

2

AD-A241 064



NAVAL POSTGRADUATE SCHOOL

Monterey, California



DTIC
ELECTE
OCT 3 1991
S C D

THESIS

ANALYSIS OF A PERTURBATION SOLUTION OF
THE MAIN PROBLEM IN
ARTIFICIAL SATELLITE THEORY

by

Scott David Krambeck

September 1990

Thesis Advisor

Donald A. Danielson

Approved for public release; distribution is unlimited.

91-12244



91-12244-113

Unclassified

security classification of this page

REPORT DOCUMENTATION PAGE

1a Report Security Classification Unclassified			1b Restrictive Markings		
2a Security Classification Authority			3 Distribution/Availability of Report		
2b Declassification/Downgrading Schedule			Approved for public release; distribution is unlimited.		
4 Performing Organization Report Number(s)			5 Monitoring Organization Report Number(s)		
6a Name of Performing Organization Naval Postgraduate School		6b Office Symbol (if applicable) 31	7a Name of Monitoring Organization Naval Postgraduate School		
6c Address (city, state, and ZIP code) Monterey, CA 93943-5000			7b Address (city, state, and ZIP code) Monterey, CA 93943-5000		
8a Name of Funding, Sponsoring Organization		8b Office Symbol (if applicable)	9 Procurement Instrument Identification Number		
8c Address (city, state, and ZIP code)			10 Source of Funding Numbers		
			Program Element No	Project No	Task No
			Work Unit Accession No		
11 Title (include security classification) ANALYSIS OF A PERTURBATION SOLUTION OF THE MAIN PROBLEM IN ARTIFICIAL SATELLITE THEORY					
12 Personal Author(s) Scott David Krambeck					
13a Type of Report Engineer's Thesis		13b Time Covered From To		14 Date of Report (year, month, day) September 1990	15 Page Count 142
16 Supplementary Notation The views expressed in this thesis are those of the author and do not reflect the official policy or position of the Department of Defense or the U.S. Government.					
17 Cosati Codes			18 Subject Terms (continue on reverse if necessary and identify by block number)		
Field	Group	Subgroup	Oblateness, Perturbation, First Order Solution, Numerical Solution Comparison, Measured Satellite Data Comparison.		
19 Abstract (continue on reverse if necessary and identify by block number)					
<p>The development of a universal solution of the main problem in artificial satellite theory has only recently been accomplished with the aid of high powered computers. The solution to this long standing problem is an analytical expression that is similar in form to the two-body solution. An analysis is presented in which the solution is compared with the two-body solution, a proven numerical solution, and actual measured satellite data. The solution is shown to be significantly more accurate than the two-body solution. The theoretical accuracy of the solution is confirmed. The solution compares extremely well with a proven numerical solution for at least 41 orbits with a relative error on the order of J^20. The solution compares extremely well with measured satellite data for satellites in near Earth orbits. For a satellite in orbit at an altitude of approximately 1000 kilometers, the solution reduces the error of the two-body solution by about 95%. For satellites in orbit at semisynchronous and geosynchronous altitudes, the solution reduces the error of the two-body solution by at least 50%. The solution is free of singularities and is valid for all eccentricities and inclinations.</p>					
20 Distribution/Availability of Abstract			21 Abstract Security Classification		
<input checked="" type="checkbox"/> unclassified unlimited <input type="checkbox"/> same as report <input type="checkbox"/> DTIC users			Unclassified		
22a Name of Responsible Individual Donald A. Danielson			22b Telephone (include Area code) (408) 646-2622		22c Office Symbol MA Dd

DD FORM 1473,84 MAR

83 APR edition may be used until exhausted
All other editions are obsolete

security classification of this page

Unclassified

Approved for public release; distribution is unlimited.

Analysis of a Perturbation Solution of the Main Problem in
Artificial Satellite Theory

by

Scott David Krambeck
Lieutenant, United States Navy
B.S., Iowa State University, 1982

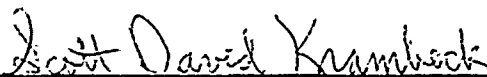
Submitted in partial fulfillment of the
requirements for the degrees of

MASTER OF SCIENCE IN AERONAUTICAL ENGINEERING
and
AERONAUTICAL AND ASTRONAUTICAL ENGINEER

from the

NAVAL POSTGRADUATE SCHOOL
September 1990

Author:



Scott David Krambeck

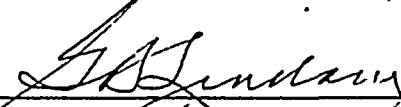
Approved by:



Donald A. Danielson, Thesis Advisor



Richard M. Howard, Second Reader



E. R. Wood, Chairman,
Department of Aeronautics and Astronautics



DEAN OF FACULTY
AND GRADUATE STUDIES

ABSTRACT

The development of a universal solution of the main problem in artificial satellite theory has only recently been accomplished with the aid of high powered computers. The solution to this long standing problem is an analytical expression that is similar in form to the two-body solution. An analysis is presented in which the solution is compared with the two-body solution, a proven numerical solution, and actual measured satellite data. The solution is shown to be significantly more accurate than the two-body solution. The theoretical accuracy of the solution is confirmed. The solution compares extremely well with a proven numerical solution for at least 41 orbits with a relative error on the order of $J^2\theta$. The solution compares extremely well with measured satellite data for satellites in near Earth orbits. For a satellite in orbit at an altitude of approximately 1000 kilometers, the solution reduces the error of the two-body solution by about 95%. For satellites in orbit at semisynchronous and geosynchronous altitudes, the solution reduces the error of the two-body solution by at least 50%. The solution is free of singularities and is valid for all eccentricities and inclinations.



Accession For	
NTIS GRA&I	<input checked="" type="checkbox"/>
DTIC TAB	<input type="checkbox"/>
Unannounced	<input type="checkbox"/>
Justification	
By	
Distribution/	
Availability Codes	
Dist	Avail and/or Special
A-1	

TABLE OF CONTENTS

I. INTRODUCTION	1
II. BACKGROUND	2
A. ORBITAL KINEMATICS	2
B. EQUATIONS OF MOTION	4
C. SOLUTION	7
D. SIMPLIFIED SOLUTION	10
E. THE CRITICAL INCLINATIONS	12
F. SPECIFIC MECHANICAL ENERGY	14
III. METHOD OF ANALYSIS	16
A. ORBITAL PARAMETERS	16
1. Argument of Latitude (θ)	16
2. Radius Magnitude (r)	18
3. Inclination (i)	18
4. Longitude of the Ascending Node (Ω)	18
B. ROMBERG INTEGRATION TECHNIQUE	19
IV. METHOD OF COMPARISON	22
A. NUMERICAL INTEGRATION COMPARISON	22
1. Delta Radius Vector	22
2. Earth Arc Angle	23
3. Delta Omega, Delta Inclination, Delta Theta	24
4. Relative Errors	24
5. Track Errors	24
B. MEASURED DATA COMPARISON	27
V. RESULTS	28
A. NUMERICAL INTEGRATION COMPARISON	28
1. Delta Radius Vector Comparison	29
2. Earth Arc Angle Comparison	30

3. Delta Omega Comparison	30
4. Delta Inclination Comparison	31
5. Delta Theta Comparison	31
6. Delta Theta Relative Error Comparison	31
7. Delta Radius Relative Error Comparison	32
8. Radial Track Error Comparison	32
9. Along Track Error Comparison	32
10. Cross Track Error Comparison	33
B. MEASURED DATA COMPARISON	33
1. Near Earth Orbit Comparison	34
2. Semisynchronous Orbit Comparison	36
3. Geosynchronous Orbit Comparison	38
VI. CONCLUSIONS AND RECOMMENDATIONS	40
APPENDIX A. NUMERICAL SOLUTION COMPARISON RESULTS	42
APPENDIX B. NEAR EARTH ORBIT COMPARISON RESULTS	70
APPENDIX C. SEMISYNCHRONOUS ORBIT COMPARISON RESULTS ...	83
APPENDIX D. GEOSYNCHRONOUS ORBIT COMPARISON RESULTS ..	94
APPENDIX E. COMPUTER PROGRAM :.....	105
LIST OF REFERENCES	126
INITIAL DISTRIBUTION LIST	128

LIST OF TABLES

Table 1. A SCHEMATIC OF ROMBERG INTEGRATION	20
Table 2. ROMBERG INTEGRATION	21

LIST OF FIGURES

Figure 1.	Spherical coordinate system.	2
Figure 2.	Orbital plane.	3
Figure 3.	Delta radius vector and Earth arc angle.	23
Figure 4.	Track errors.	26
Figure 5.	Delta radius vector (1 day)	43
Figure 6.	Delta radius vector (1 day)	44
Figure 7.	Delta radius vector (3 days)	45
Figure 8.	Earth arc angle (1 day)	46
Figure 9.	Earth arc angle (1 day)	47
Figure 10.	Earth arc angle (3 days)	48
Figure 11.	Delta omega (1 day)	49
Figure 12.	Delta omega (3 days)	50
Figure 13.	Delta inclination (1 day)	51
Figure 14.	Delta inclination (3 days)	52
Figure 15.	Delta theta (1 day)	53
Figure 16.	Delta theta (1 day)	54
Figure 17.	Delta theta (3 days)	55
Figure 18.	Delta theta relative error (1 day)	56
Figure 19.	Delta theta relative error (1 day)	57
Figure 20.	Delta theta relative error (3 days)	58
Figure 21.	Delta radius relative error (1 day)	59
Figure 22.	Delta radius relative error (1 day)	60
Figure 23.	Delta radius relative error (3 days)	61
Figure 24.	Radial track error (1 day)	62
Figure 25.	Radial track error (1 day)	63
Figure 26.	Radial track error (3 days)	64
Figure 27.	Along track error (1 day)	65
Figure 28.	Along track error (1 day)	66
Figure 29.	Along track error (3 days)	67
Figure 30.	Cross track error (1 day)	68
Figure 31.	Cross track error (3 days)	69

Figure 32. Delta radius vector (21 days)	71
Figure 33. Earth arc angle (21 days)	72
Figure 34. Delta omega (21 days)	73
Figure 35. Delta omega (21 days)	74
Figure 36. Delta inclination (21 days)	75
Figure 37. Delta theta (21 days)	76
Figure 38. Delta theta relative error (21 days)	77
Figure 39. Delta radius relative error (21 days)	78
Figure 40. Radial track error (21 days)	79
Figure 41. Along track error (21 days)	80
Figure 42. Cross track error (21 days)	81
Figure 43. Cross track error (21 days)	82
Figure 44. Delta radius vector (30 days)	84
Figure 45. Earth arc angle (30 days)	85
Figure 46. Delta omega (30 days)	86
Figure 47. Delta inclination (30 days)	87
Figure 48. Delta theta (30 days)	88
Figure 49. Delta theta relative error (30 days)	89
Figure 50. Delta radius relative error (30 days)	90
Figure 51. Radial track error (30 days)	91
Figure 52. Along track error (30 days)	92
Figure 53. Cross track error (30 days)	93
Figure 54. Delta radius vector (28 days)	95
Figure 55. Earth arc angle (28 days)	96
Figure 56. Delta omega (28 days)	97
Figure 57. Delta inclination (28 days)	98
Figure 58. Delta theta (28 days)	99
Figure 59. Delta theta relative error (28 days)	100
Figure 60. Delta radius relative error (28 days)	101
Figure 61. Radial track error (28 days)	102
Figure 62. Along track error (28 days)	103
Figure 63. Cross track error (28 days)	104

LIST OF SYMBOLS

<i>ATE</i>	along track error
<i>a</i>	semi-major axis
<i>a</i> ₀	initial value of <i>a</i>
<i>B</i> _{<i>n</i>}	rotating orthonormal base vectors (<i>n</i> = 1, 2, 3)
<i>b</i> _{<i>n</i>}	fixed orthonormal base vectors (<i>n</i> = 1, 2, 3)
<i>CTE</i>	cross track error
<i>c</i>	cos <i>i</i> ₀
<i>e</i>	eccentricity
<i>e</i> ₀	initial value of <i>e</i>
<i>f</i>	function
<i>G</i>	universal gravitational constant (<i>G</i> = 6.662 × 10 ⁻²⁰ km ³ /kg-s ²)
<i>h</i>	angular momentum
<i>h</i> ₀	initial value of <i>h</i>
<i>I</i>	integration result
<i>i</i>	inclination
<i>i</i> ₀	initial value of <i>i</i>
<i>J</i>	normalized <i>J</i> ₂ (<i>J</i> = $\frac{3}{2} \frac{J_2 R^2}{p_0^3}$)
<i>J</i> _{<i>n</i>}	coefficient of the <i>n</i> th zonal harmonic of a planet's gravitational potential
<i>M</i>	planet mass (<i>Earth</i> , <i>M</i> = 5.98319478 × 10 ²⁴ kg)
<i>O</i>	center of the planet and the coordinate system
<i>O</i>	order
<i>p</i>	semi-latus rectum (<i>p</i> = <i>a</i> (1 - <i>e</i> ²)) (<i>p</i> = <i>h</i> ² / <i>GM</i>)
<i>p</i> ₀	initial value of <i>p</i> (<i>p</i> ₀ = <i>a</i> ₀ (1 - <i>e</i> ₀ ²)) (<i>p</i> ₀ = <i>h</i> ₀ ² / <i>GM</i>)
<i>R</i>	equatorial radius of a planet (<i>Earth</i> , <i>R</i> = 6378.137 km)
<i>RTE</i>	radial track error
<i>r</i>	radial vector from the center of a planet to the satellite
<i>r</i> _{<i>n</i>}	radial vector from the center of a planet to the satellite for the reference solution

r	magnitude of the radial vector from the center of a planet to the satellite
r_n	magnitude of the radial vector from the center of a planet to the satellite for the reference solution
S	satellite
s	$\sin i_0$
T	specific kinetic energy
t	time
t_0	initial value of t
u	p_0/r
V	specific potential energy
y	variable used in the r , i , and Ω equations
Z	Greenwich mean time (ZULU time)
α	right ascension angle
β	declination or latitude
β_0	initial value of β
γ	fixed direction of the vernal equinox
Δ	a finite increment
θ	argument of latitude
θ_0	initial value of θ
θ_n	argument of latitude for the reference solution
Ψ	Earth arc angle
Ω	longitude of the ascending node
Ω_0	initial value of Ω
ω	argument of periapsis
ω_0	initial value of ω

ACKNOWLEDGMENT

Sir Issac Newton once remarked, "If I have seen a little farther than others it is because I have stood on the shoulders of giants." In completing this endeavor there are several giants I wish to acknowledge.

My special thanks to Professor Don Danielson for his encouragement, inspiration, and patience as he guided me through this project. I will be forever grateful for his confidence and trust.

Several words of thanks go to LTC Jim Snider, USA, and LT Chris Sagovac, USN, whose research cleared the path such that this thesis could be attempted. Their numerous and timely suggestions were extremely helpful.

I must thank John Rodell from the Colorado Center for Astrodynamic Research (CCAR) for producing the numerical data needed in this analysis. His quick response to my requests were greatly appreciated.

I must also thank CAPT Greg Petrick, USAF, and 1stLT Bruce Hibbert, USAF, from the First Satellite Control Squadron (ISCS) for supplying the measured satellite data needed in this analysis. I extend my sincere appreciation for their help and cooperation.

I convey special gratitude to my lovely wife Susan for her support, sacrifice, and understanding which made the completion of this thesis a reality.

I. INTRODUCTION

With the development of any new method or theory the question always arises on whether the approach is valid or practical for ordinary use. This is particularly true in the prediction of satellite motion. Ever since Sir Issac Newton's discovery of the law of universal gravitation, new methods have been developed to better predict the motion of the heavenly bodies. Usually the method contains one or more restrictions that limits the practical use of the solution. The goal, of course, is to develop a solution that is valid and possesses no restrictions. Recently, such a solution has been formulated.

This analysis continues the work that was begun by Snider [Ref. 1] and Sagovac [Ref. 2]. From their research, a higher order universal solution of the motion of an artificial satellite around an oblate planet was developed. The solution is free of singularities and is theoretical valid for all orbital parameters. The purpose and scope of this work is to compare the solution with proven numerical solutions and actual measured satellite data in order to determine whether the theoretical work is valid and practical.

The first chapter summarizes the development of the theory and presents the solution in its entirety. Also included is a somewhat less accurate simplified solution. An explanation of the solution near the critical inclinations is presented. The chapter concludes with a discussion on the conservation of specific mechanical energy. The next chapter describes the method of analysis and explains the type of integration routine exercised in the evaluation. The method of comparison is presented next in which the error parameters are described in detail. The results follow which include both a detailed discussion and a graphic representation.

The analysis is objective in nature and designed to demonstrate both the advantages and disadvantages of the theory and the solution. Before the solution can be applied extensively, a general understanding of its strengths and weaknesses must be determined.

II. BACKGROUND

A. ORBITAL KINEMATICS

A reference system for a planet in spherical coordinates (r, α, β) is shown in Figure 1. The radial distance (r) is measured from the center of the planet (O) to the satellite (S). The line (O γ) is in a direction fixed with respect to an inertial coordinate system. For Earth, the line (O γ) is in the direction of the vernal equinox. The right ascension angle (α) is measured in the planet's equatorial plane eastward from the line (O γ). The declination or latitude (β) is the angle measured northward from the equator. The position vector (r) of the satellite in the spherical coordinate system is:

$$r = r (\cos \alpha \cos \beta) b_1 + r (\sin \alpha \cos \beta) b_2 + r (\sin \beta) b_3 \quad (1)$$

where (b_1, b_2, b_3) are orthonormal base vectors fixed in the direction shown.

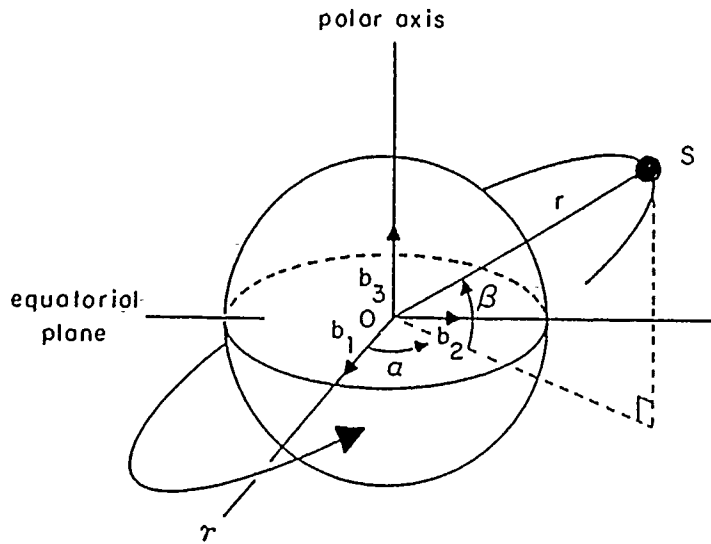


Figure 1. Spherical coordinate system.

A reference system for a satellite in polar coordinates (r, θ) within a rotating orbital plane is shown in Figure 2. The satellite's position and velocity vectors are contained within the orbital plane. The argument of latitude (θ) is measured in the orbital plane

from the ascending node to the satellite. The inclination (i) of the orbital plane is the angle measured between the equatorial plane and the orbital plane. The longitude of the ascending node (Ω) is measured from the line ($O \gamma$) to the ascending node. The ascending node lies on the line of nodes which form the intersection of the equatorial and orbital planes.

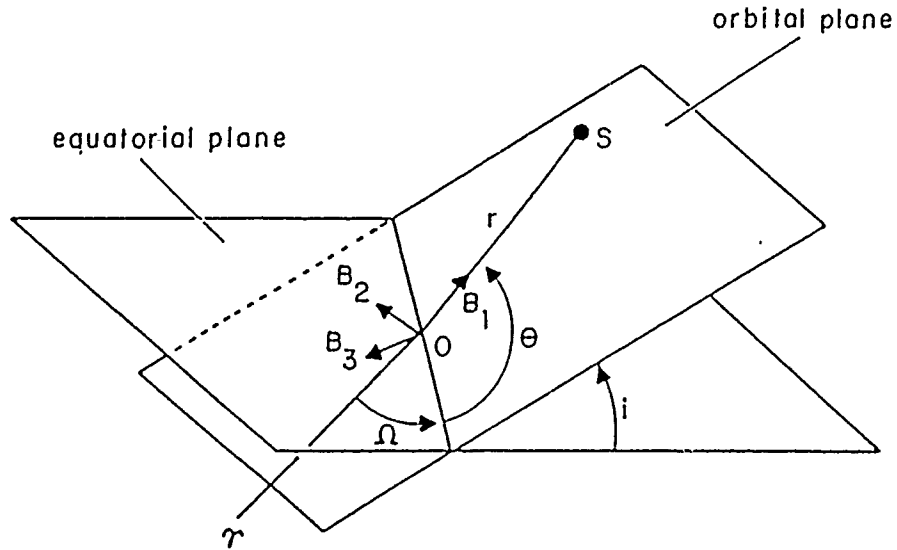


Figure 2. Orbital plane.

The basis (b_1, b_2, b_3) may be transformed into another orthonormal basis (B_1, B_2, B_3) by a succession of three rotations. First the basis (b_1, b_2, b_3) is rotated about the b_3 direction by the angle Ω . The basis is then rotated about the new first coordinate vector by the angle i . The final rotation is about the new third coordinate vector by the angle θ . The position vector (r) has only one component in the rotating basis.

$$r = r B_1 \quad (2)$$

The components of \mathbf{r} in the fixed basis are:

$$\begin{aligned} \mathbf{r} = & r (\cos \theta \cos \Omega - \sin \theta \cos i \sin \Omega) \mathbf{b}_1 \\ & + r (\cos \theta \sin \Omega + \sin \theta \cos i \cos \Omega) \mathbf{b}_2 + r (\sin \theta \sin i) \mathbf{b}_3 \end{aligned} \quad (3)$$

Equating the components of equations (1) and (3), the following relations among the angles (α, β) of the spherical coordinate system and the astronomical angles (i, Ω, θ) can be obtained.

$$\sin \beta = \sin \theta \sin i \quad (4)$$

$$\cos \beta = \cos \theta \sec(\alpha - \Omega) \quad (5)$$

The velocity $(d\mathbf{r}/dt)$ of the satellite is obtained by differentiating equation (2) with respect to time (t) which results in:

$$\frac{d\mathbf{r}}{dt} = \frac{dr}{dt} \mathbf{B}_1 + r \frac{d\theta}{dt} \left(1 + \tan \theta \cot i \frac{di}{d\theta} \right) \mathbf{B}_2 \quad (6)$$

Equations (2) and (6) represent the orbital kinematics of a satellite in the polar coordinate system. The position and velocity vector expressions describe the motion of a satellite in a particular reference system and provide the information needed to develop the equations of motion in that system. These expressions are referenced to the *true*, rather than *mean*, orbital plane and were originally formulated by Struble [Ref. 3, 4, 5].

B. EQUATIONS OF MOTION

The motion of all objects is mathematically described by the equations of motion that govern them. For an oblate planet, the expressions for the kinetic and potential energies per unit mass of an orbiting satellite in spherical coordinates are respectively:

$$T = \frac{1}{2} \left[\left(\frac{dr}{dt} \right)^2 + r^2 \left(\frac{d\beta}{dt} \right)^2 + r^2 \cos^2 \beta \left(\frac{d\alpha}{dt} \right)^2 \right] \quad (7)$$

$$V = -\frac{GM}{r} \left[1 + \frac{J_2 R^2}{2r^2} (1 - 3 \sin^2 \beta) \right] \quad (8)$$

In the above equations, (M) is the mass of the planet, (G) is the universal gravitational constant, (R) is the equatorial radius of the planet, and (J_2) is the coefficient of the second zonal harmonic of the planet's gravitational potential. The governing equations of motion can be determined by substituting equations (7) and (8) into Lagrange's equations which are represented by:

$$\frac{d}{dt} \left[\frac{\partial(T-V)}{\partial \left(\frac{dq}{dt} \right)} \right] - \frac{\partial}{\partial q} (T-V) = 0 \quad (9)$$

where: $q = \alpha, r$, and β

Three equations result from Lagrange's equations which describe the motion of the satellite. The three equations are:

$$\frac{d}{dt} \left(r^2 \cos^2 \beta \frac{d\alpha}{dt} \right) = 0 \quad (10)$$

$$\frac{d^2 r}{dt^2} - r \left(\frac{d\beta}{dt} \right)^2 - r \cos^2 \beta \left(\frac{d\alpha}{dt} \right)^2 = - \frac{\partial V}{\partial r} \quad (11)$$

$$\frac{d}{dt} \left(r^2 \frac{d\beta}{dt} \right) + r^2 \sin \beta \cos \beta \left(\frac{d\alpha}{dt} \right)^2 = - \frac{\partial V}{\partial \beta} \quad (12)$$

From the equations of motion, two integrals result which are:

$$r^2 \cos^2 \beta \frac{d\alpha}{dt} = \text{constant} \quad (13)$$

$$T + V = \text{constant} \quad (14)$$

Equation (13) results from integrating equation (10) and equation (14) simply states that the specific mechanical energy of the satellite remains constant. To change the independent variable from t to θ , equations (1), (2), and (6) are used in conjunction with equation (13) and some initial conditions to form:

$$\frac{dt}{d\theta} = \frac{r^2 \cos i}{h_0 \cos i_0} \left(1 + \tan \theta \cot i \frac{di}{d\theta} \right) \quad (15)$$

Letting $u = p_0/r$, and using equation (15), the remaining equations of motion (11) - (12) can be rewritten as:

$$\frac{di}{d\theta} = \frac{-2Ju \sin \theta \cos \theta \sin i \cos^2 i}{\left(\frac{c^2}{\cos i} \right) + 2Ju \sin^2 \theta \cos^3 i} \quad (16)$$

$$\begin{aligned} \frac{d^2 u}{d\theta^2} + u = & \left\{ c^2 \cos^2 i - Jc^2 u \cos^2 i \left[2 \frac{du}{d\theta} \sin \theta \cos \theta (3 \cos^2 i - 1) - u \right] \right. \\ & \left. - 4J^2 u^2 \frac{du}{d\theta} \sin^3 \theta \cos \theta \cos^6 i (3 - \cos^2 i) \right\} / \{ c^4 + 4Juc^2 \sin^2 \theta \cos^4 i \\ & + 4u^2 J^2 \sin^4 \theta \cos^8 i \} \end{aligned} \quad (17)$$

$$\frac{d\Omega}{d\theta} = \frac{\tan \theta}{\sin i} \frac{di}{d\theta} \quad (18)$$

$$\begin{aligned} \text{where: } c &= \cos i_0 \\ s &= \sin i_0 \\ J &= \frac{3J_2 R^2}{2p_0^2} \end{aligned}$$

Equation (18) results from uncoupling the equations for Ω and i . The angles Ω and i can be uncoupled by applying the fact that the orbital plane must contain the velocity vector. The differential equations (16) - (18) are coupled by nonlinear terms and apparently cannot be solved analytically. If the right sides of equations (16) - (18) are expanded in a Taylor series expansion in powers of J , the equations simplify to:

$$\frac{di}{d\theta} = \frac{-2Ju \sin \theta \cos \theta \sin i \cos^3 i}{c^2} + 4J^2 u^2 s c^3 \sin^3 \theta \cos \theta + O(J^3) \quad (19)$$

$$\begin{aligned}
\frac{d^2 u}{d\theta^2} + u = & \frac{\cos^2 i}{c^2} + \frac{J \cos^2 i}{c^2} \left\{ \frac{-4u \sin^2 \theta \cos^4 i}{c^2} + u^2 [1 + \sin^2 \theta (7 \cos^2 i \right. \\
& - 3)] + 2u \frac{du}{d\theta} \sin \theta \cos \theta (1 - 3 \cos^2 i) - 2 \left(\frac{du}{d\theta} \right)^2 \sin^2 \theta \cos^2 i \Big\} \\
& + \frac{4J^2 u \sin^2 \theta \cos^6 i}{c^4} \{ u^2 [3 \sin^2 \theta (1 - 2 \cos^2 i) - 1] \\
& + \frac{3u \sin^2 \theta \cos^4 i}{c^2} + u \frac{du}{d\theta} \sin \theta \cos \theta [4 \sin^2 i + \sin^2 \theta (1 \\
& - 3 \cos^2 i)] + \left(\frac{du}{d\theta} \right)^2 \sin^2 \theta \cos^2 i \Big\} + O(J^3)
\end{aligned} \tag{20}$$

$$\frac{d\Omega}{d\theta} = -2Juc \sin^2 \theta + 4J^2 u^2 c^3 \sin^4 \theta + O(J^3) \tag{21}$$

Each of the neglected terms in equations (19) - (21) are indicated by the (O) symbols. These are terms which will be multiplied by J to the third power or higher. Equations (19) - (21) are identical to those used as a starting point in the analysis of Eckstein, Shi and Kevorkian [Ref. 6].

C. SOLUTION

The initial breakthrough of an analytical solution of the equations of motion represented by equations (15), (19), (20), and (21) was obtained by Danielson and Snider [Ref. 1, 7]. Further refinement of the solution was later formulated by Danielson, Sagovac, and Snider [Ref. 2, 8]. The three authors developed the solution through the extensive use of an algebraic manipulation computer program called MACSYMA. Through the use of an algorithm, MACSYMA was able to solve for the variables u (or r), i , Ω , and $dt/d\theta$ in terms of θ . The solution includes all terms multiplied by J and excludes terms of order J^2 and higher. In order to maintain a solution of order J when $\theta \leq 1/J$, the solutions also need to appropriately include terms multiplied by $J^2 \theta$. The solutions which analytically demonstrate a relative accuracy of order $J^2 \theta$ are:

$$\begin{aligned}
r = & p_0 / \left\{ 1 + e_0 \cos y + J \left[1 - \frac{3s^2}{2} + e_0^2 \left(1 - \frac{5s^2}{4} \right) + \frac{e_0^2}{8} (3s^2 - 2) \cos(2y - 2\theta) \right. \right. \\
& + \frac{e_0 [15(2 + e_0^2)s^4 - 14(4 + e_0^2)s^2 + 24] \sin \left[J\theta \left(\frac{5s^2}{2} - 2 \right) \right] \sin[\theta + \omega_0]}{6(s^2 - 4)} \\
& + \frac{1}{4} [(6 + 5e_0^2)s^2 - 4(1 + e_0^2)] \cos(y - \theta_0 + \omega_0) + \frac{e_0 s^2}{3} \cos(3\theta_0 - \omega_0) \\
& + \frac{e_0^2 s^2 (15s^2 - 14) \sin \left[J\theta \left(\frac{5s^2}{2} - 2 \right) \right] \sin \left[2\omega_0 - J\theta \left(\frac{5s^2}{2} - 2 \right) \right]}{6(5s^2 - 4)} \\
& + \frac{e_0^2}{48} (9s^2 - 4) \cos(y + 3\theta_0 - \omega_0) + \frac{e_0^2}{8} (6 - 7s^2) \cos(y + \theta_0 - \omega_0) \\
& + \frac{1}{8} [(5e_0^2 - 2)s^2 - 2e_0^2] \cos(y + \theta_0 + \omega_0) + e_0 s^2 \cos(\theta_0 + \omega_0) \\
& - \frac{e_0^2 s^2}{16} \cos(y - 5\theta_0 + 3\omega_0) + \frac{e_0}{4} (3s^2 - 2) \cos(y - 2\theta_0 + 2\omega_0) \\
& - \frac{e_0^2 s^2}{16} \cos(y - \theta_0 + 3\omega_0) + \frac{e_0^2}{24} (3s^2 - 2) \cos(y - 3\theta_0 + 3\omega_0) \\
& + \frac{e_0}{4} (1 - 3s^2) \cos(y - 2\theta_0) + \frac{e_0}{4} (2 - 3s^2) \cos y + s^2 \cos 2\theta_0 \\
& + \frac{e_0^2}{16} (4 - 5s^2) \cos(y - \theta_0 - \omega_0) + \frac{e_0}{4} (2s^2 - 1) \cos(y + 2\theta_0) \\
& + \frac{e_0}{24} (6 - 11s^2) \cos(y + 2\theta) + \frac{e_0^2}{24} (2 - 3s^2) \cos(2y + 2\theta) \\
& + \frac{1}{12} [2e_0^2 - (2 + 5e_0^2)s^2] \cos 2\theta + \frac{e_0^2}{12} (9s^2 - 8) \cos 2y \\
& - \frac{3e_0 s^2}{8} \cos(y - 4\theta_0 + 2\omega_0) - \frac{e_0}{4} (s^2 + 1) \cos(y + 2\omega_0) \\
& + \left. \frac{1}{24} [2e_0^2 - (14 + 5e_0^2)s^2] \cos(y - 3\theta_0 + \omega_0) \right] + O(J^2, J^3\theta, \dots) \}
\end{aligned} \tag{22}$$

$$\begin{aligned}
y &= \theta - \omega_0 + J \left\{ \left(\frac{5s^2}{2} - 2 \right) (\theta - \theta_0) \right. \\
&\quad + \frac{e_0^2 (112 - 75s^6 + 260s^4 - 296s^2) \sin \left[J\theta \left(\frac{5s^2}{2} - 2 \right) \right] \cos \left[2\omega_0 - J\theta \left(\frac{5s^2}{2} - 2 \right) \right]}{24(5s^2 - 4)^2} \Big\} \\
&\quad + J^2 \theta \left\{ \frac{e_0^2 s^2 (14 - 15s^2) (15s^2 - 13) \cos 2\omega_0}{24(5s^2 - 4)} + \frac{s^2}{2} (15s^2 - 13) \cos 2\theta_0 \right. \\
&\quad + \frac{e_0 s^2}{2} (15s^2 - 13) \cos(\theta_0 + \omega_0) + \frac{e_0 s^2}{6} (15s^2 - 13) \cos(3\theta_0 - \omega_0) \\
&\quad \left. + \frac{1}{96} [5(9e_0^2 + 34)s^4 + 4(2e_0^2 - 34)s^2 - 56e_0^2] \right\} + O(J^2, J^3\theta, \dots) \tag{23}
\end{aligned}$$

$$\begin{aligned}
i &= i_0 + scJ \left\{ \frac{1}{2} \cos 2\theta + \frac{e_0}{6} \cos(y + 2\theta) + \frac{e_0}{2} \cos(y - 2\theta) - \frac{1}{2} \cos 2\theta_0 \right. \\
&\quad + \frac{e_0^2 (14 - 15s^2) \sin \left[J\theta \left(\frac{5s^2}{2} - 2 \right) \right] \sin \left[2\omega_0 - J\theta \left(\frac{5s^2}{2} - 2 \right) \right]}{12(5s^2 - 4)} \\
&\quad \left. - \frac{e_0}{6} \cos(3\theta_0 - \omega_0) - \frac{e_0}{2} \cos(\theta_0 + \omega_0) \right\} + O(J^2, J^3\theta, \dots) \tag{24}
\end{aligned}$$

$$\begin{aligned}
\Omega &= \Omega_0 + cJ \left\{ \theta_0 - \theta + \frac{1}{2} \sin 2\theta - e_0 \sin y + \frac{e_0}{6} \sin(y + 2\theta) - \frac{e_0}{2} \sin(y - 2\theta) \right. \\
&\quad + \frac{e_0^2 (15s^4 - 45s^2 + 28) \sin \left[J\theta \left(\frac{5s^2}{2} - 2 \right) \right] \cos \left[2\omega_0 - J\theta \left(\frac{5s^2}{2} - 2 \right) \right]}{6(5s^2 - 4)^2} \\
&\quad - \frac{1}{2} \sin 2\theta_0 + e_0 \sin(\theta_0 - \omega_0) - \frac{e_0}{6} \sin(3\theta_0 - \omega_0) - \frac{e_0}{2} \sin(\theta_0 + \omega_0) \Big\} \\
&\quad + cJ^2 \theta \left\{ \frac{e_0^2 s^2 (15s^2 - 14)}{12(5s^2 - 4)} \cos 2\omega_0 - e_0 s^2 \cos(\theta_0 + \omega_0) + \frac{e_0^2}{24} (7s^2 - 4) \right. \\
&\quad \left. - \frac{e_0 s^2}{3} \cos(3\theta_0 - \omega_0) - s^2 \cos 2\theta_0 + \frac{1}{12} (6 - s^2) \right\} + O(J^2, J^3\theta, \dots) \tag{25}
\end{aligned}$$

$$\begin{aligned}
t = & t_0 + \frac{1}{h_0} \int_{\theta_0}^{\theta} r^2 \left\{ 1 + J \left[\frac{(2-3s^2)}{2} \cos 2\theta + e_0(s^2-1) \cos y + \frac{e_0 s^2}{6} \cos(3\theta_0 - \omega_0) \right. \right. \\
& + \frac{e_0^2 s^2 (15s^2 - 14) \sin \left[J\theta \left(\frac{5s^2}{2} - 2 \right) \right] \sin \left[2\omega_0 - J\theta \left(\frac{5s^2}{2} - 2 \right) \right]}{12(5s^2 - 4)} + s^2 - 1 \quad (26) \\
& + \frac{e_0(1-2s^2)}{2} \cos(y-2\theta) + \frac{s^2}{2} \cos 2\theta_0 + \frac{e_0(3-4s^2)}{6} \cos(y+2\theta) \\
& \left. + \frac{e_0 s^2}{2} \cos(\theta_0 + \omega_0) \right\} + O(J^2, J^3\theta, \dots) d\theta
\end{aligned}$$

D. SIMPLIFIED SOLUTION

As shown in equations (22) - (25), if θ is restricted such that $\theta \leq 1/J$, the solution should be of order J and the neglected terms should be of order J^2 . For an Earth satellite, $J < 3/2 \times 10^{-3}$, so for at least 100 revolutions the relative error should be on the order of 10^{-6} . If θ is restricted such that $\theta \leq 1$, all of the terms of order $J^2\theta$ in equations (22) - (26) can be neglected if a relative error of order J is desired. By neglecting terms of order $J^2\theta$, the solution simplifies considerably to:

$$\begin{aligned}
r = & p_0 \left\{ 1 + e_0 \cos \left[\theta - \omega_0 + J(\theta - \theta_0) \left(\frac{5s^2}{2} - 2 \right) \right] \right. \\
& + J \left[1 - \frac{3s^2}{2} + e_0^2 \left(1 - \frac{5s^2}{4} \right) + \frac{1}{12} [2e_0^2 - (2 + 5e_0^2)s^2] \cos 2\theta \right. \\
& + \frac{e_0^2}{48} (9s^2 - 4) \cos(\theta + 3\theta_0 - 2\omega_0) + \frac{e_0^2}{8} (6 - 7s^2) \cos(\theta + \theta_0 - 2\omega_0) \\
& + \frac{e_0^2}{16} (4 - 5s^2) \cos(\theta - \theta_0 - 2\omega_0) + \frac{e_0}{4} (2s^2 - 1) \cos(\theta + 2\theta_0 - \omega_0) \\
& - \frac{e_0^2 s^2}{16} \cos(\theta - \theta_0 + 2\omega_0) + \frac{e_0^2}{24} (3s^2 - 2) \cos(\theta - 3\theta_0 + 2\omega_0) \\
& - \frac{e_0^2 s^2}{16} \cos(\theta - 5\theta_0 + 2\omega_0) + \frac{e_0}{4} (3s^2 - 2) \cos(\theta - 2\theta_0 + \omega_0) \\
& \left. \left. + \frac{e_0}{4} (1 - 3s^2) \cos(\theta - 2\theta_0 - \omega_0) + \frac{e_0}{4} (2 - 3s^2) \cos(\theta - \omega_0) \right] \right\} \quad (27)
\end{aligned}$$

$$\begin{aligned}
& + \frac{e_0^2}{12} (9s^2 - 8) \cos(2\theta - 2\omega_0) + \frac{e_0}{24} (6 - 11s^2) \cos(3\theta - \omega_0) \\
& + \frac{1}{8} [(5e_0^2 - 2)s^2 - 2e_0^2] \cos(\theta + \theta_0) + e_0 s^2 \cos(\theta_0 - \omega_0) \\
& + \frac{e_0^2}{24} (2 - 3s^2) \cos(4\theta + 2\omega_0) + \frac{e_0^2}{8} (3s^2 - 2) \cos 2\omega_0 \\
& - \frac{3e_0 s^2}{8} \cos(\theta - 4\theta_0 + \omega_0) - \frac{e_0}{4} (s^2 + 1) \cos(\theta + \omega_0) \\
& + \frac{1}{24} [2e_0^2 - (14 + 5e_0^2)s^2] \cos(\theta - 3\theta_0) + s^2 \cos 2\theta_0 \\
& + \frac{1}{4} [(6 + 5e_0^2)s^2 - 4(1 + e_0^2)] \cos(\theta - \theta_0) \\
& + \frac{e_0 s^2}{3} \cos(3\theta_0 - \omega_0) \Big] + O(J^2, J^2\theta, \dots) \Big\}
\end{aligned}$$

$$\begin{aligned}
i = i_0 + scJ \Big[& \frac{1}{2} \cos 2\theta + \frac{e_0}{6} \cos(3\theta - \omega_0) + \frac{e_0}{2} \cos(\theta + \omega_0) - \frac{1}{2} \cos 2\theta_0 \\
& - \frac{e_0}{6} \cos(3\theta_0 - \omega_0) - \frac{e_0}{2} \cos(\theta_0 + \omega_0) \Big] + O(J^2, J^2\theta, \dots) \quad (28)
\end{aligned}$$

$$\begin{aligned}
\Omega = \Omega_0 + cJ \Big\{ & \theta_0 - \theta + \frac{1}{2} \sin 2\theta - e_0 \sin(\theta - \omega_0) + \frac{e_0}{6} \sin(3\theta - \omega_0) \\
& + \frac{e_0}{2} \sin(\theta + \omega_0) - \frac{1}{2} \sin 2\theta_0 + e_0 \sin(\theta_0 - \omega_0) - \frac{e_0}{6} \sin(3\theta_0 - \omega_0) \\
& - \frac{e_0}{2} \sin(\theta_0 + \omega_0) \Big\} + O(J^2, J^2\theta, \dots) \quad (29)
\end{aligned}$$

$$\begin{aligned}
t = t_0 + \frac{1}{h_0} \int_{\theta_0}^{\theta} r^2 \Big\{ & 1 + J \Big[\frac{(2 - 3s^2)}{2} \cos 2\theta + e_0(s^2 - 1) \cos(\theta - \omega_0) \\
& + \frac{e_0(3 - 4s^2)}{6} \cos(3\theta - \omega_0) + \frac{e_0(1 - 2s^2)}{2} \cos(\theta + \omega_0) + s^2 - 1 \\
& + \frac{e_0 s^2}{2} \cos(\theta_0 + \omega_0) + \frac{e_0 s^2}{6} \cos(3\theta_0 - \omega_0) \\
& + \frac{s^2}{2} \cos 2\theta_0 \Big] + O(J^2, J^3\theta, \dots) \Big\} d\theta \quad (30)
\end{aligned}$$

E. THE CRITICAL INCLINATIONS

As shown in equations (22) - (26), the solution appears to be well bounded for almost all inclinations. However, two particular inclinations immediately appear that may produce a singularity. A possible singularity occurs when the inclination is equal to either 63.43 degrees or 116.57 degrees. These two inclinations have produced mountains of literature and are well known as the critical inclinations. However, if the solution is replaced by the limit as the inclination approaches either critical inclination, the solution remains finite. More specifically, the solution at either critical inclination is as follows:

$$\begin{aligned}
 r = & p_0 / \left\{ 1 + e_0 \cos y + J \left[1 - \frac{3s^2}{2} + e_0^2 \left(1 - \frac{5s^2}{4} \right) + \frac{e_0^2}{8} (3s^2 - 2) \cos(2y - 2\theta) \right. \right. \\
 & + \frac{1}{4} [(6 + 5e_0^2)s^2 - 4(1 + e_0^2)] \cos(y - \theta_0 + \omega_0) + \frac{e_0 s^2}{3} \cos(3\theta_0 - \omega_0) \\
 & + \frac{e_0^2}{48} (9s^2 - 4) \cos(y + 3\theta_0 - \omega_0) + \frac{e_0^2}{8} (6 - 7s^2) \cos(y + \theta_0 - \omega_0) \\
 & + \frac{1}{8} [(5e_0^2 - 2)s^2 - 2e_0^2] \cos(y + \theta_0 + \omega_0) + e_0 s^2 \cos(\theta_0 + \omega_0) \\
 & - \frac{e_0^2 s^2}{16} \cos(y - 5\theta_0 + 3\omega_0) + \frac{e_0}{4} (3s^2 - 2) \cos(y - 2\theta_0 + 2\omega_0) \\
 & - \frac{e_0^2 s^2}{16} \cos(y - \theta_0 + 3\omega_0) + \frac{e_0^2}{24} (3s^2 - 2) \cos(y - 3\theta_0 + 3\omega_0) \\
 & + \frac{e_0}{4} (1 - 3s^2) \cos(y - 2\theta_0) + \frac{e_0}{4} (2 - 3s^2) \cos y + s^2 \cos 2\theta_0 \\
 & + \frac{e_0^2}{16} (4 - 5s^2) \cos(y - \theta_0 - \omega_0) + \frac{e_0}{4} (2s^2 - 1) \cos(y + 2\theta_0) \\
 & + \frac{e_0}{24} (6 - 11s^2) \cos(y + 2\theta) + \frac{e_0^2}{24} (2 - 3s^2) \cos(2y + 2\theta) \\
 & + \frac{1}{12} [2e_0^2 - (2 + 5e_0^2)s^2] \cos 2\theta + \frac{e_0^2}{12} (9s^2 - 8) \cos 2y \\
 & - \frac{3e_0 s^2}{8} \cos(y - 4\theta_0 + 2\omega_0) - \frac{e_0}{4} (s^2 + 1) \cos(y + 2\omega_0) \\
 & \left. + \frac{1}{24} [2e_0^2 - (14 + 5e_0^2)s^2] \cos(y - 3\theta_0 + \omega_0) \right\} \quad (31)
 \end{aligned}$$

$$+ J^2 \theta \left[\frac{e_0}{24} [15(2 + e_0^2)s^4 - 14(4 + e_0^2)s^2 + 24] \sin(\theta + \omega_0) \right. \\ \left. + \frac{e_0^2 s^2}{12} (15s^2 - 14) \sin 2\omega_0 \right] + O(J^2, J^3 \theta, \dots) \}$$

$$y = \theta - \omega_0 + J \left\{ \left(\frac{5s^2}{2} - 2 \right) (\theta - \theta_0) \right\} \\ + J^2 \theta \left\{ \frac{e_0^2}{48} (130s^2 - 105s^4 - 28) \cos 2\omega_0 + \frac{s^2}{2} (15s^2 - 13) \cos 2\theta_0 \right. \quad (32) \\ + \frac{e_0 s^2}{2} (15s^2 - 13) \cos(\theta_0 + \omega_0) + \frac{e_0 s^2}{6} (15s^2 - 13) \cos(3\theta_0 - \omega_0) \\ \left. + \frac{1}{96} [5(9e_0^2 + 34)s^4 + 4(9e_0^2 - 34)s^2 - 56e_0^2] \right\} + O(J^2, J^3 \theta, \dots)$$

$$i = i_0 + scJ \left\{ \frac{1}{2} \cos 2\theta + \frac{e_0}{6} \cos(y + 2\theta) + \frac{e_0}{2} \cos(y - 2\theta) \right. \\ - \frac{1}{2} \cos 2\theta_0 - \frac{e_0}{6} \cos(3\theta_0 - \omega_0) - \frac{e_0}{2} \cos(\theta_0 + \omega_0) \Big\} \quad (33) \\ + J^2 \theta \frac{sc e_0^2}{24} (14 - 15s^2) \sin 2\omega_0 + O(J^2, J^3 \theta, \dots)$$

$$\Omega = \Omega_0 + cJ \left\{ \theta_0 - \theta + \frac{1}{2} \sin 2\theta - e_0 \sin y + \frac{e_0}{6} \sin(y + 2\theta) - \frac{e_0}{2} \sin(y - 2\theta) \right. \\ - \frac{1}{2} \sin 2\theta_0 + e_0 \sin(\theta_0 - \omega_0) - \frac{e_0}{6} \sin(3\theta_0 - \omega_0) - \frac{e_0}{2} \sin(\theta_0 + \omega_0) \Big\} \quad (34) \\ + cJ^2 \theta \left\{ \frac{e_0^2}{12} (6s^2 - 7) \cos 2\omega_0 - e_0 s^2 \cos(\theta_0 + \omega_0) + \frac{e_0^2}{24} (7s^2 - 4) \right. \\ \left. - \frac{e_0 s^2}{3} \cos(3\theta_0 - \omega_0) - s^2 \cos 2\theta_0 + \frac{1}{12} (6 - s^2) \right\} + O(J^2, J^3 \theta, \dots)$$

$$t = t_0 + \frac{1}{h_0} \int_{\theta_0}^{\theta} r^2 \left\{ 1 + J \left[\frac{(2 - 3s^2)}{2} \cos 2\theta + e_0(s^2 - 1) \cos y + s^2 - 1 \right. \right. \\ \left. \left. + \frac{e_0(1 - 2s^2)}{2} \cos(y - 2\theta) + \frac{s^2}{2} \cos 2\theta_0 + \frac{e_0(3 - 4s^2)}{6} \cos(y + 2\theta) \right] \right\} \quad (35)$$

$$\begin{aligned}
& + \frac{e_0 s^2}{2} \cos(\theta_0 + \omega_0) + \frac{e_0 s^2}{6} \cos(3\theta_0 - \omega_0) \Big] \\
& + J^2 \theta \frac{e_0^2 s^2}{24} (15s^2 - 14) \sin 2\omega_0 + O(J^2, J^3 \theta, \dots) \Big\} \dot{\alpha} \theta
\end{aligned}$$

Clearly, equations (31) - (35) demonstrate that the solution is indeed finite for both critical inclinations. Equations (31) - (35) are only valid for the critical inclinations and were first developed by Sagovac [Ref. 2] . The primary purpose in developing these equations was over a concern in computer programming. Some computers have major problems when a denominator approaches zero, and unlike humans, will not replace a solution with its limit. Therefore, depending upon the accuracy of a computer, equations (22) - (26) can replace equations (31) - (35) for inclinations near the critical inclinations. It should be noted, however, that the solution itself is valid and bounded for all inclinations. It is the limitation of the computer that creates the singularity.

The simplified solution which is shown in equations (27) - (30) , is valid for all inclinations. Since all terms of order $J^2 \theta$ have been neglected, the troublesome denominators mentioned earlier do not appear.

F. SPECIFIC MECHANICAL ENERGY

For all satellites under the influence of conservative forces, the specific mechanical energy remains constant. Therefore, an ideal analytical check of the solution would be to see if indeed the specific mechanical energy at any time is a constant. This simple check was performed by Danielson, Sagovac, and Snider [Ref 1, 2, 7, 8] by substituting equations (22) - (26) into equations (7) and (8). The substitution yields:

$$T + V = -\frac{GM(1 - e_0^2)}{2p_0} - \frac{GMJ_2 R^2 (1 - 3 \sin^2 \beta_0)}{2[r(t_0)]^3} + O(J^2, J^3, \dots) \quad (36)$$

The first two terms on the right side of equation (36) represent the initial specific mechanical energy. All other terms multiplied by J in equations (22) - (26) combine to zero when substituted into equations (7) and (8). Equation (36) demonstrates that by neglecting all terms of order J^2 and higher, the specific mechanical energy at any time

is precisely equal to the initial specific mechanical energy. Obviously, the solution satisfies the requirement of constant specific mechanical energy.

III. METHOD OF ANALYSIS

A. ORBITAL PARAMETERS

1. Argument of Latitude (θ)

Figure 2 illustrates that the position of a satellite at a particular time can be described by the argument of latitude (θ), the radius magnitude (r), the inclination (i), and the longitude of the ascending node (Ω). As shown in both the solution and the simplified solution, r , i , and Ω are only functions of J and the argument of latitude (θ). Since J is a constant for all planets, a simple determination of these terms is trivial once θ is known. However, the determination of θ is not trivial. Although it would be ideal for all of the equations to be analytical expressions, equations (26), (30), and (35) contain an integral that must be evaluated in order for θ to be determined. Herein lies the key to the solution. Given an elapsed time between observations, how can θ be precisely determined? Since the initial angular momentum (h_0) is known, this term can be moved to the left side of equations (26), (30), and (35) to yield equations in the form of:

$$(t - t_0)h_0 = \int_{\theta_0}^{\theta} r^2(J, \theta) \{1 + f(J, \theta)\} d\theta \quad (37)$$

If r was not a function of θ , an evaluation of the right side of equation (37) could easily be conducted that would yield an analytic expression. However, r is also a function of θ and the only practical technique in evaluating the integral is through numerical means.

Several numerical methods could be used to evaluate the integral depending on the speed and accuracy one desires. Since accuracy and not speed is desired in this analysis, a Romberg integration routine was used to evaluate the integral. Since the right side of equations (26), (30), and (35) are sinusoidal in nature, the Romberg scheme converged quickly and accurately.

Since θ defines the upper limit of the integral, in order to arrive at a solution, an initial θ must be estimated. Once θ is estimated, the integral can be numerically integrated and the result can be compared to the left side of equation (37). If the comparison is accurate within some predetermined error, the iteration is complete and θ has been determined. If the comparison produces an error that is unacceptable, θ can be incremented either up or down and the integral can be reevaluated. Eventually, the iteration will converge and θ will be determined. An algorithm of the iteration procedure is as follows:

1. Estimate θ .
2. Evaluate the integral.
3. Compare the result with the left side of equation (37).
4. If outside the limit, go to (5). If within the limit, stop.
5. Increment θ up or down as needed, go to (2).

The determination of θ involves a combination of two errors. The first error is contained in the numerical evaluation of the integral itself, while the second error involves the comparison of the result of the integration with the left side of equation (37). Unfortunately, the errors do not linearly combine, but rather multiply since the numerical evaluation of the integral is inherently nonlinear. In order to make the comparison error meaningful, the evaluation of the integral must be made as precise as possible. In order to avoid determining whether an error is due to computing or truncation errors, the numerical technique used in this analysis did not rely on a step size constraint. Therefore, the relative error, in general, can be specifically controlled. Since in this analysis, accuracy and not speed is desired, the Romberg integration technique was utilized. The Romberg technique does not depend on any specific step size and the evaluation of the integral is determined through a converging algorithm. Also, the relative error of the integration can be specifically controlled. In general, the relative error normally demanded in the integral evaluation was on the order of 10^{-12} , and the relative error of the comparison was on the order of 10^{-10} . Since the computer program utilized in the analysis was written for double precision accuracy, these types of relative errors presented no significant problems. The double precision accuracy enabled the computer program to calculate up to sixteen digit precision.

2. Radius Magnitude (r)

From equations (22), (27), and (31), it can be seen that the radius magnitude (r) is a function of J and θ . Once θ is known, r can be evaluated. From the appearance of equations (22), (27), and (31), it is not obvious how r will behave as the orbit of a satellite progresses. However, from observations of actual satellite motion, it is clear that the orbit should behave elliptically with r varying from a minimum value at periapsis to a maximum value at apoapsis. The magnitude of J plays an important role and fortunately for most planets, oblateness effects act as a perturbation in comparison to the main gravitational force. Therefore, a large value of J causes larger variations in r . Since equations (22), (27), and (31) contain a number of sine and cosine terms, a sinusoidal behavior should be expected.

3. Inclination (i)

The solution of the inclination is shown in equations (24) and (33), and the inclination for the simplified solution is shown in equation (28). In general, these three solutions are quite similar. Again, once θ is known, i can be evaluated easily. It can be seen from equations (24), (28), and (33), that i will vary slightly from an initial inclination as the orbit of a satellite progresses. Also, since a number of sine and cosine terms are present, the variation should be sinusoidal in nature. From inspection it is clear that the magnitude of the variation is dependent upon the magnitude of J and the initial inclination. The variation of the inclination should not behave in a diverging fashion, but rather in an oscillatory fashion about some arbitrary mean inclination. This behavior is consistent with observations of actual measured satellite data. The driving factor in all inclination variations is the magnitude of J . Since for Earth, J_2 is on the order of 10^{-3} , these variations should be quite small.

4. Longitude of the Ascending Node (Ω)

The solution of the longitude of the ascending node (Ω) is shown in equations (25) and (34), and the longitude of the ascending node for the simplified solution is shown in equation (29). As expected, all solutions are quite similar. As with the case of r and i , Ω can easily be determined once θ is known. Unlike the behavior of r and i , the variation of Ω is very predictable and highly meaningful. With the presence of θ alone in equations (25), (29), and (34), Ω possesses a linear relationship with θ and

as θ increases with time, the variation of Ω from Ω_0 should be linear. Depending upon the initial inclination, this variation will be either positive or negative. This type of behavior is clearly consistent with the classical behavior known as nodal regression. For an oblate planet, nodal regression is a linear property whose magnitude and direction depends upon the radius magnitude and inclination of the satellite. In equations (25), (29), and (34), the radius magnitude is contained in the J term. Therefore, the magnitude of the nodal regression is entirely dependent upon the magnitude of J . From the analysis of the behavior of Ω as θ increases, the nodal regression behavior should be extremely obvious.

B. ROMBERG INTEGRATION TECHNIQUE

The Romberg integration technique is a powerful integration method in which arbitrary accuracy can be achieved in a relatively efficient manner. The method combines any type of relatively inaccurate quadrature method with a Richardson extrapolation in order to quickly and accurately converge on a solution. In this analysis, a simple trapezoidal quadrature was initially used to estimate the integral and then a Richardson extrapolation was used to improve the integration to the desired accuracy level. The trapezoidal quadrature first estimates the integral with a single interval. The estimate is then improved by using 2 intervals, 4 intervals, 8 intervals, etc. For purposes of identification, the results can be labeled I_0^1 , I_0^2 , I_0^4 , and so on. These results can be arranged in column form in preparation for a Richardson extrapolation and each new member represents the technique of halving the prior interval. The length of the column is determined by the accuracy that one desires. Once the first column is arranged, a Richardson extrapolation can be performed by the following equation.

$$I_l^n = \frac{4^l I_{l-1}^n - I_{l-1}^{n/2}}{4^l - 1} \quad (38)$$

The values of I_l^n can be arranged in tabular form as shown in Table 1.

Table 1. A SCHEMATIC OF ROMBERG INTEGRATION

I_0^1	-	-	-	-
I_0^2	I_1^2	-	-	-
I_0^4	I_1^4	I_2^4	-	-
I_0^8	I_1^8	I_2^8	I_3^8	-
I_0^{16}	I_1^{16}	I_2^{16}	I_3^{16}	I_4^{16}

To test for convergence, the value represented by $I_n^{2^n}$ is compared with the value represented by $I_{n-1}^{2^n}$. If these two values are within some predetermined error, then $I_n^{2^n}$ becomes the evaluation of the integral. If convergence has not been reached, then another row is calculated and the process continues. An excellent example of the Romberg integration technique is shown in Ferziger [Ref. 9]. In this example the following solution of the integral is desired.

$$I = \int_0^1 e^x dx \quad (39)$$

From elementary calculus, the exact solution is:

$$I_{exact} = 2.718281828 \quad (40)$$

The technique of Romberg integration of the integral is shown in Table 2. The relative error of I_3^8 to I_2^8 is 7.81×10^{-9} . The relative error of I_3^8 to I_{exact} is 1.97×10^{-10} . As can easily be seen, the integration is converging very nicely and the error found in the final solution is less than the error demanded within the Romberg integration scheme itself.

Table 2. ROMBERG INTEGRATION

n	I_0^n	I_1^n	I_2^n	I_3^n
1	1.859140914	-	-	-
2	1.753931092	1.718861152	-	-
4	1.727221905	1.718318842	1.718282688	-
8	1.720518592	1.718284155	1.718281842	1.718281829

The advantage of the Romberg integration technique over a simple quadrature method is obvious. The number of intervals that must be evaluated is very small and the relative accuracy is very high. In order to attain the accuracy that the Romberg technique delivers, the trapezoidal method would need to divide the integral into several more intervals. This would be highly inefficient. For smooth functions, the Romberg technique is very effective and efficient. Since equation (37) is sinusoidal in nature and thus relatively smooth, the Romberg integration technique was used to evaluate the integral. If equation (37) had not been so well behaved, another integration technique might have been warranted. The Romberg integration scheme is the heart of the analysis and can be found in the computer program shown in Appendix E.

IV. METHOD OF COMPARISON

A. NUMERICAL INTEGRATION COMPARISON

In order to verify that the theory is valid for practical application, the solution must be compared with proven numerical solutions and measured satellite data. By comparing the solution with a numerical integration of the equations of motion, theoretical accuracy can be specifically determined. As shown in equations (22) - (26), theoretically the solution is accurate to order $J^2\theta$. A numerical integration comparison will determine whether this prediction is correct. In order to verify the solution, the following parameters will be compared.

1. Delta-radius vector ($|\Delta r|$)
2. Earth arc angle (Ψ)
3. Delta omega ($\Delta\Omega$)
4. Delta inclination (Δi)
5. Delta theta ($\Delta\theta$)
6. Delta radius relative error ($|\Delta r|/r_n$)
7. Delta theta relative error ($\Delta\theta/\theta_n$)
8. Radial track error (RTE)
9. Along track error (ATE)
10. Cross track error (CTE)

1. Delta Radius Vector

A graphical representation of the delta radius vector ($|\Delta r|$) and the Earth arc length (Ψ) is shown in Figure 3. The delta radius vector is the magnitude of the vector separating the solution radius vector (r) from the numerical integration radius vector (r_n). Mathematically, the delta radius vector can be expressed as:

$$\Delta r = r - r_n \quad (41)$$

The delta radius vector describes in overall terms the global error in the solution. Another common name for this error is the Euclidean normed difference in ephemerides. Although the delta radius vector provides ample information on the global error in the solution, this error can also be expressed by a different parameter that will be called Earth arc angle.

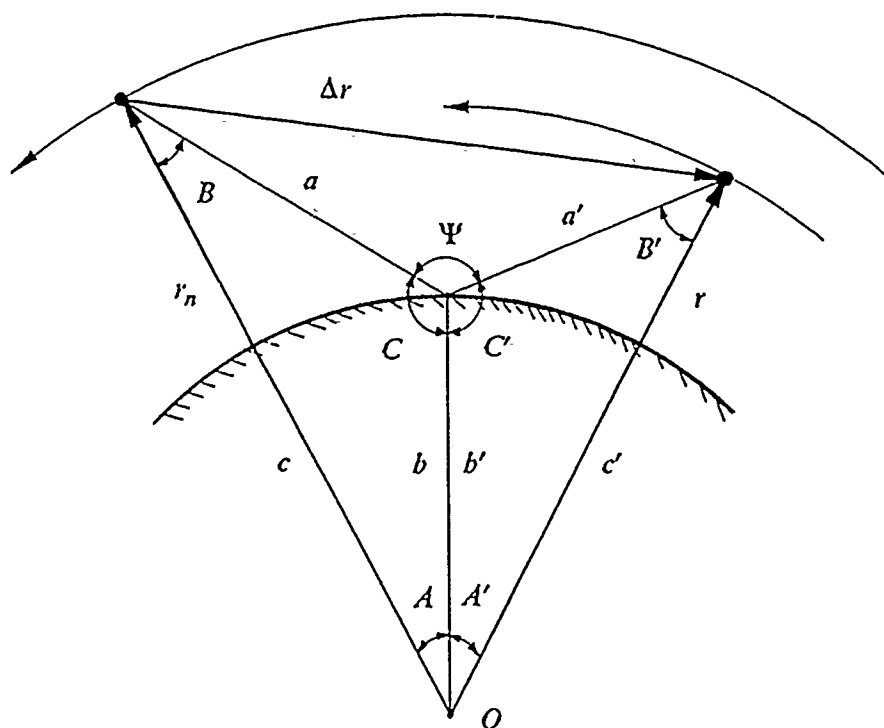


Figure 3. Delta radius vector and Earth arc angle.

2. Earth Arc Angle

Earth arc angle (Ψ) is simply the angle between the two positions if viewed from sea level on Earth. For simplicity, the position at sea level was chosen such that the arc angle from the center of the Earth was bisected. By using the law of sines and cosines, the Earth arc angle is easily determined. Since satellites are tracked by instruments on the surface of the Earth, a better feel for the global error can be attained by determining the angle between the two positions. Most satellite tracking radars possess beamwidth

and field of view limitations; therefore, Ψ will provide useful information on whether the solution is accurate enough for satellite tracking radars.

3. Delta Omega, Delta Inclination, Delta Theta

A break down of the global error can be described in the errors of delta omega ($\Delta\Omega$), delta inclination (Δi), and delta theta ($\Delta\theta$). As mentioned previously, $\Delta\Omega$ will provide an insight on the motion of the line of nodes, and specifically if nodal regression is present. The change in inclination will provide information on the movement and stability of the orbital plane. The parameter in which all errors are based, $\Delta\theta$, will provide much information on the source of the global error. It is clear that small errors in $\Delta\theta$ will contribute significantly to the accuracy of the solution.

4. Relative Errors

The verification of the solution will lie in the confirmation of the relative errors. The delta radius relative error and the delta theta relative error will demonstrate the actual accuracy of the solution. Both parameters, Δr and $\Delta\theta$, demonstrate a theoretical error of $J^2\theta$. Therefore, the delta radius relative error should be on the order of $J^2\theta$, while the delta theta relative error should be on the order of J^2 . Comparisons of the relative errors between the solution and the numerical integration solution will provide the evidence for theoretical confirmation.

5. Track Errors

Another method to break down the global error is in terms of track errors. Figure 4 shows a graphical representation of radial track error (RTE), along track error (ATE), and cross track error (CTE). These errors can better be described by referring also to Figures 1 and 2. The radial track error is the error in the radial direction or in the B_1 direction. The along track error is the arc length error in the plane defined by the solution radius vector (r) and the B_2 direction. Together, these errors describe errors in three orthogonal directions or planes as compared with some reference position. The reference position in this case is the numerical integration solution. A mathematical derivation of these errors is as follows:

$$\Delta r = r(r_n + \Delta r, \theta + \Delta\theta, i + \Delta i, \Omega + \Delta\Omega) - r(r_n, \theta, i, \Omega) \quad (42)$$

Using equation (1),

$$\Delta r = (r_n + \Delta r)(B_1 + \Delta B_1) - r_n B_1 \quad (43)$$

$$\Delta r = r_n B_1 + \Delta r B_1 + r_n \Delta B_1 + \Delta r \Delta B_1 - r_n B_1 \quad (44)$$

Neglecting higher order terms,

$$\Delta r = \Delta r B_1 + r_n \Delta B_1 \quad (45)$$

Continuing, defining ΔB_1 ,

$$\Delta B_1 = (B_1 \cdot \Delta B_1)B_1 + (B_2 \cdot \Delta B_1)B_2 + (B_3 \cdot \Delta B_1)B_3 \quad (46)$$

Using the rotation transformation and after performing considerable algebra,

$$B_1 \cdot \Delta B_1 = 0 \quad (47)$$

$$B_2 \cdot \Delta B_1 = (\Delta \theta + \Delta \Omega \cos i) \quad (48)$$

$$B_3 \cdot \Delta B_1 = (\Delta i \sin \theta - \Delta \Omega \cos \theta \sin i) \quad (49)$$

Therefore, using equation (45),

$$\Delta r = (\Delta r)B_1 + r_n(\Delta \theta + \Delta \Omega \cos i)B_2 + r_n(\Delta i \sin \theta - \Delta \Omega \cos \theta \sin i)B_3 \quad (50)$$

From equation (50), the track errors can easily be defined.

$$RTE = r - r_n \quad (51)$$

$$ATE = r_n(\Delta \theta + \Delta \Omega \cos i) \quad (52)$$

$$CTE = r_n(\Delta i \sin \theta - \Delta \Omega \cos \theta \sin i) \quad (53)$$

A graphical representation of the track errors is shown in Figure 4.

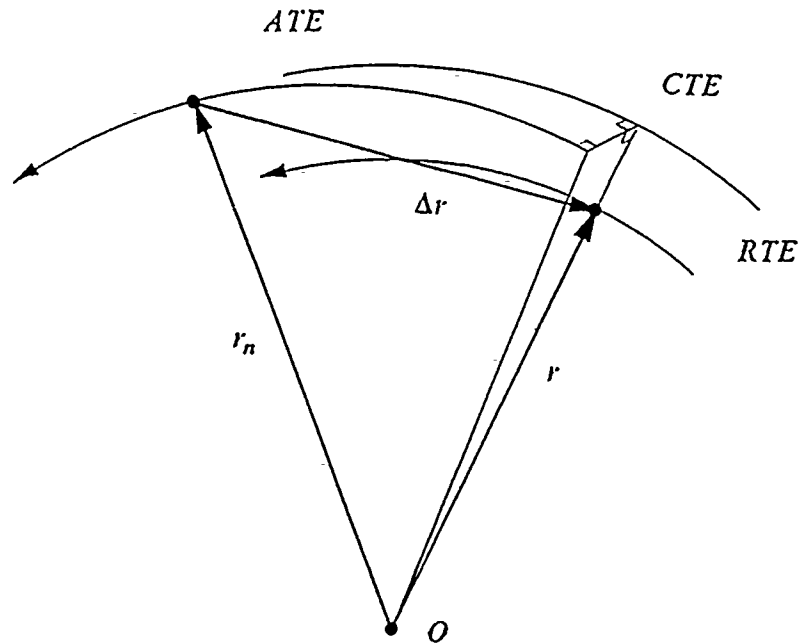


Figure 4. Track errors.

Examination of equations (51) - (53) demonstrates that the track errors divide the global error into three distinct regions. Radial track errors obviously describe errors in the radial direction. Along track errors are similar in nature to Earth arc angle errors, but also include errors due to nodal regression. Cross track errors describe orbital plane errors in terms of both inclination errors and errors due to nodal regression.

In general, all these parameters should give an excellent insight into the accuracy of the solution. Also included in the numerical comparison will be the simplified solution and the two-body solution. The simplified solution has been previously presented. The two-body solution can easily be determined by simply setting $J = 0$. The analysis of the numerical comparison will demonstrate the strengths and weaknesses of all the different solutions.

B. MEASURED DATA COMPARISON

In order to observe how well the solution models actual satellite motion, the solution will be compared with actual measured data from operational satellites. To properly evaluate the solution, a wide range of orbit characteristics will be compared. These characteristics include orbits of various altitudes, inclinations, and eccentricities. Also included in this comparison will be the simplified solution, the two-body solution, and if available, some particular numerical solutions.

The numerical solutions will consist of two forms. The first is a numerical solution that only includes perturbations involving J_2 , J_3 , J_4 , and J_5 . The second numerical solution will include the following perturbation effects.

1. J_2 , J_3 , J_4 , and J_5 .
2. Atmospheric drag.
3. Sun gravitational effects.
4. Moon gravitational effects.
5. Solar pressure effects.

From the analysis, the accuracy of the solution and the simplified solution can be compared to a numerical solution as well as to actual measured data. The weakness of the two-body solution will also be demonstrated. In addition, the strengths of a well modeled numerical solution will clearly be seen. The identical error parameters described in the previous section will also be used in the measured data comparison. From this comparison, the advantages and disadvantages of the solution in regard to actual satellite motion will clearly be demonstrated.

V. RESULTS

A. NUMERICAL INTEGRATION COMPARISON

To verify that the theory is valid for practical applications, the solution was compared with a proven numerical solution. A numerical integration computer program called UTOPIA is currently in use at the Colorado Center for Astrodynamics Research (CCAR) located on the campus of the University of Colorado, Boulder, Colorado. UTOPIA is primarily used to model a wide range of perturbations and can predict satellite motion with a high degree of accuracy. The UTOPIA computer program was developed at the University of Texas, Austin, Texas, and is currently in use at several universities and research centers. The solution was compared with the UTOPIA solution for a satellite with the following initial conditions:

$$\begin{aligned}r_0 &= 7,386.18 \text{ km} \\i_0 &= 90.03 \text{ degrees} \\e_0 &= 0.003991 \\\omega_0 &= 224.38 \text{ degrees} \\\theta_0 &= 104.05 \text{ degrees} \\\Omega_0 &= 322.63 \text{ degrees} \\h_0 &= 54,205.18 \text{ km}^2/\text{s} \\p_0 &= 7,371.29 \text{ km} \\t_0 &= 0.00 \text{ seconds}\end{aligned}$$

In general, these initial conditions represent a slightly retrograde orbit of small eccentricity at an altitude of approximately 1000 kilometers. Essentially, it is a polar orbit at an altitude where several satellites are currently in motion. From the initial conditions, the orbit should demonstrate a slight easterly nodal regression. But, since the inclination is so close to 90 degrees, some integration routines might predict zero nodal regression. In this comparison, UTOPIA only modeled the J_2 perturbation; therefore, the solution should compare well if the theory is valid. All error parameters depicted in the comparison were calculated in the following manner.

$$\Delta(\text{Error Parameter}) = \text{Theoretical Solution} - \text{UTOPIA Numerical Solution} \quad (54)$$

All solutions were compared at one hour intervals over two separate periods of time. One comparison is for a time period of one day while the second is for a time period of three days. The three day comparison was constructed to illustrate the effect of long term errors while the one day comparison allows for a more detailed analysis during the first few hours of motion. The period of rotation for the satellite is about 105.26 minutes which equates to approximately 13.68 orbits per day. The results of the numerical solution comparison are shown in Appendix A.

1. Delta Radius Vector Comparison

The comparison of the delta radius vector is shown in Figures 5, 6, and 7 in Appendix A. Figure 5 includes the comparison of the solution, the simplified solution, and the two-body solution to the numerical solution. If the solution matched the numerical solution exactly, the delta radius vector would be zero. As shown in Figure 5, the solution and the simplified solution match extremely well with the numerical solution while the two-body solution contains gross errors.

A more detailed plot of the delta radius vector comparison is shown in Figures 6 and 7. In these figures, the two-body solution is excluded. The difference in the solution and the simplified solution can clearly be seen. The simplified solution produces a diverging sinusoidal response about the solution. However, up to approximately four hours of motion, the solution and the simplified solution are nearly identical. The sinusoidal behavior of the simplified solution can be attributed to the fact that all terms multiplied by $J^2\theta$ have been neglected. As θ grows with time, these terms become significant in the solution. As shown specifically in Figure 7, the average delta radius vector of the simplified solution clearly diverges from the solution.

Figures 5, 6, and 7 also demonstrate that for at least one day, the delta radius vector for the solution and the two-body solution are nearly linear as a function of time. Other comparisons will determine whether this relationship holds true and will be shown later. As mentioned earlier, the delta radius vector is a global error. As shown in Figures 5, 6, and 7, the solution compares well globally with the numerical solution and demonstrates a great improvement over the two-body solution.

2. Earth Arc Angle Comparison

The comparison of the Earth arc angle is shown in Figures 8, 9, and 10 in Appendix A. From inspection, these plots are nearly identical in appearance to the delta radius vector plots. This is expected since both the delta radius vector and the Earth arc angle represent global errors. Figure 8 clearly illustrates the large error generated by the two-body solution. The two-body solution produces unsatisfactory long term satellite position prediction. After one day, a tracking radar would have a difficult time detecting a satellite with a position error of over 80 degrees.

Figures 9 and 10 present much more encouraging results. Again, the simplified solution responds in a sinusoidal behavior about the solution. After one day, the position error of the solution is only approximately 0.15 degrees. Clearly, the solution and the simplified solution are superior to the two-body solution. Most tracking radars can easily handle daily position errors of 0.15 degrees. In general, the solution and the simplified solution agree very well with the numerical solution.

3. Delta Omega Comparison

The comparison of the delta omega angle is shown in Figures 11 and 12 in Appendix A. At first glance, the solution and the simplified solution in Figure 11 appear not to agree well with the numerical solution. However, the scale of delta omega is multiplied by 10^{-4} . The numerical solution parallels the two-body solution nearly exactly and predicts almost no change in Ω . In other words, the numerical solution predicts no nodal regression. Easterly nodal regression is represented by a positive delta omega; therefore, it is clear that the solution and the simplified solution predict greater nodal regression than the numerical solution.

On a larger scale, all three solutions are essentially identical. Since the initial inclination is so close to 90 degrees, small discrepancies are not surprising. The delta omega plot does, however, invoke confidence in the solution. Although the initial inclination is very close to 90 degrees, the solution, the simplified solution, and the numerical solution predict easterly nodal regression. This result is significant. Even initial inclinations close to 90 degrees produce nodal regression in the correct direction for the solution, the simplified solution, and the numerical solution.

4. Delta Inclination Comparison

The comparison of the delta inclination angle is shown in Figures 13 and 14 in Appendix A. On a larger scale, all of the solutions compare very well. On the scale shown in Figure 10, the two-body solution and the numerical solution are nearly identical. The solution and the simplified solution oscillate about an error of approximately -2.0×10^{-5} degrees. Obviously, this error is extremely small. In general, the solution and the numerical solution agree very well.

An interesting aspect of the delta inclination comparison is the sinusoidal behavior of the solution and the simplified solution. This type of behavior is precisely what was predicted in the earlier analysis. Figure 14 demonstrates that this behavior continues for even longer periods of time. On a larger scale, this type of motion would not be detectable.

5. Delta Theta Comparison

The comparison of the delta theta angle is shown in Figures 15, 16, and 17 in Appendix A. This comparison confirms the results found in the earlier comparisons. The two-body solution produces very large errors, while the solution and the simplified solution agree very well with the numerical solution. Figures 16 and 17 again illustrate the typical sinusoidal response of the simplified solution about the solution. Since the delta theta error produces all other errors, the excellent results found in the earlier comparisons are now not surprising.

6. Delta Theta Relative Error Comparison

The comparison of the delta theta relative error is shown in Figures 18, 19, and 20 in Appendix A. As shown in Figure 18, the two-body solution demonstrates a relative error of $2.3J$, while the relative errors of the solution and the simplified solution are much smaller. In more detail, Figures 19 and 20 indicate that the relative error of the solution is $2.8J^2$. This result confirms the theoretical prediction that the delta theta relative error of the solution would be on the order of J^2 . Figures 19 and 20 illustrate that initially the relative error of the simplified solution is also on the order of J^2 . But as θ increases with time, the relative error grows in a sinusoidal fashion. This result is expected since the simplified solution neglects all the terms multiplied by J^3 . In gen-

eral, the results shown in Figures 18, 19, and 20 confirm the theoretical relative accuracy of delta theta that was predicted in the earlier analysis.

7. Delta Radius Relative Error Comparison

The comparison of the delta radius relative error is shown in Figures 21, 22, and 23 in Appendix A. As shown in Figure 21, the two-body solution produces a relative error that is linear in time and proportional to $2.3J^2\theta$. Again, the relative errors of the solution and the simplified solution are magnitudes smaller.

Figures 22 and 23 present in more detail the relative errors of the solution and the simplified solution. The relative error of the solution is very linear and proportional to $2.8J^2\theta$. The relative error of the simplified solution is sinusoidal in nature and diverges from the solution. However, for up to four hours of motion, the relative error of the solution and the simplified solution are nearly indistinguishable. Again, the results from this comparison confirm the theoretical prediction that the delta radius relative error of the solution would be on the order of $J^2\theta$.

8. Radial Track Error Comparison

The comparison of the radial track error is shown in Figures 24, 25, and 26 in Appendix A. As shown in Figure 24, the two-body solution oscillates about an error of approximately -11.0 kilometers, while the solution and the simplified solution both produce errors that are dramatically smaller. From inspection, the two-body solution also appears to be slowly converging as time increases.

In Figures 25 and 26, the solution and the simplified solution produce contrasting behaviors. While the solution remains relatively constant, the simplified solution slowly diverges from zero. These two different responses continue even after three days of motion. Again, the neglected $J^2\theta$ terms cause the significant divergence of the simplified solution. Not surprisingly, the solution and the simplified solution are clearly superior to the two-body solution.

9. Along Track Error Comparison

The comparison of the along track error is shown in Figures 27, 28, and 29 in Appendix A. The results presented in this comparison parallel the results found in the earlier comparisons. Since the inclination is so close to 90 degrees, the $\Delta\Omega$ contribution

is negligible and the $\Delta\theta$ contribution strongly influences the responses. As a result, the along track error comparison is practically a mirror image of the delta theta comparison.

10. Cross Track Error Comparison

The comparison of the cross track error is shown in Figures 30 and 31 in Appendix A. The cross track error is strongly influenced by Δi and $\Delta\Omega$. Since the two-body solution produced good results with these two parameters, it is not surprising that the two-body solution agrees well with the numerical solution. Fortunately, the errors produced by the solution and the simplified solution are also very small. The solution produces a maximum cross track error of approximately ± 0.5 kilometers after one day of motion, and approximately ± 1.3 kilometers after three days of motion.

Clearly in this comparison, the two-body solution is superior. However, the large errors produced by the two-body solution in the other comparisons easily overwhelm these results. In global terms, the two-body solution is no match for either the solution or the simplified solution.

B. MEASURED DATA COMPARISON

The solution was compared with actual measured satellite data to determine the altitude band where the theory works best. The measured satellite data was obtained from the First Satellite Control Squadron (ISCS) located at Falcon Air Force Base, Colorado. The First Satellite Control Squadron tracks several satellites for the Air Force and was able to supply measured data for three separate satellites. The three satellites are currently in motion and occupy orbits that are labeled Near Earth, Semisynchronous, and Geosynchronous, respectively. All error parameters compared in the earlier numerical comparison were also compared in this comparison using the measured data as a reference.

Included in all the comparisons were the solution, the simplified solution, the two-body solution, and two numerical solutions. The two numerical solutions were also supplied by the First Satellite Control Squadron and are labeled Spacom 1 and Spacom 2, respectively. The Spacom 1 solution includes all perturbation effects, while the Spacom 2 solution only includes the Earth's harmonic perturbations. All error parameters in this comparison were calculated in the following manner.

$$\Delta(\text{ErrorParameter}) = \text{Test Solution} - \text{Measured Data Solution} \quad (55)$$

Unfortunately, the First Satellite Control Squadron only records measured data when an update of their numerical solution is required. Routine updates are usually conducted after about seven days of motion. Therefore, satellite data for one month usually consists of only four data points. Although more data points are needed for a more detailed analysis, a long term analysis can still be conducted. The analysis of each type of orbit will be presented separately.

1. Near Earth Orbit Comparison

The near Earth orbit comparison possesses the following initial conditions.

$$\begin{aligned} r_0 &= 7,776.58 \text{ km} \\ i_0 &= 98.81 \text{ degrees} \\ e_0 &= 0.0003071 \\ \omega_0 &= 9.57 \text{ degrees} \\ \theta_0 &= 149.14 \text{ degrees} \\ \Omega_0 &= 37.10 \text{ degrees} \\ h_0 &= 53,664.37 \text{ km}^2/\text{s} \\ p_0 &= 7,224.89 \text{ km} \\ t_0 &= 0000Z \text{ 26 July 1990} \end{aligned}$$

The initial conditions of this satellite represent a retrograde orbit of small eccentricity at an altitude of approximately 850 kilometers. The period of rotation for the satellite is about 101.89 minutes which equates to approximately 14.13 orbits per day. From the initial conditions, J_2 should be the dominant perturbation. The orbit should demonstrate noticeable easterly nodal regression. If the theory is valid, both the solution and the simplified solution should agree well with the numerical solutions and the measured data.

The results of the near Earth orbit comparison are shown in Figures 32 - 43 in Appendix B. As shown in the figures, the solution and the simplified solution agree very well with both the Spacom 1 solution and the measured data. The fact that the solution and the simplified solution produce such excellent results verifies that J_2 is the dominant

perturbation for this satellite. Figures 32 - 43 also demonstrate the larger errors produced by the two-body solution. In almost every comparison, both the solution and the simplified solution are far superior to the two-body solution.

One surprising result is the poor comparison produced by the Spacom 2 solution. In every comparison the Spacom 2 solution either models the two-body solution exactly or produces results that are inferior to the two-body solution. It is clear that the Spacom 2 solution does not model the Earth's harmonic forces correctly. An explanation for the poor results cannot be determined in this analysis. A detailed analysis of the force modeling in the Spacom 2 solution must be completed in order to adequately explain the unsatisfactory results.

The delta omega comparison in Figure 34 demonstrates the easterly nodal regression produced by the solution, the simplified solution, the Spacom 1 solution, and the measured data. The two-body solution represents zero nodal regression. Figure 35 presents the delta omega comparison at a much smaller scale and excludes the two-body solution. In this figure, much more detail can be observed.

There is only one comparison in which the results are mixed. The radial track error comparison in Figure 40 indicates that the solution produces a small improvement over the two-body solution while the simplified solution actually produces a greater error. In comparison with the along track errors, these errors are small. It is interesting, however, that the radial track error comparison produces such mixed results. In general, both the solution and the simplified solution produce results that are in excellent agreement with the measured data for this near Earth satellite.

2. Semisynchronous Orbit Comparison

The semisynchronous orbit comparison possesses the following initial conditions.

$$\begin{aligned}r_0 &= 26,407.70 \text{ km} \\i_0 &= 63.66 \text{ degrees} \\e_0 &= 0.005860 \\\omega_0 &= 318.19 \text{ degrees} \\\theta_0 &= 328.49 \text{ degrees} \\\Omega_0 &= 92.13 \text{ degrees} \\h_0 &= 102,892.59 \text{ km}^2/\text{s} \\p_0 &= 26,559.96 \text{ km} \\t_0 &= 0000Z \text{ 22 March 1990}\end{aligned}$$

The initial conditions of this satellite represent a direct orbit of small eccentricity at an altitude of approximately 20,000 kilometers. The period of rotation for the satellite is about 717.96 minutes which equates to approximately 2.01 orbits per day. An important aspect of the orbit is that the initial inclination is very close to the critical inclination of 63.43 degrees. Although the initial inclination is not exactly that of the critical inclination, an evaluation of the solution and the simplified solution near this important inclination can be made. From the initial conditions, the orbit should demonstrate substantial westerly nodal regression. Also, at this altitude, the dominance of the J_2 perturbation should be diminished. Other perturbations that are not modeled should make a considerable contribution to the errors in the comparison. If the theory is valid, both the solution and the simplified solution should show a great improvement over the two-body solution.

The results of the semisynchronous orbit comparison are shown in Figures 44 - 53 in Appendix C. As predicted earlier, the solution and simplified solution produce results that are superior to the results produced by the two-body solution. Figures 44 and 45 present the global errors of all the solutions. In global terms, the solution and the simplified solution reduce the error of the two-body solution by nearly one half. In effect, the J_2 perturbation accounts for approximately one half the error produced by the two-body solution. The remaining error which is represented by the solution and the simplified solution is caused by other perturbing forces. Unfortunately, the results of the Spacom 2 solution were not available.

The delta omega comparison in Figure 46 demonstrates the easterly nodal regression produced by the solution, the simplified solution, the Spacom 1 solution, and the measured data. Again, the two-body solution represents zero nodal regression. It is clear that at this altitude, the J_2 perturbation produces the majority of the nodal regression. The delta inclination comparison in Figure 47 indicates that the solution and the simplified solution produce results that are not much better than the results produced by the two-body solution. However, the error after 30 days of motion is extremely small. On a larger scale, the solutions would seem identical. Since the inclination is very near the critical inclination, these results produce more evidence in support of the theory. Clearly, the solution and the simplified solution are bounded at this inclination. The delta theta comparison in Figure 48 demonstrates that the majority of the error produced by the solution and the simplified solution originates in the delta theta error. It is clear that the two-body solution underestimates the value of θ while the solution and the simplified solution overestimate the value of θ .

The relative error comparisons are shown in Figures 49 and 50. While the delta theta relative error for the solution, the simplified solution, and the two-body solution is approximately 15.0×10^{-6} , the relative error produced by the Spacom 1 solution is far superior. This result is expected since the Spacom 1 solution models several more influential perturbations. The delta radius relative error comparison again demonstrates in global terms the amount of improvement that the solution and the simplified solution provide over that of the two-body solution.

The track error comparisons in Figures 51 - 53 produce mixed results. While the two-body solution produces less radial and along track errors, the solution and the simplified solution produce much less cross track error. In comparison with the along track and cross track errors, the radial track errors are small. The poor results produced by the solution and the simplified solution in the along track error comparison is due primarily to the large error in $\Delta\theta$. The very large error produced by the two-body solution in the cross track error comparison is due primarily to the very large error in $\Delta\Omega$.

In summary, although the solution and the simplified solution are superior to the two-body solution, the Spacom 1 solution models the satellite motion more precisely. However, the primary reason that the solution and the simplified solution are superior to the two-body solution is due exclusively to a better modeling of nodal regression or the angle Ω . It is clear that the solution and the simplified solution model the J_2 perturbation extremely well. The Spacom 1 solution is expected to perform better since it models more perturbing forces.

3. Geosynchronous Orbit Comparison

The geosynchronous orbit comparison possesses the following initial conditions.

$$\begin{aligned}r_0 &= 42,156.57 \text{ km} \\i_0 &= 1.09 \text{ degrees} \\e_0 &= 0.0002341 \\\omega_0 &= 320.06 \text{ degrees} \\\theta_0 &= 331.32 \text{ degrees} \\\Omega_0 &= 334.85 \text{ degrees} \\h_0 &= 129,644.14 \text{ km}^2/\text{s} \\p_0 &= 42,166.25 \text{ km} \\t_0 &= 0000Z \text{ 21 July 1990}\end{aligned}$$

The initial conditions of this satellite represent a direct orbit of small eccentricity at an altitude of approximately 35,800 kilometers. The period of rotation for the satellite is about 1436.69 minutes which equates to approximately 1.00 orbit per day. Since the initial inclination is slightly greater than zero, the orbit should demonstrate westerly nodal regression. However, since the altitude is so large, other perturbing forces that are not modeled may influence nodal regression. At a geosynchronous altitude, the magnitude of other perturbing forces approach that of J_2 . Since at this altitude the effect of J_2 is so diminished, some comparisons of the solution, the simplified solution, and the two-body solution may be nearly identical. As a result, the theory may not be any better than the two-body theory for satellites in a geosynchronous orbit.

The results of the geosynchronous orbit comparison are shown in Figures 54 - 63 in Appendix D. The global error comparisons are shown Figures 54 and 55. In global terms, the solution and the simplified solution produce results that are surprisingly superior to the results produced by the two-body solution. Evidently, for this satellite, the J_2 perturbation is still quite dominant. However, the other comparisons may present a different picture. Once again, the Spacom 2 solution generates very poor results.

The delta omega comparison in Figure 56 indicates that the actual perturbing forces produce easterly nodal regression. Conversely, the solution and the simplified solution predict westerly nodal regression. It is obvious that other perturbing forces

influence the nodal regression of this satellite. Although the Spacom 1 solution is superior, even this accurate numerical solution has trouble predicting the value of Ω . The solution and the simplified solution also produce poor results in the delta inclination comparison in Figure 57. All solutions, except for the Spacom 1 solution, produce identical results. Again, on a larger scale, all of the solutions would seem nearly identical. However, this detailed analysis does demonstrate a weakness in the theory. The delta theta comparison in Figure 48 indicates that the solution and the simplified solution are inferior to all solutions including the two-body solution. Clearly, other perturbing forces are at work.

The relative error comparisons are shown in Figures 59 and 60. The delta theta relative error comparison simply repeats the results found in the delta theta comparison. However, the delta radius relative error comparison is much more reassuring. Again, in global terms, the solution and the simplified solution produce better results than the two-body solution.

The track error comparisons in Figures 61 - 63 produce mixed results. The radial track error comparison indicates that initially the Spacom 1 solution is inferior to all other solutions. However, after 21 days of motion, Spacom 1 is the superior solution. Once again, the radial track errors are small when compared to the along and cross track errors. The clue to the favorable global results of the solution and the simplified solution is found in the along and cross track error comparisons. The solution and the simplified solution perform much better than the two-body solution in the along track error comparison. Although the two-body solution is superior to the solution and the simplified solution in the cross track error comparison, the difference is small. It is clear that the solution and the simplified solution are superior to the two-body solution due to a much smaller along track error.

In summary, although the solution and the simplified solution are superior to the two-body solution, other perturbing forces greatly influence the satellite's motion. At this altitude, the solution and the simplified solution simply do not model the satellite's motion well. Other perturbing forces must be modeled at this altitude if proper satellite position prediction is desired.

VI. CONCLUSIONS AND RECOMMENDATIONS

An analysis was conducted on a perturbation solution of the main problem in artificial satellite theory. The purpose of the analysis was to compare the solution with proven numerical solutions and actual measured satellite data in order to determine if the theoretical work is valid and practical. From the analysis, the following conclusions can be made.

1. The solution and the simplified solution are both significantly more accurate than the two-body solution. The relative error of the two-body solution is on the order of $J\theta$ while the relative error of the solution and the simplified solution is on the order of $J^2\theta$.
2. The real physical effects of the orbit are easily distinguishable in both the solution and the simplified solution.
3. The solution and the simplified solution compare extremely well with a proven numerical solution for at least 41 revolutions with a relative error on the order of $J^2\theta$.
4. The solution and the simplified solution compare extremely well with actual measured satellite data for at least 297 revolutions at altitudes where the J_2 perturbation dominates (e.g., near Earth orbits). For a satellite in orbit at an altitude of around 1000 kilometers, the solution and the simplified solution reduce the error of the two-body solution by approximately 95%.
5. The solution and the simplified solution compare less favorably with actual measured satellite data at semisynchronous and geosynchronous altitudes. At these altitudes, however, the solution and the simplified solution reduce the error of the two-body solution by at least 50%.
6. The solution and the simplified solution are free of singularities and are valid for all orbital parameters.

Clearly, the solution and the simplified solution model the J_2 perturbation very well. The equations are easy to implement and can provide quick and accurate predictions of satellite motion. However, other types of analytical solutions exist that are more accurate than the solutions described here.

One such solution was developed by Coffey and Alfriend [Ref. 10] through research that was conducted by Depina [Ref. 11], Coffey and Deprit [Ref. 12], and Alfriend and Coffey [Ref. 13] . The solution is called the Analytic Orbit Prediction Program generator or (AOPP). Although the program is very accurate, AOPP exten-

sively utilizes four different Hamiltonian transformations. As a result, the real physical effects of the orbit are not easily distinguishable.

The beauty of the solution and the simplified solution is their similarity in form to the well known two-body solution and the fact that a satellite's position can be easily predicted by evaluating only one integral. Once θ has been determined, all other orbital parameters can be calculated easily. The structure of the solution and the simplified solution is ideal for implementation with onboard spacecraft computers.

Before the solutions can be adapted for practical applications, more examination and testing of the theory is required. In order to provide more confidence in the theory, the following recommendations are suggested.

1. The solution and the simplified solution need to be compared to a numerical integration of the equations of motion for at least 100 revolutions to confirm the theoretical accuracy for long term satellite motion.
2. The solution and the simplified solution need to be compared to several more diverse sets of actual measured satellite data.
3. To increase precision, the solution needs to include the higher order zonal harmonics of the gravitational potential (e.g., J_3 , J_4 , J_5 , etc.).
4. For spacecraft computer implementation, the Lagrangian coefficients of the state transition matrix need to be determined.

For onboard spacecraft navigation, computers make use of the state transition matrix. Currently the Lagrangian coefficients of the two-body solution are the only matrix elements that have been determined. An excellent formulation of the two-body state transition matrix is shown by Battin [Ref. 14]. Once the Lagrangian coefficients of the solution are developed, onboard spacecraft navigation can be greatly improved.

APPENDIX A. NUMERICAL SOLUTION COMPARISON RESULTS

DELTA RADIUS VECTOR

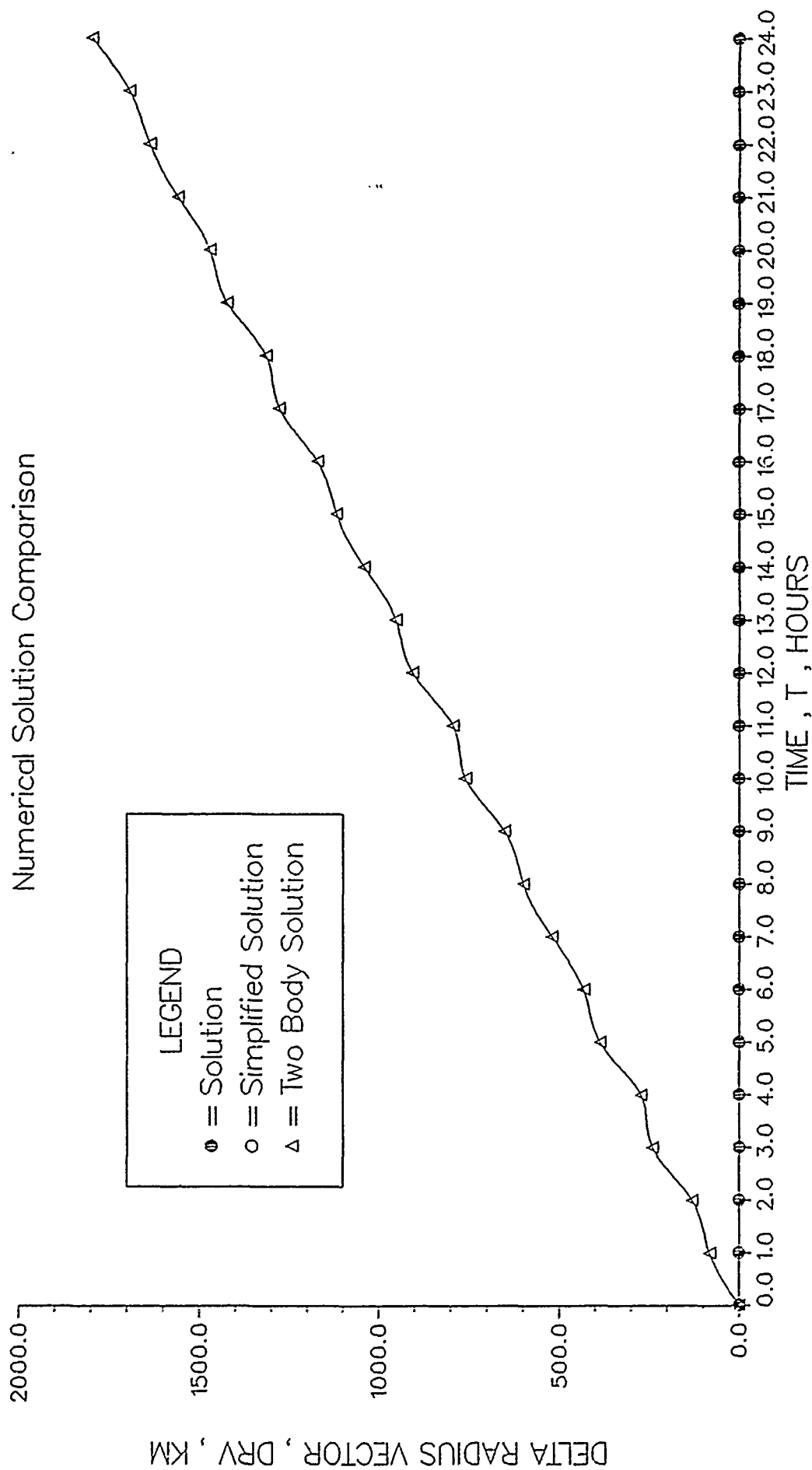


Figure 5. Delta radius vector (1 day)

DELTA RADIUS VECTOR

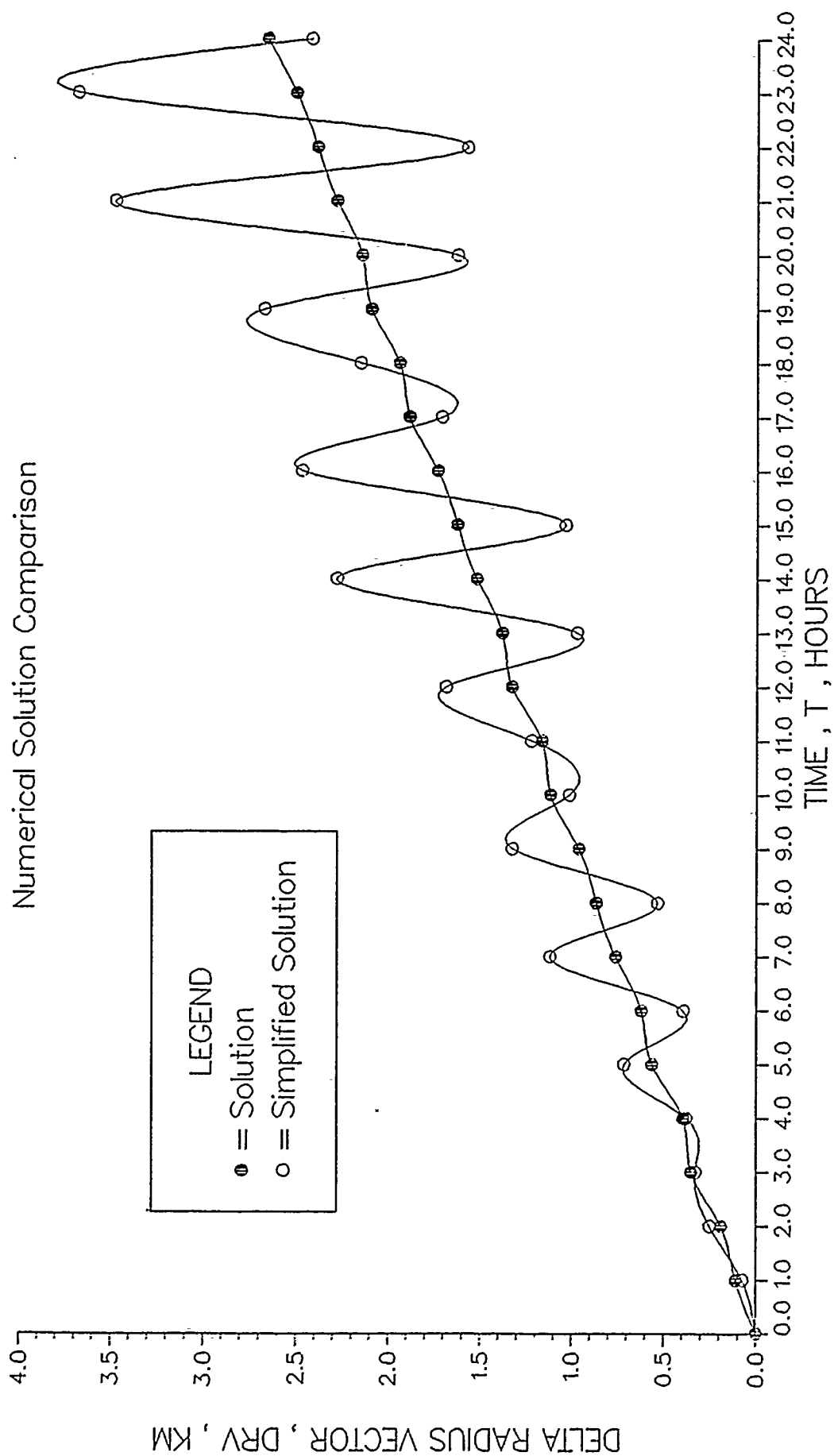


Figure 6. Delta radius vector (1 day)

DELTA RADIUS VECTOR

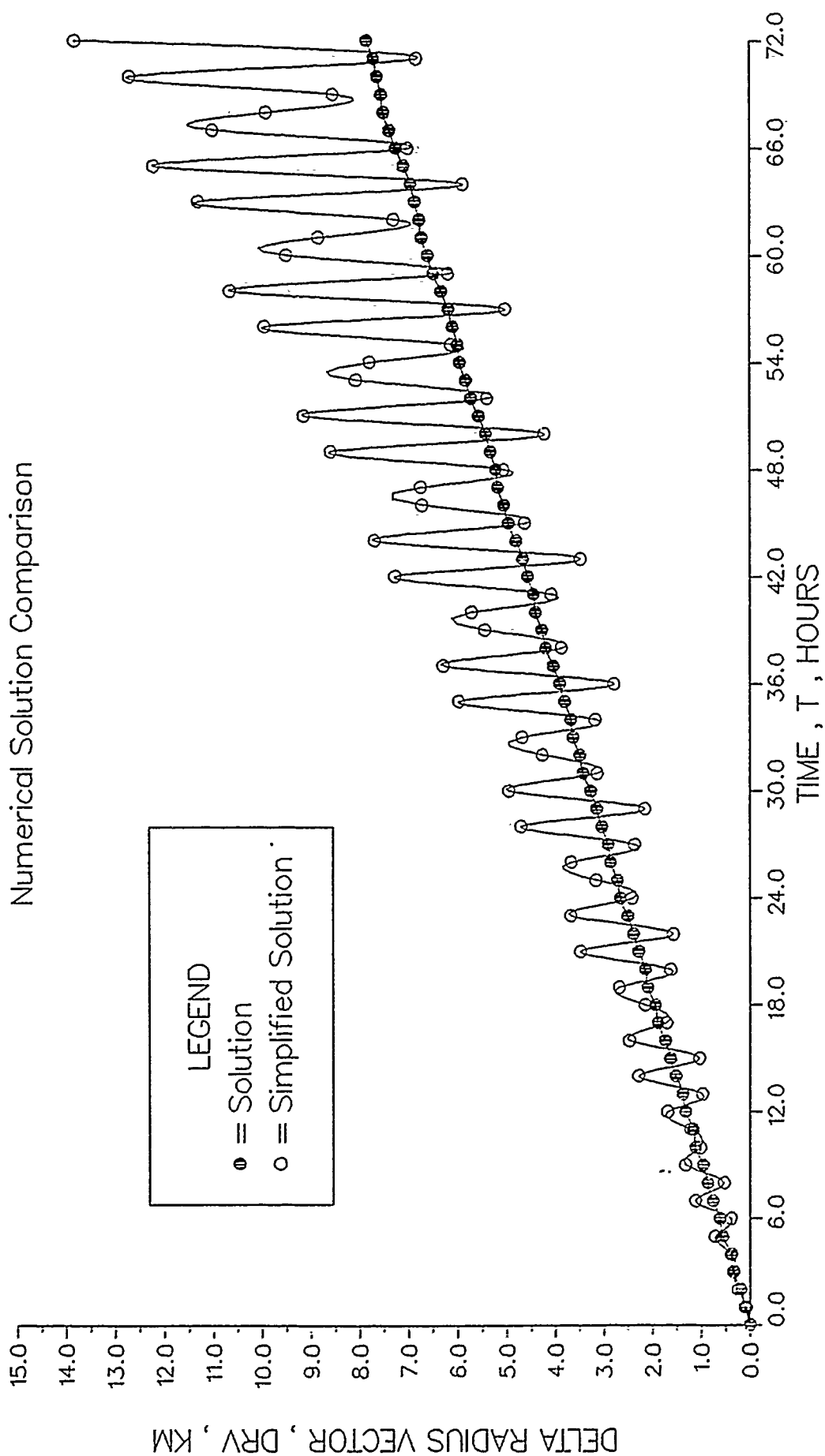


Figure 7. Delta radius vector (3 days)

EARTH ARC ANGLE

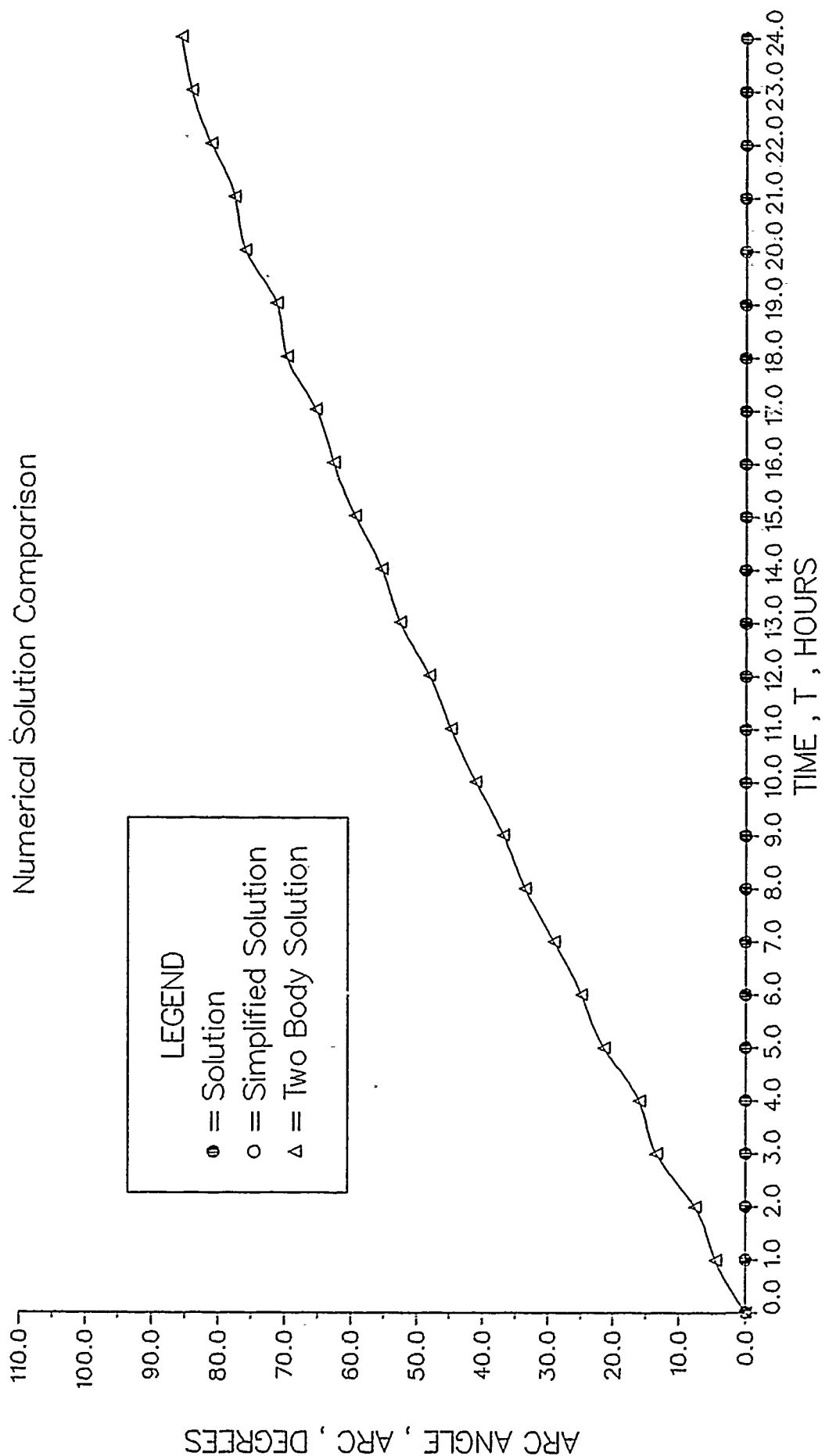


Figure 8. Earth arc angle (1 day)

EARTH ARC ANGLE

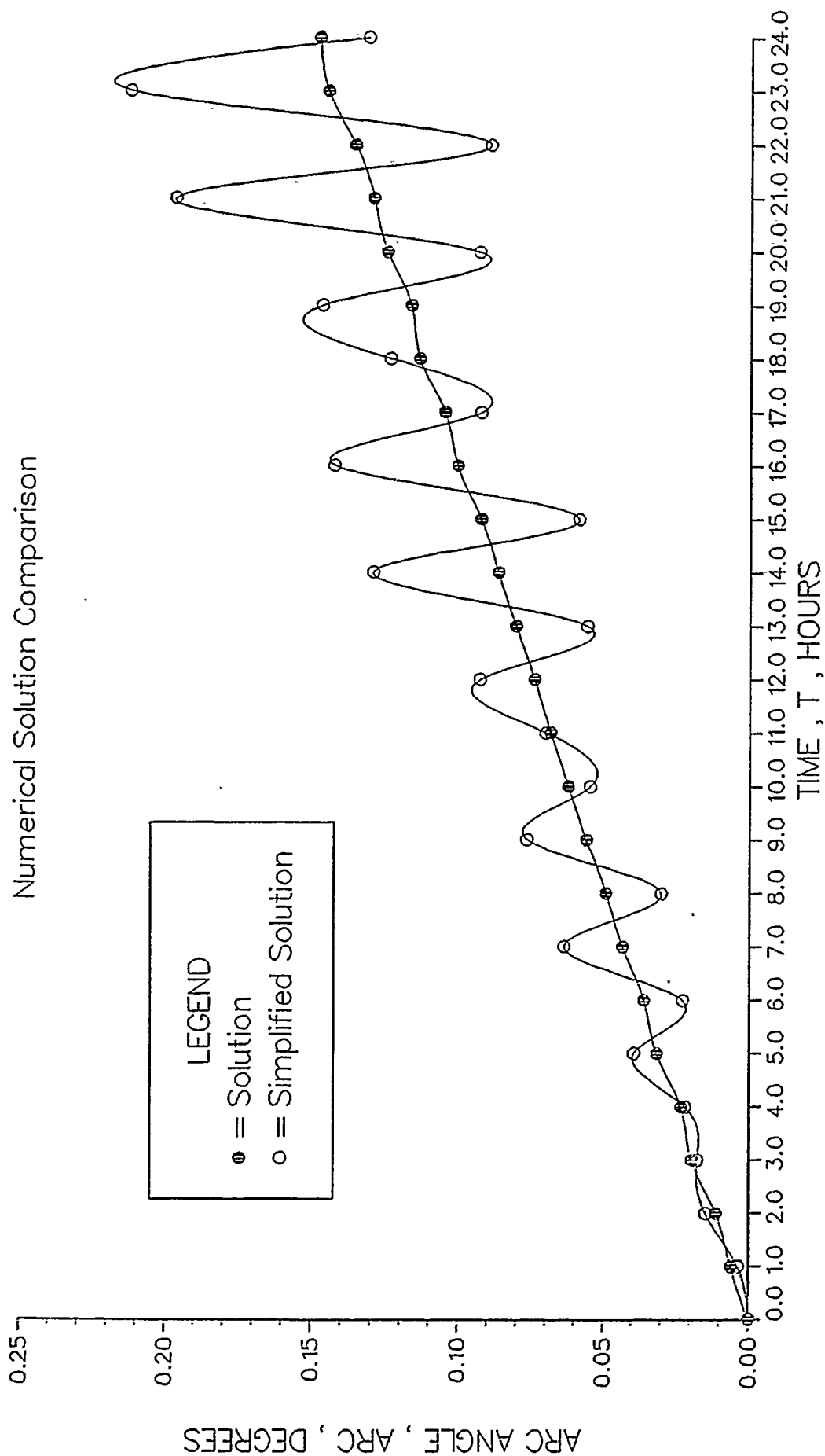


Figure 9. Earth arc angle (1 day)

EARTH ARC ANGLE

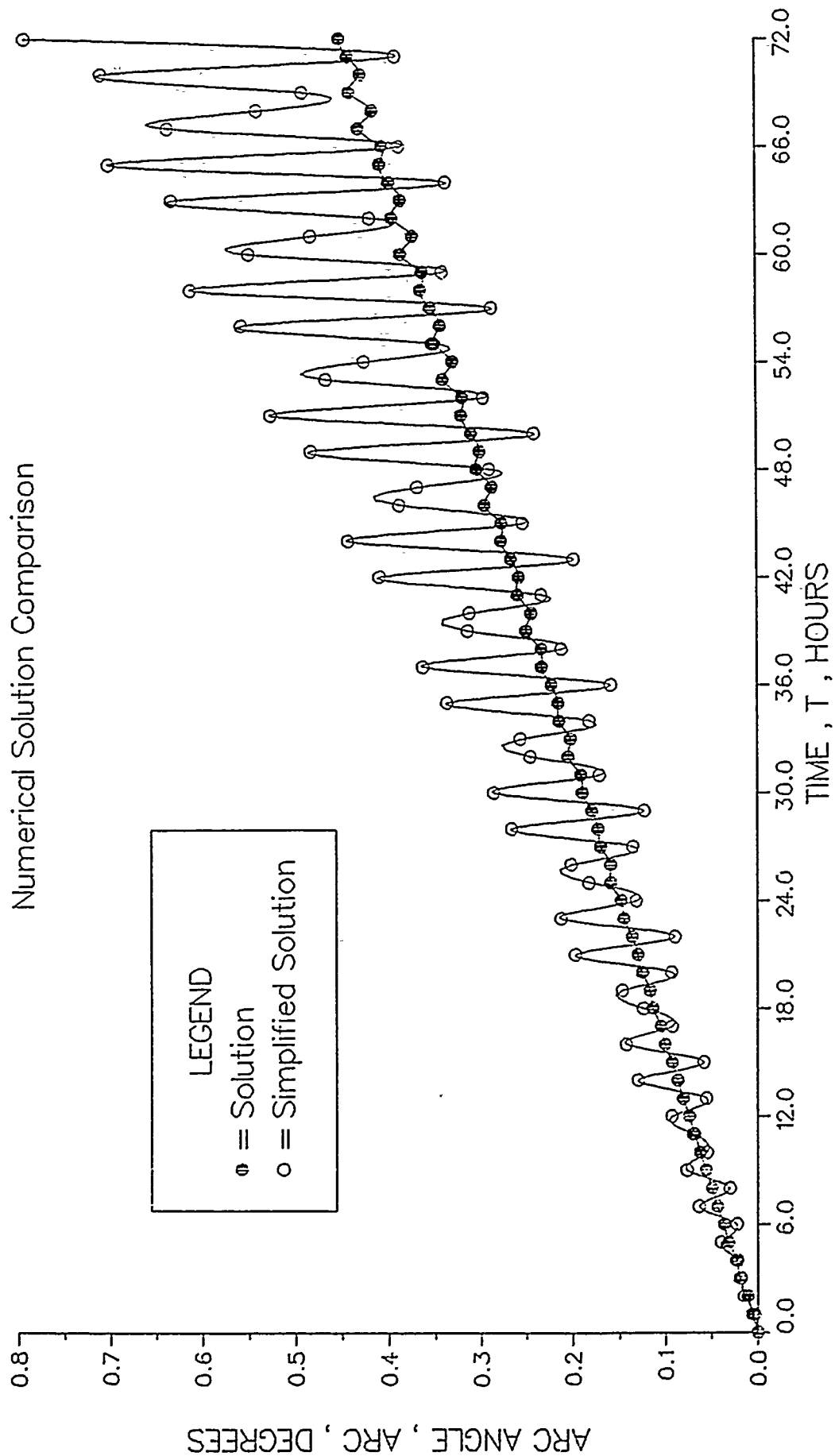


Figure 10. Earth arc angle (3 days)

DELTA OMEGA

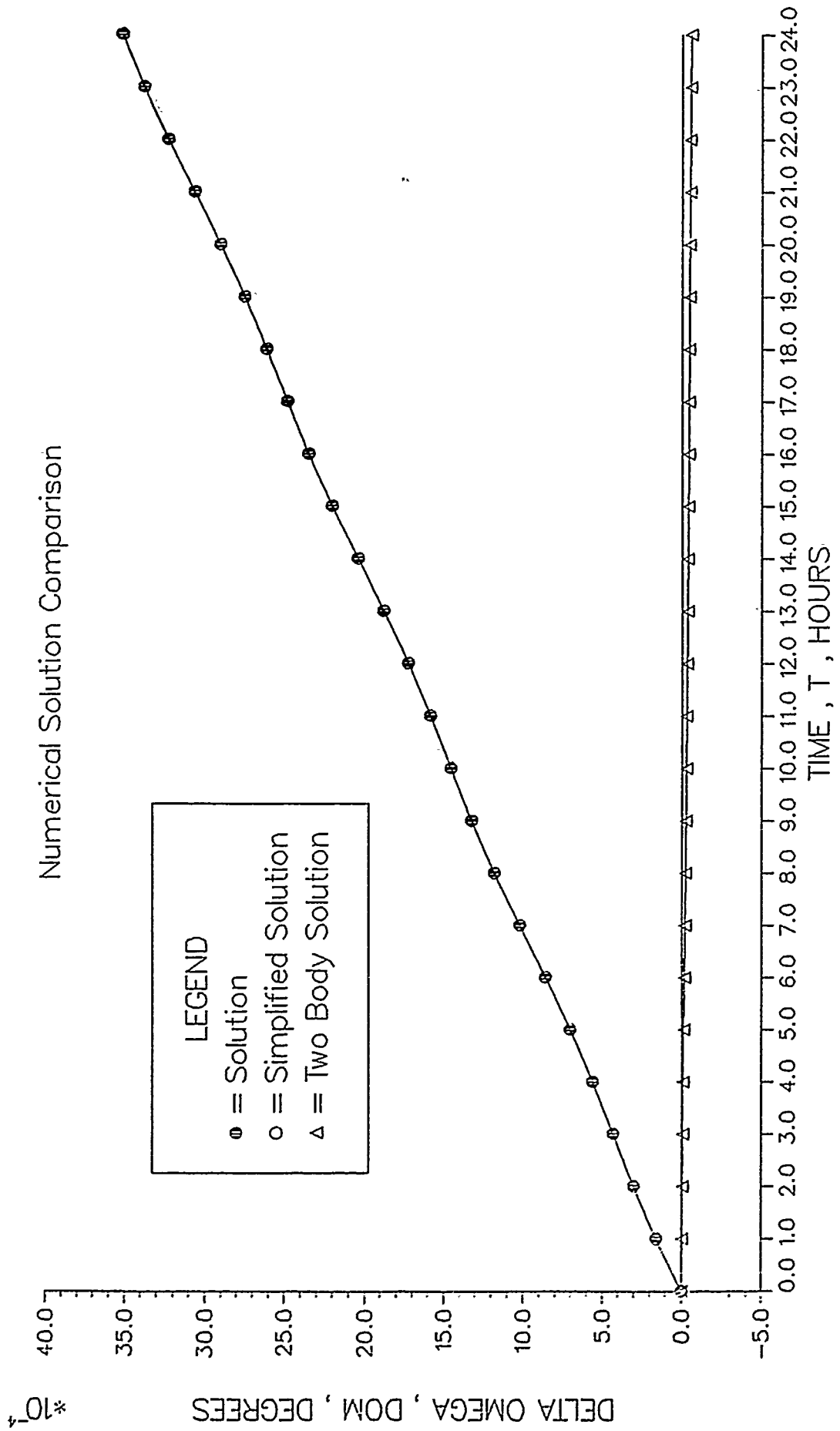


Figure 11. Delta omega (1 day)

DELTA OMEGA

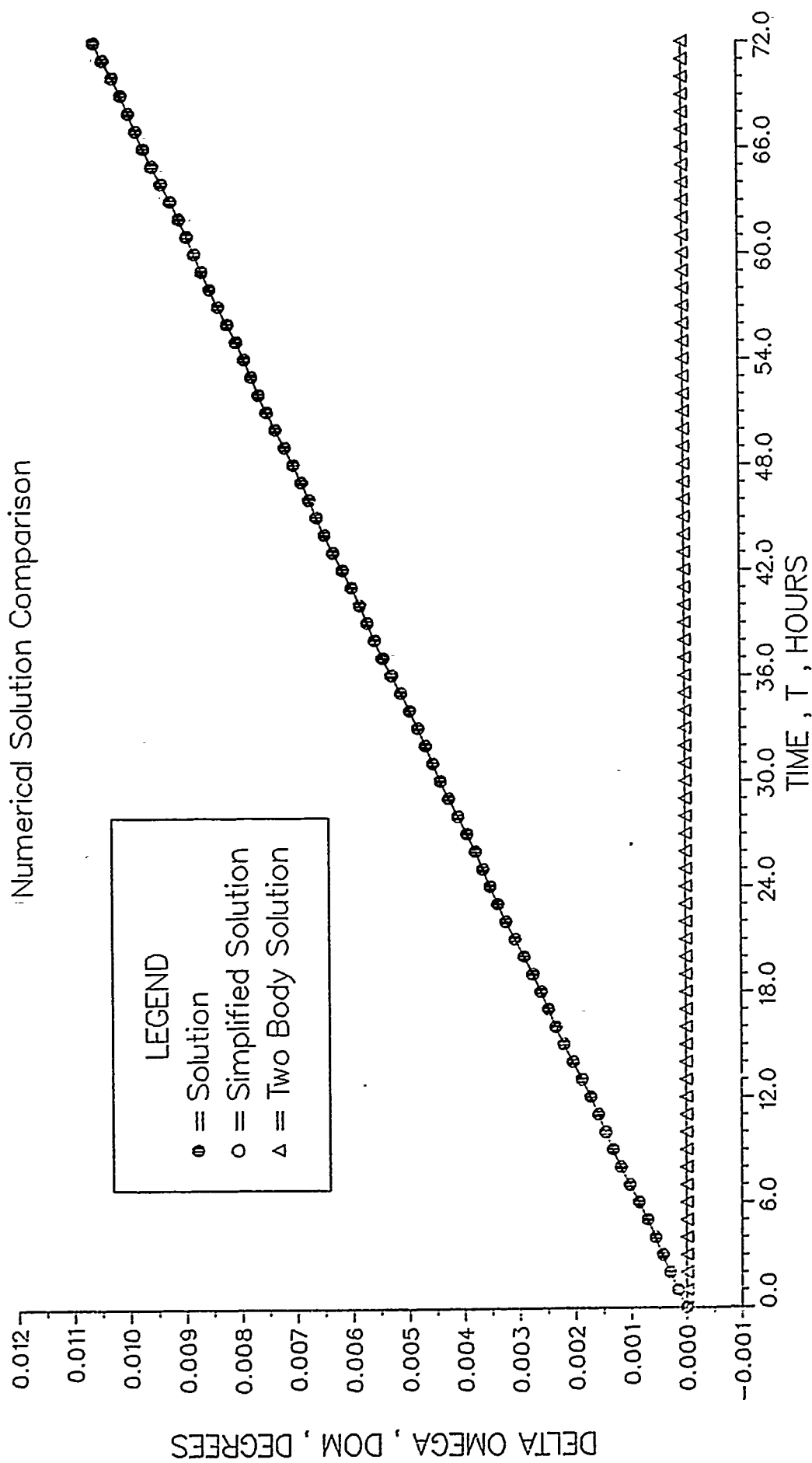


Figure 12, Delta omega (3 days)

DELTA INCLINATION

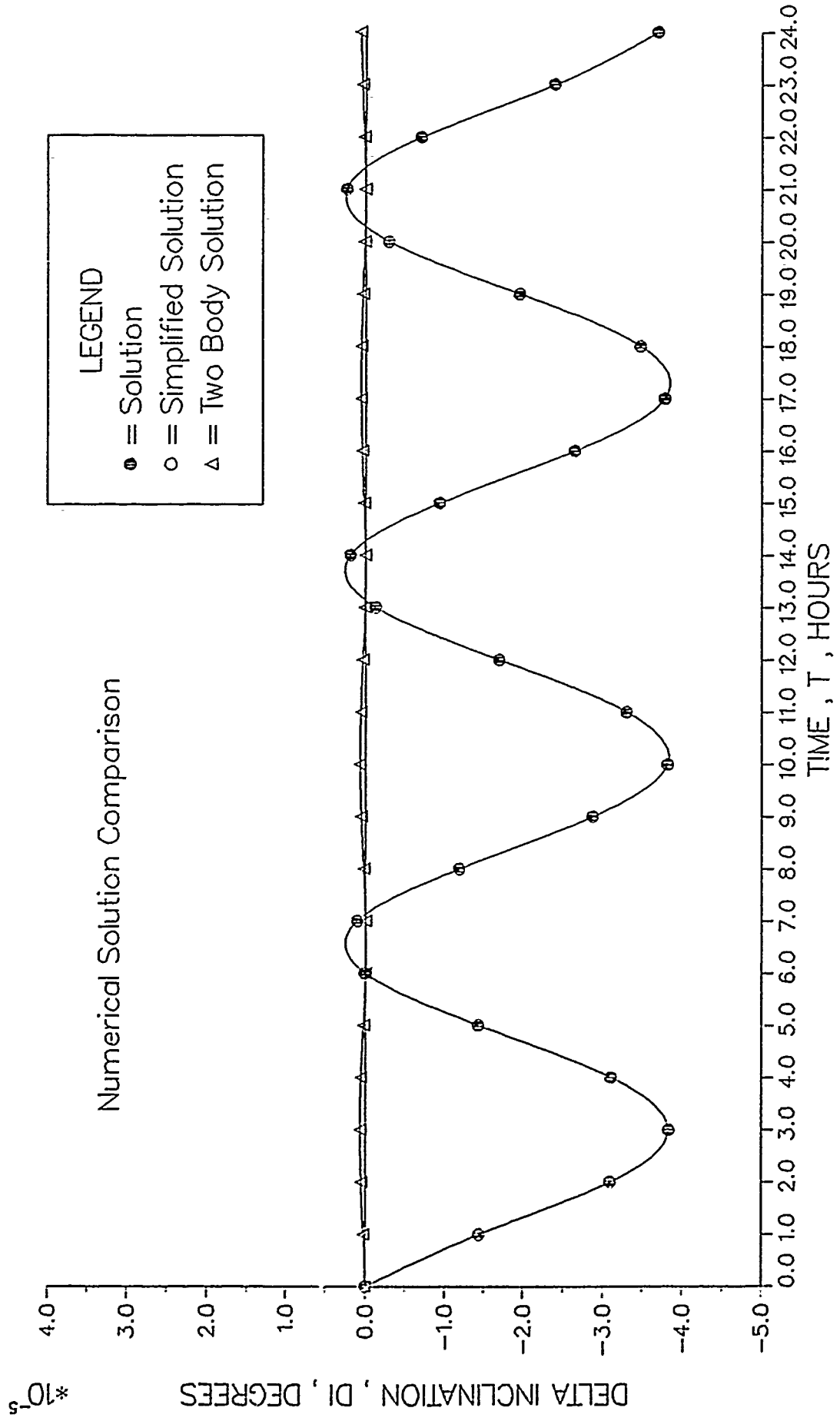


Figure 13. Delta inclination (1 day)

DELTA INCLINATION

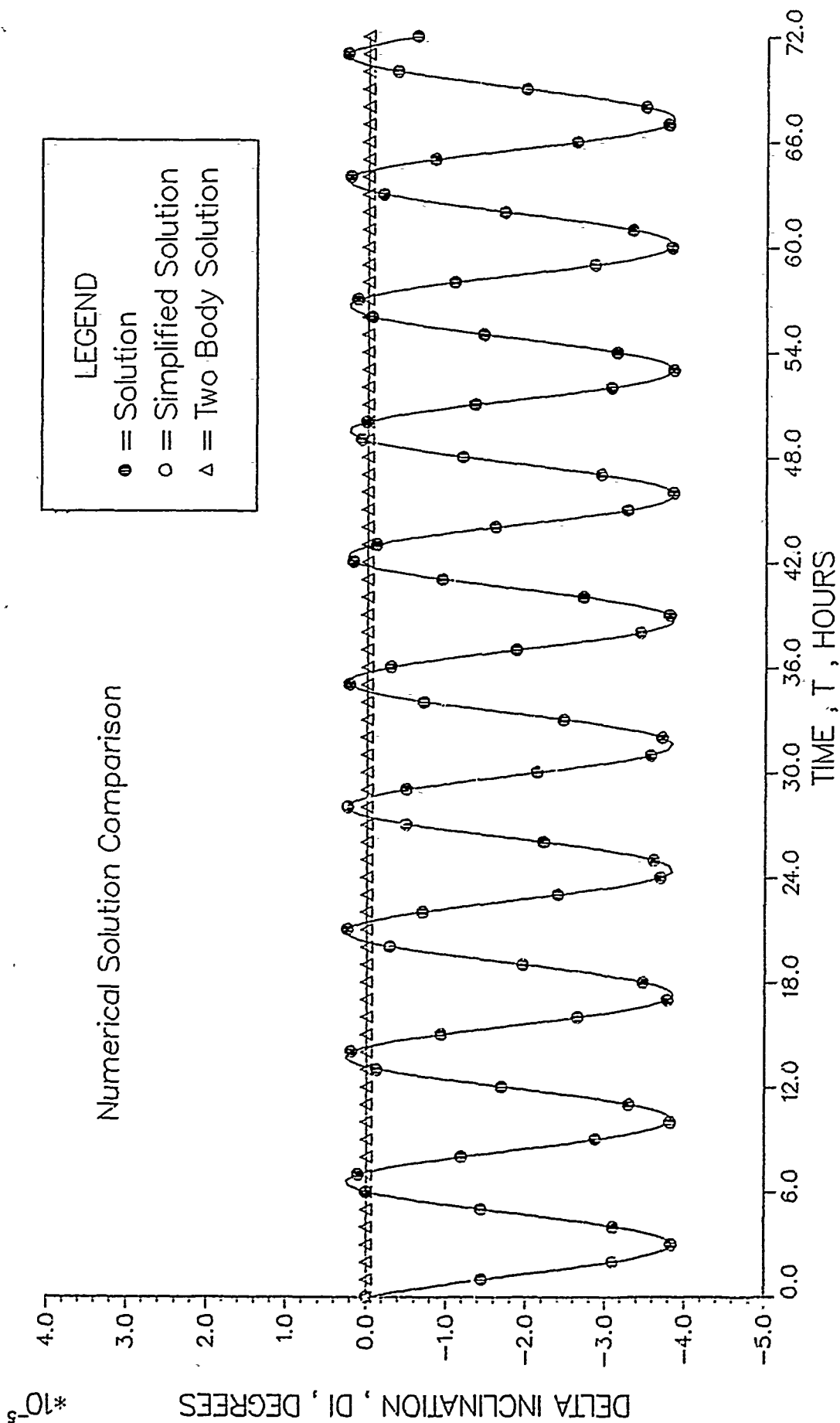


Figure 14. Delta inclination (3 days)

DELTA THETA

Numerical Solution Comparison

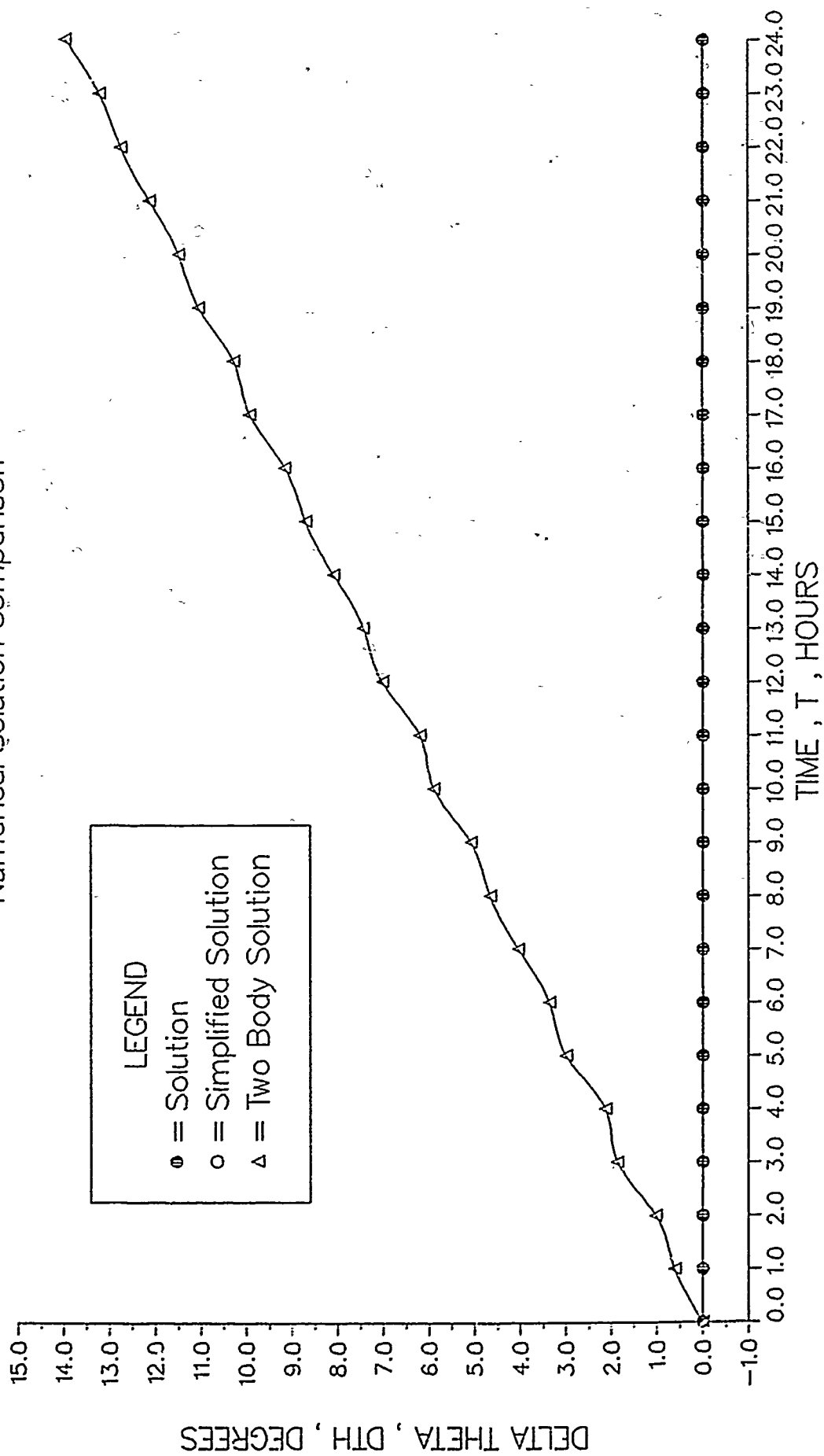


Figure 15. Delta theta (1 day)

DELTA THETA

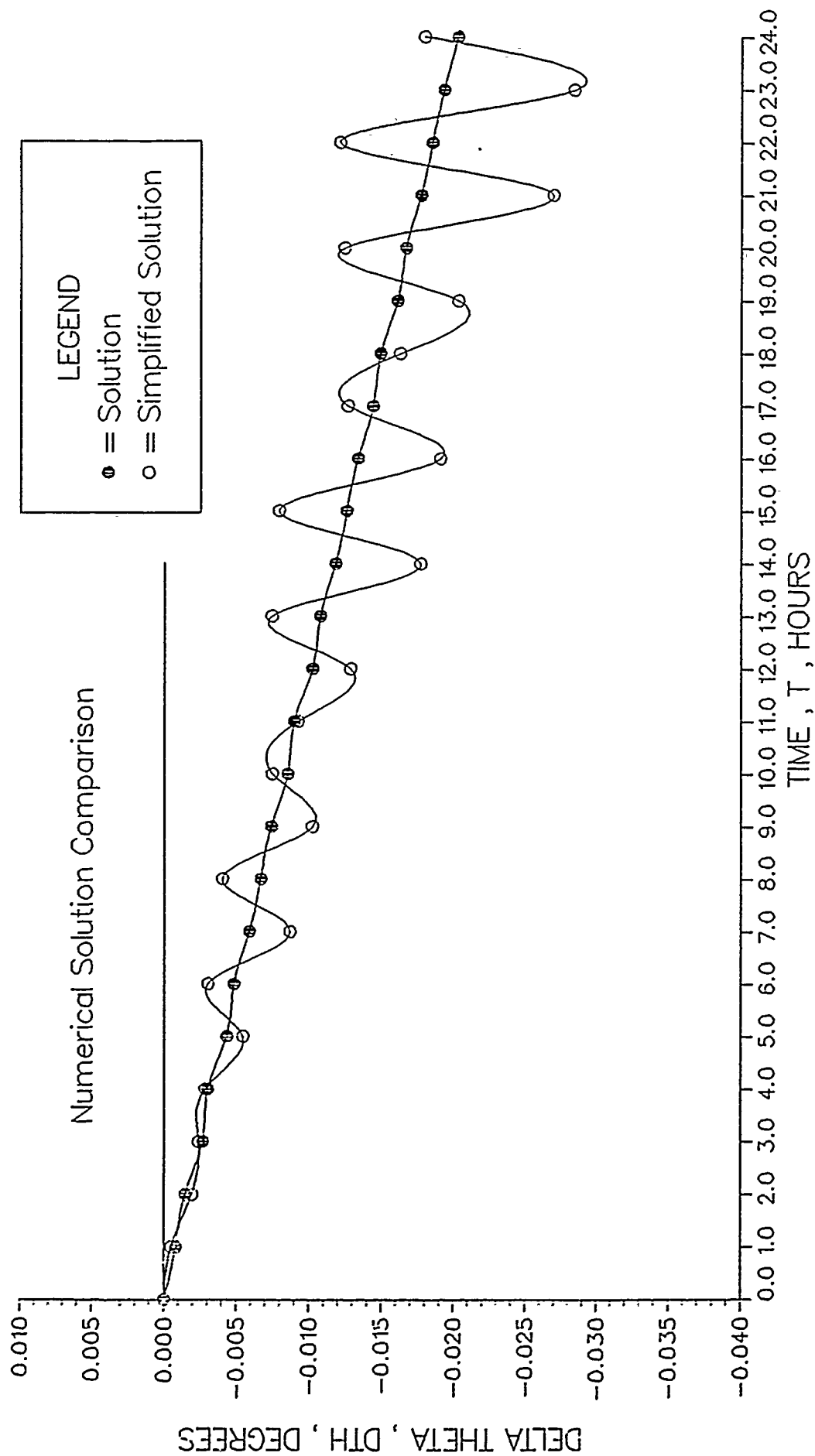


Figure 16. Delta theta (1 day)

DELTA THETA

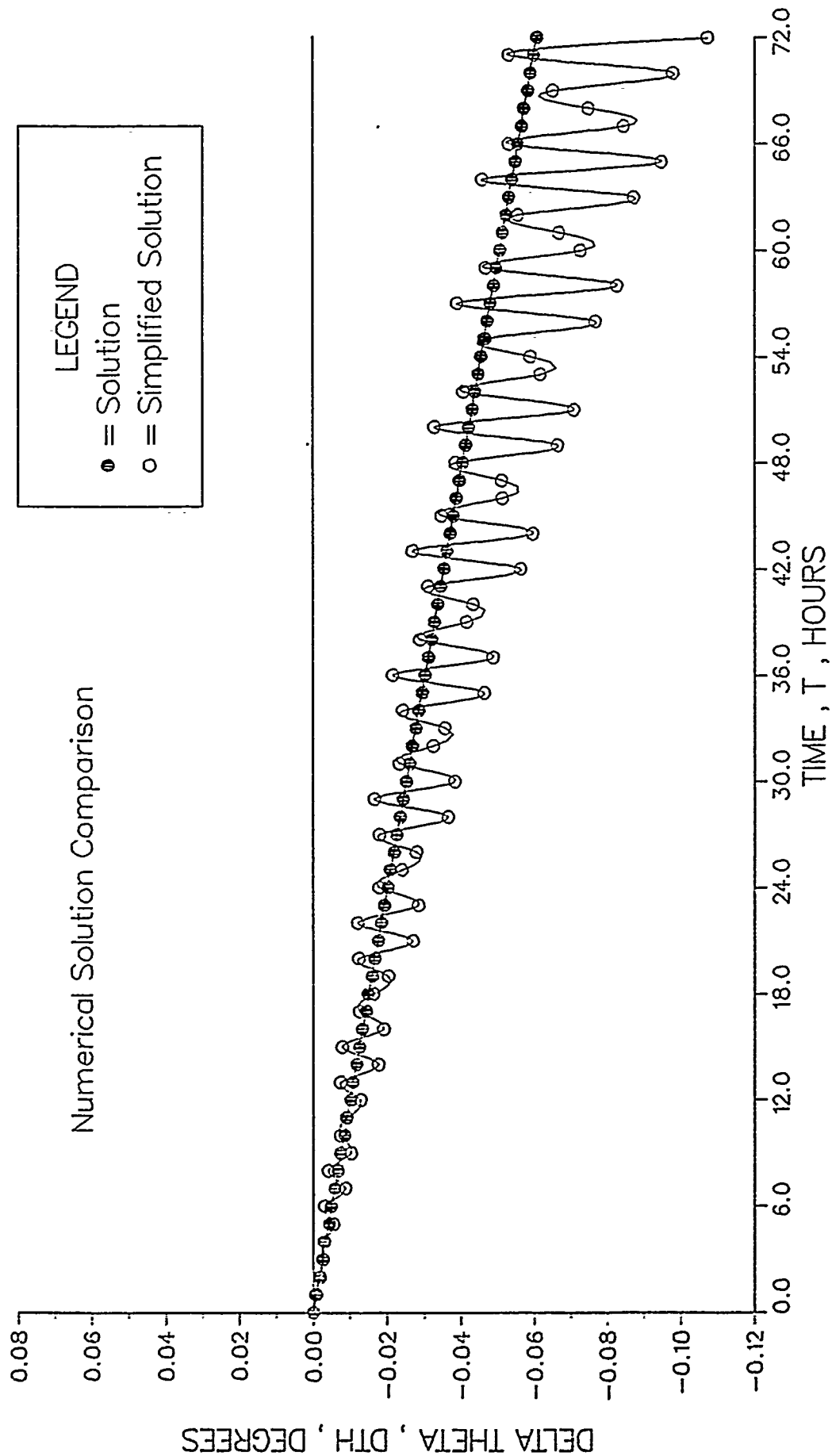


Figure 17. Delta theta (3 days)

DELTA THETA RELATIVE ERROR

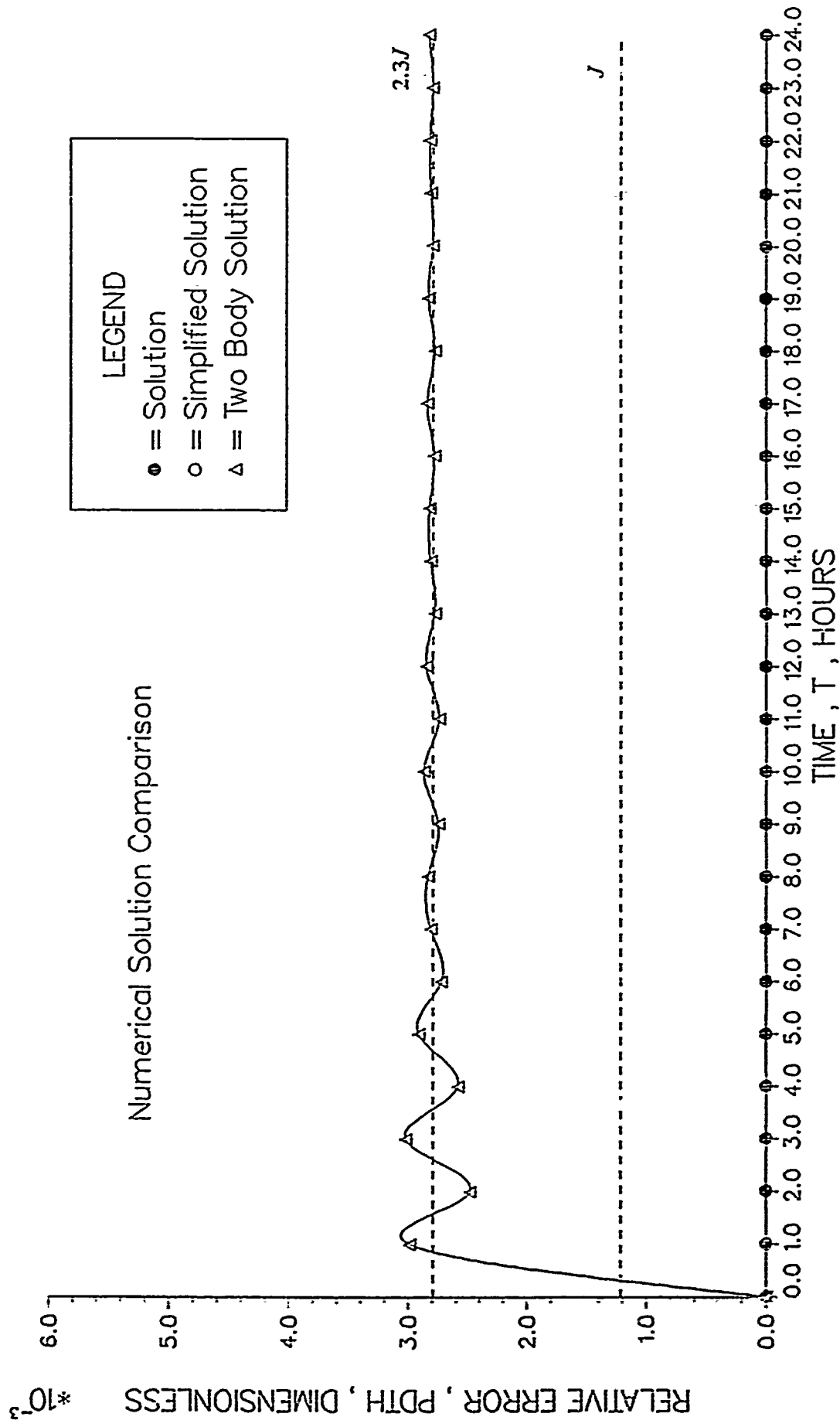


Figure 18. Delta theta relative error (1 day)

DELTA THETA RELATIVE ERROR

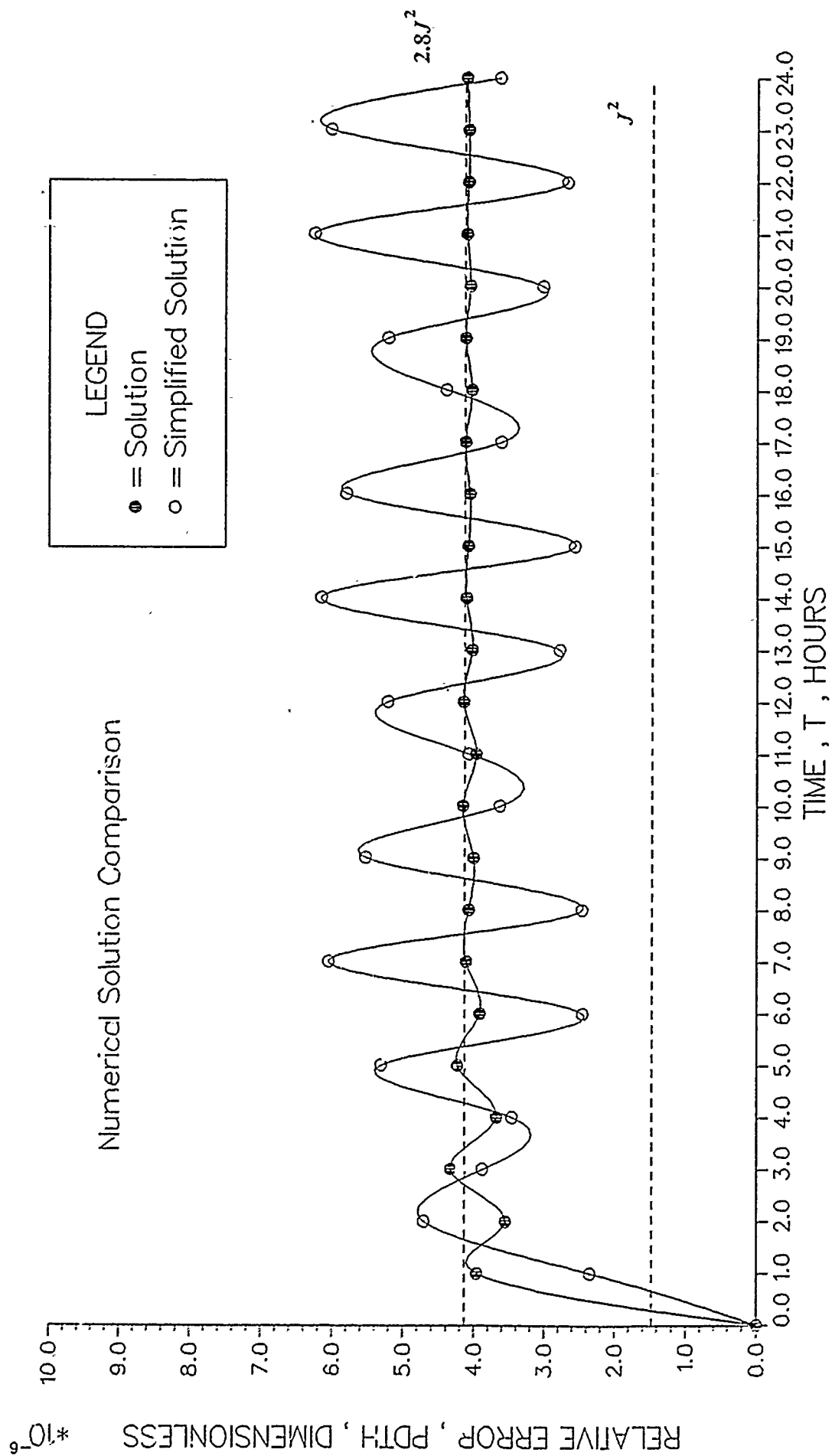


Figure 19. Delta theta relative error (1 day)

DELTA THETA RELATIVE ERROR

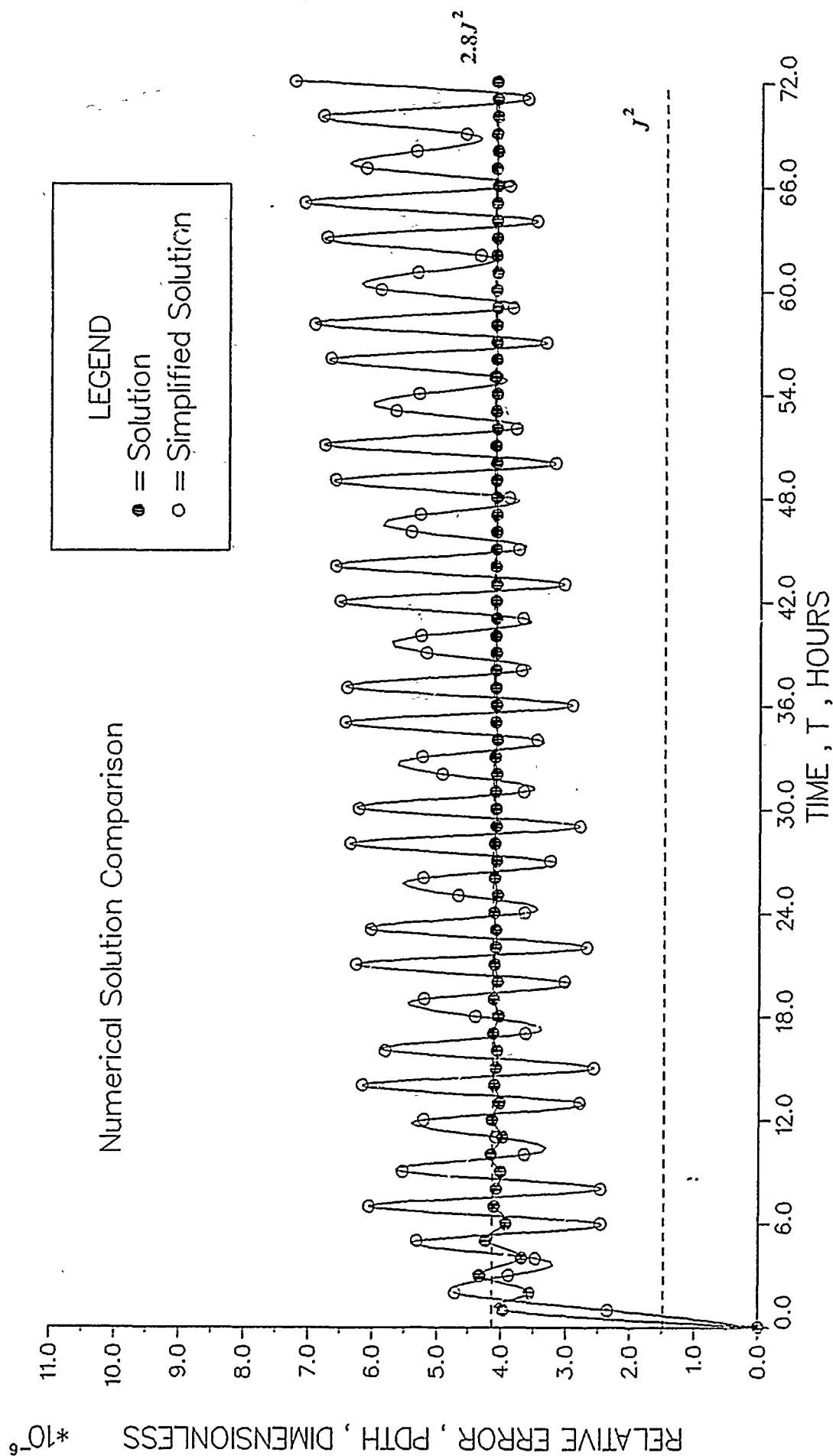


Figure 20. Delta theta relative error (3 days)

DELTA RADIUS RELATIVE ERROR

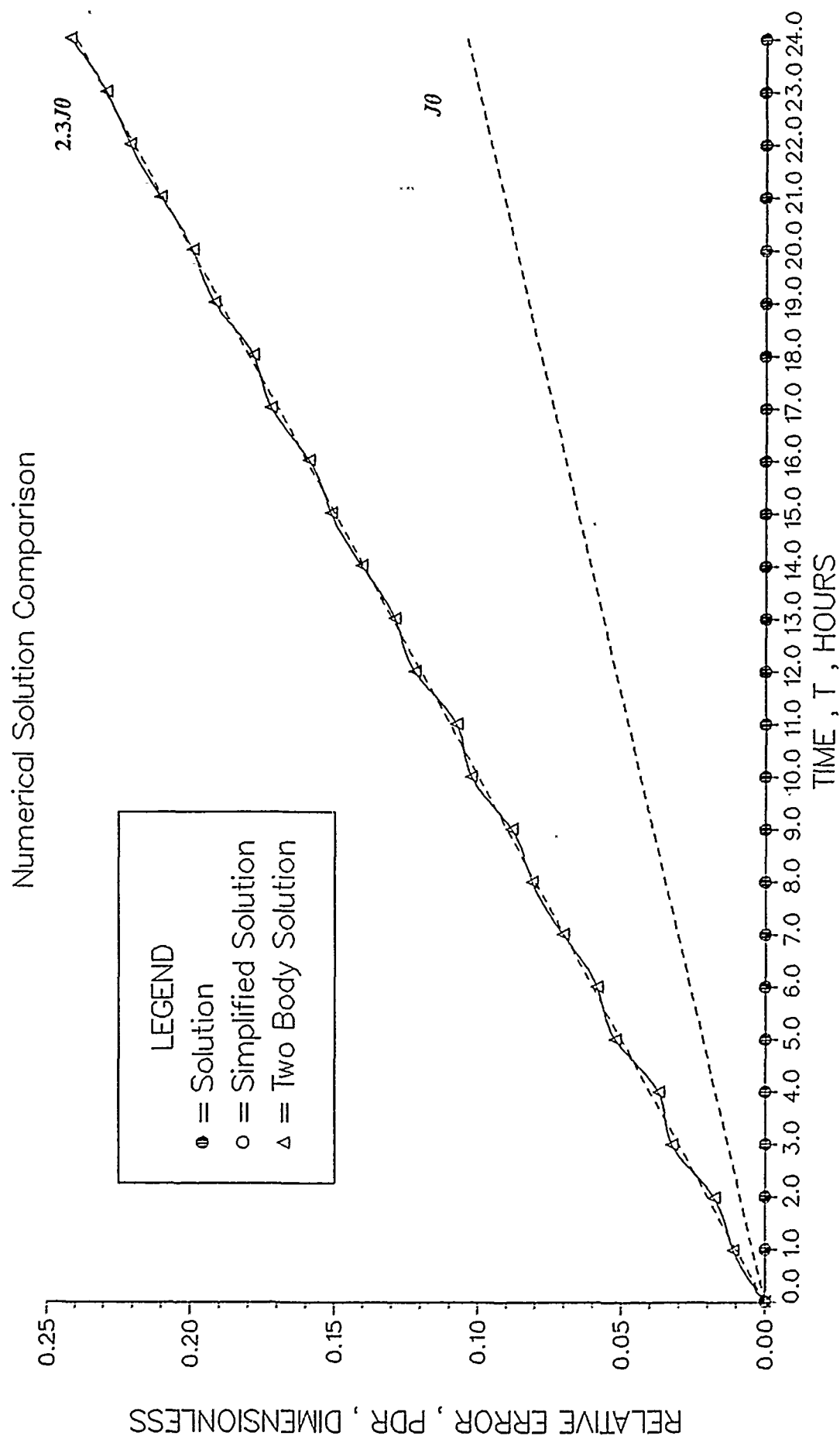


Figure 21. Delta radius relative error (1 day)

DELTA RADIUS RELATIVE ERROR

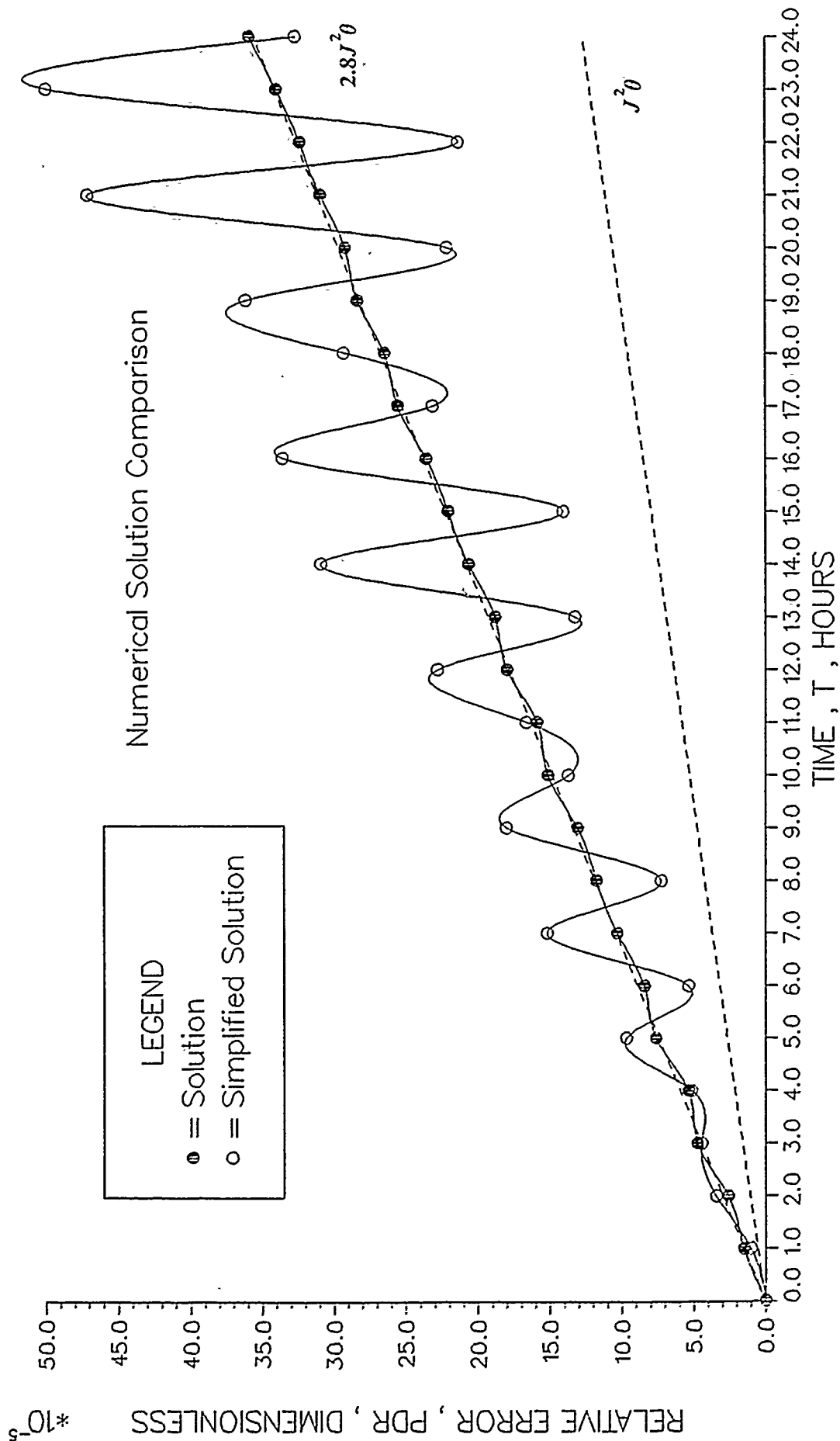


Figure 22. Delta radius relative error (1 day)

DELTA RADIUS RELATIVE ERROR

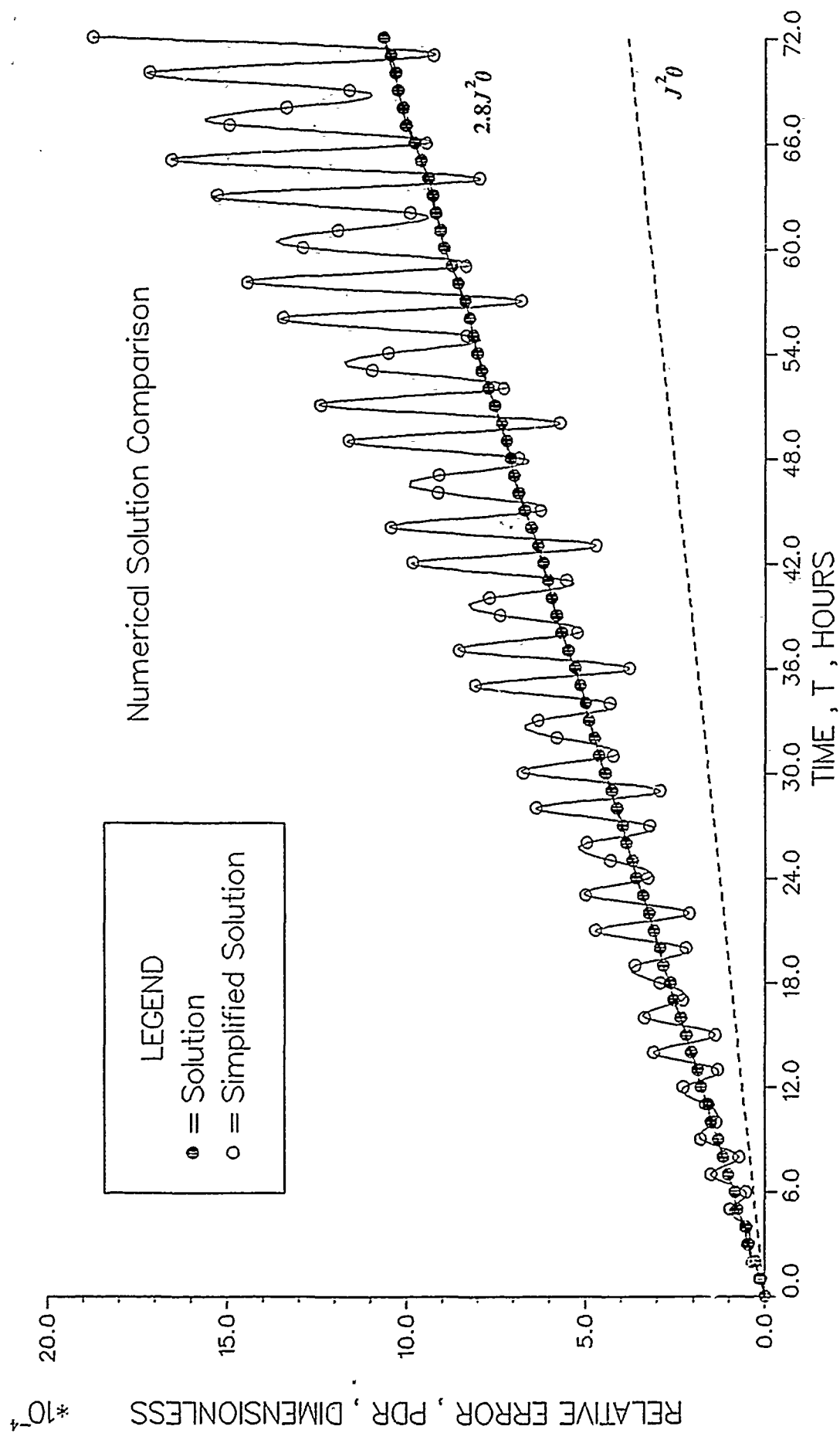


Figure 23. Delta radius relative error (3 days)

RADIAL TRACK ERROR

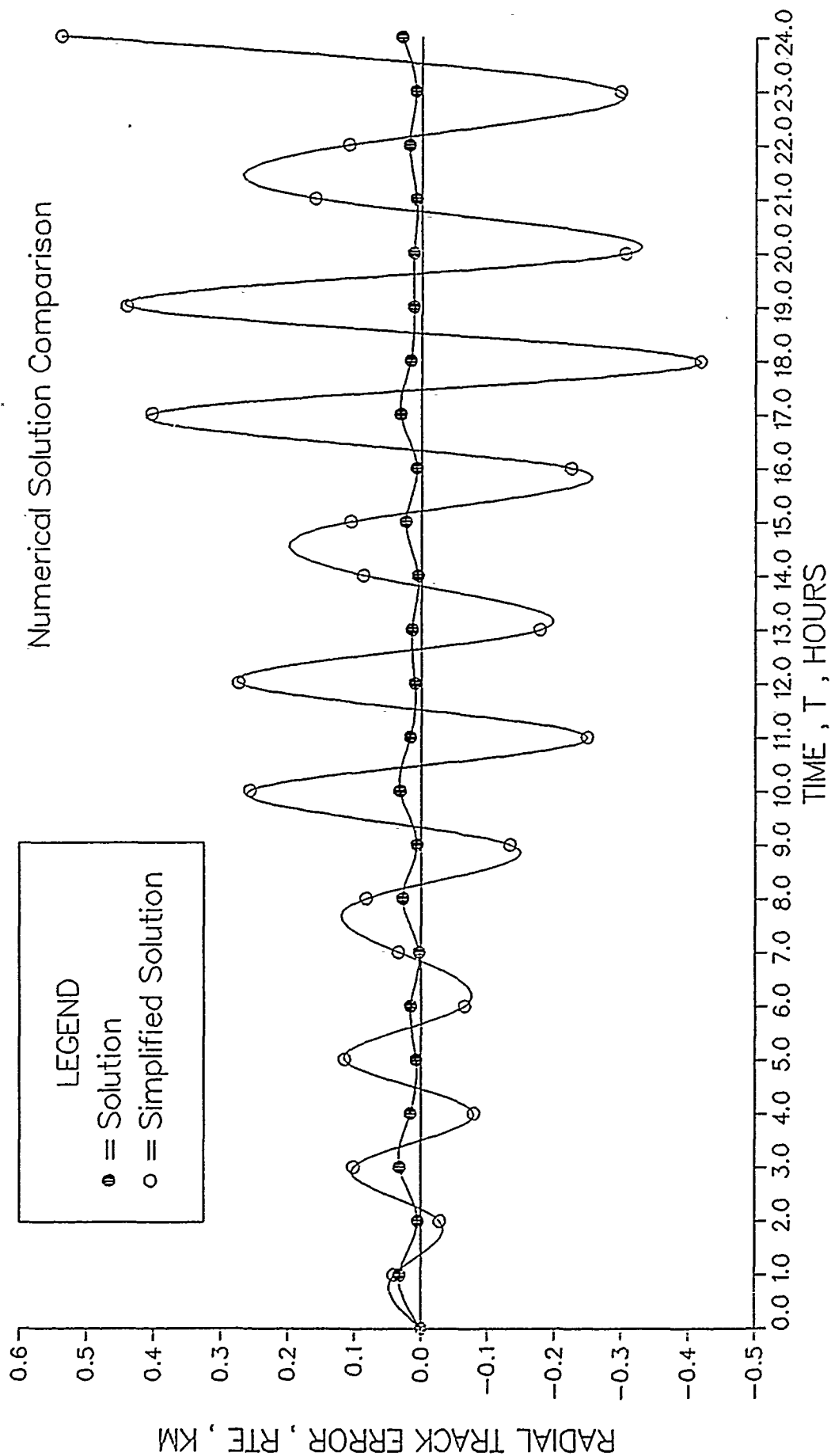


Figure 25. Radial track error (1 day)

RADIAL TRACK ERROR

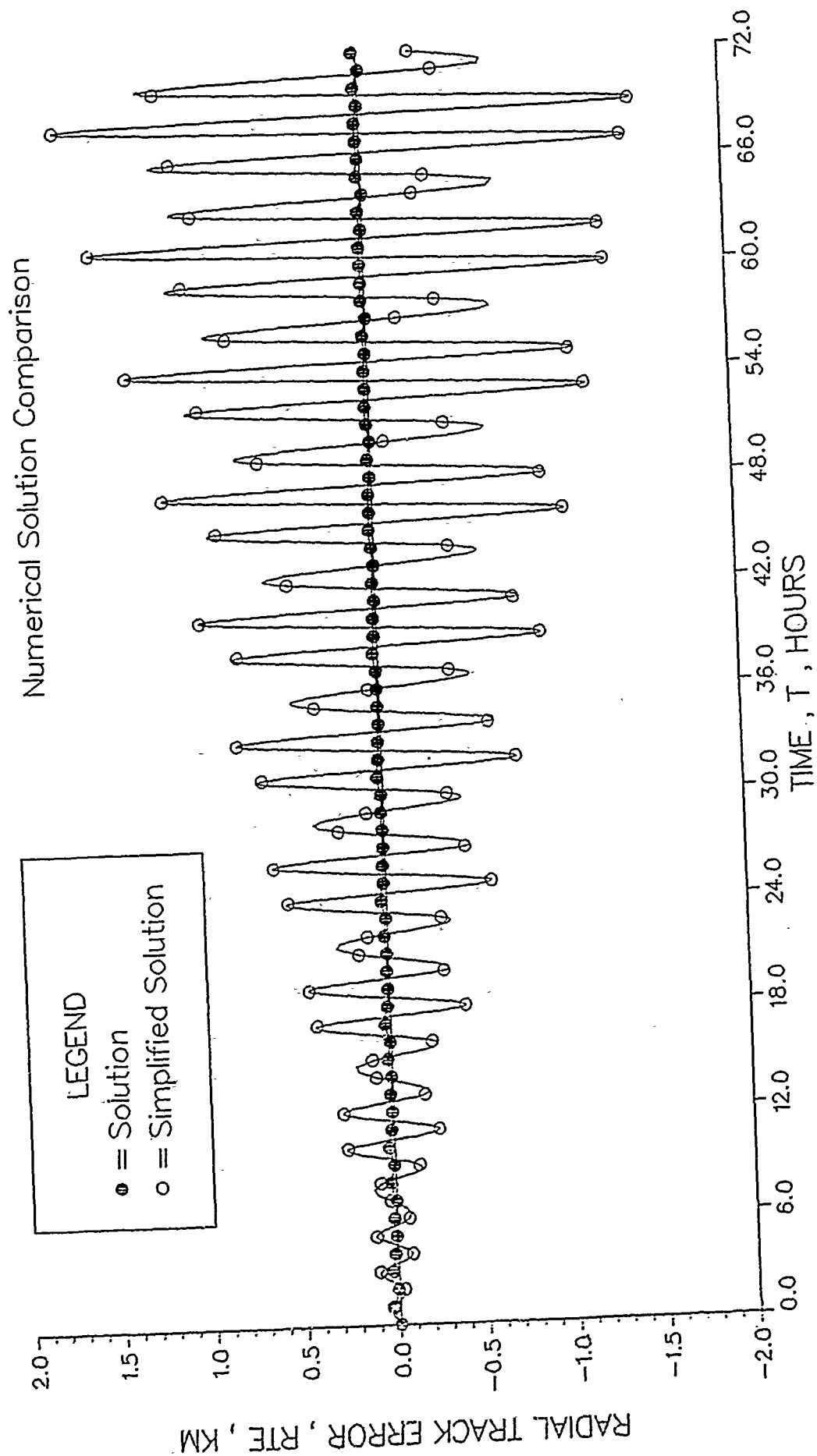


Figure 26. Radial track error (3 days)

ALONG TRACK ERROR

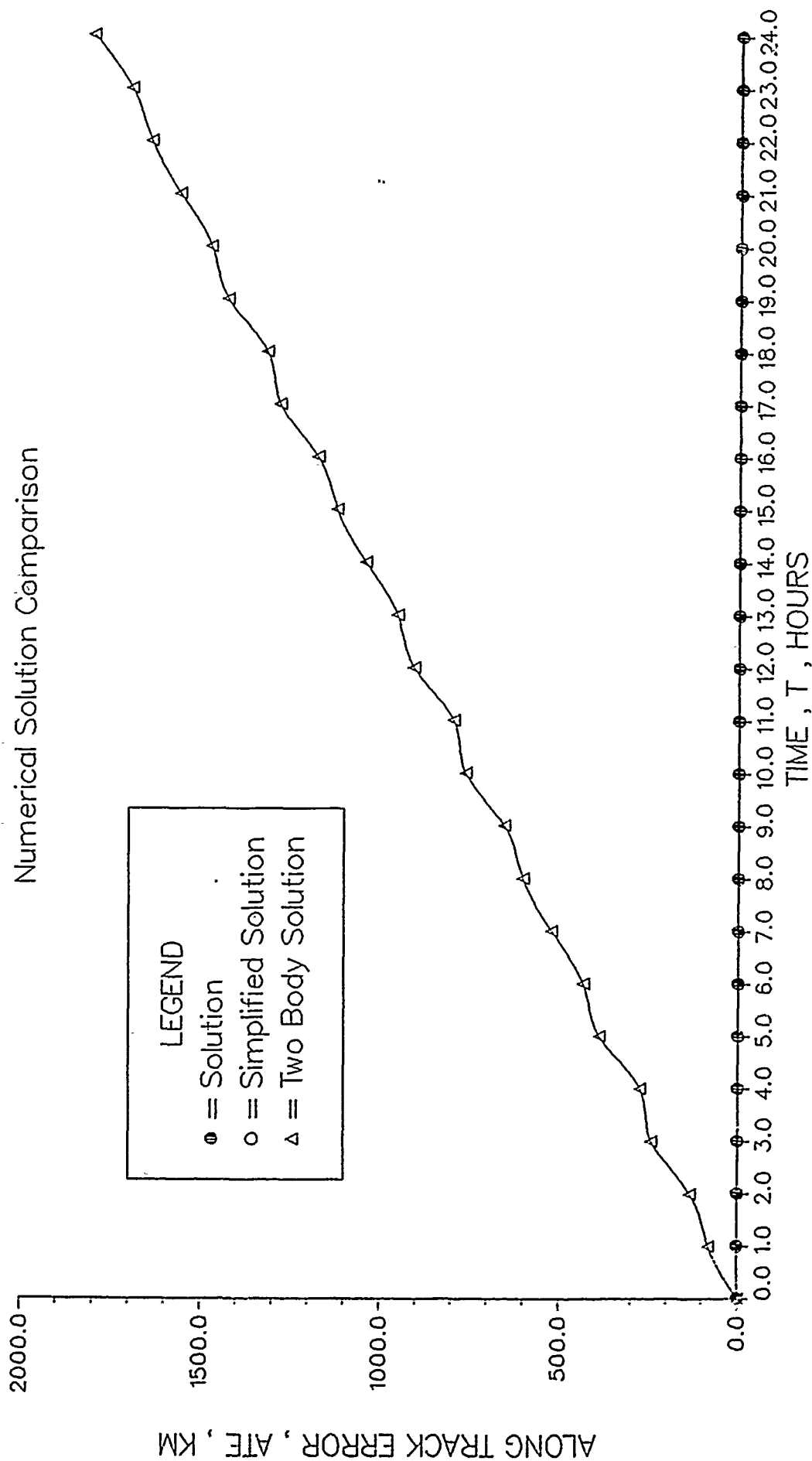


Figure 27. Along track error (1 day)

ALONG TRACK ERROR

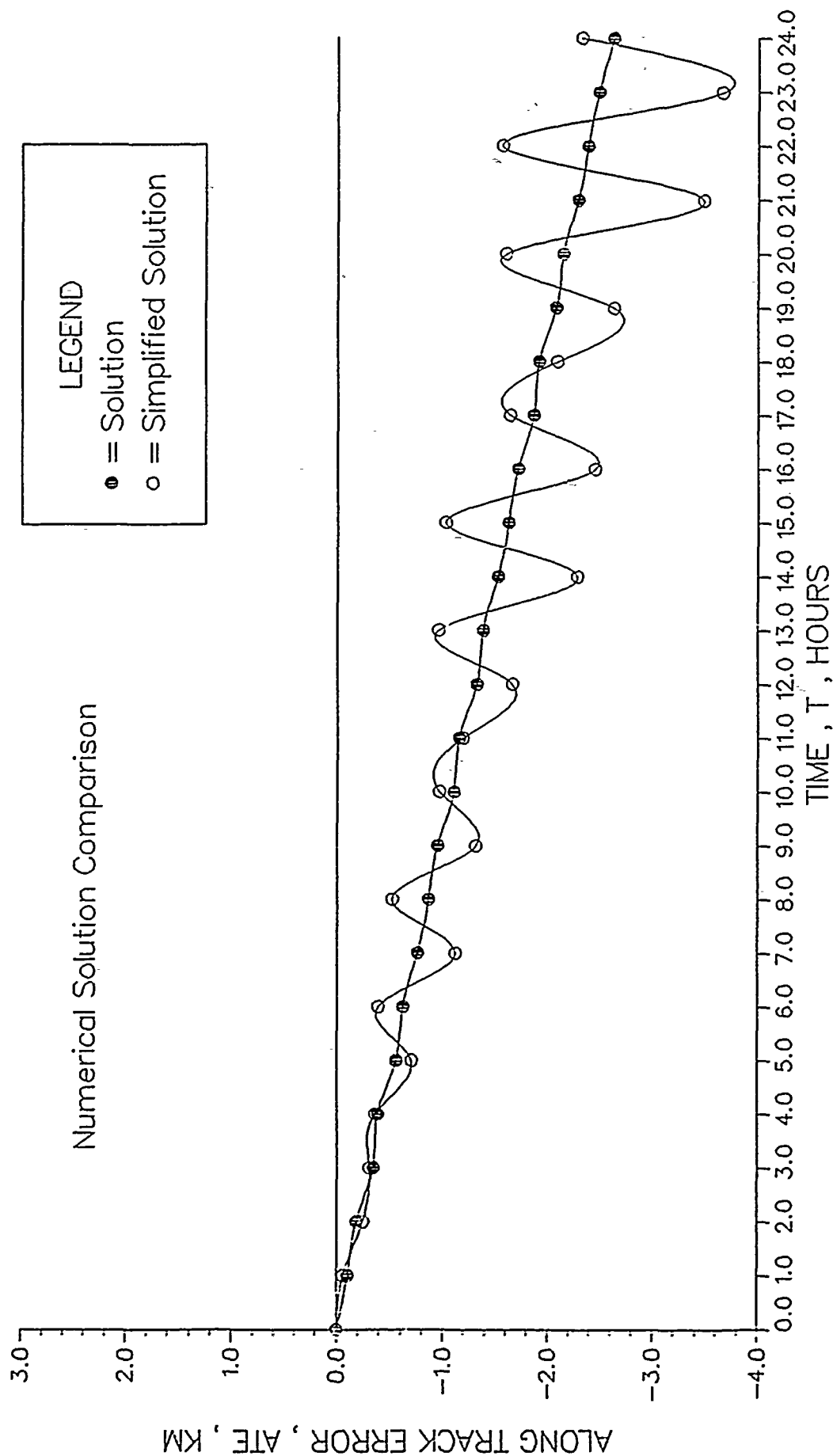


Figure 28. Along track error (1 day).

ALONG TRACK ERROR

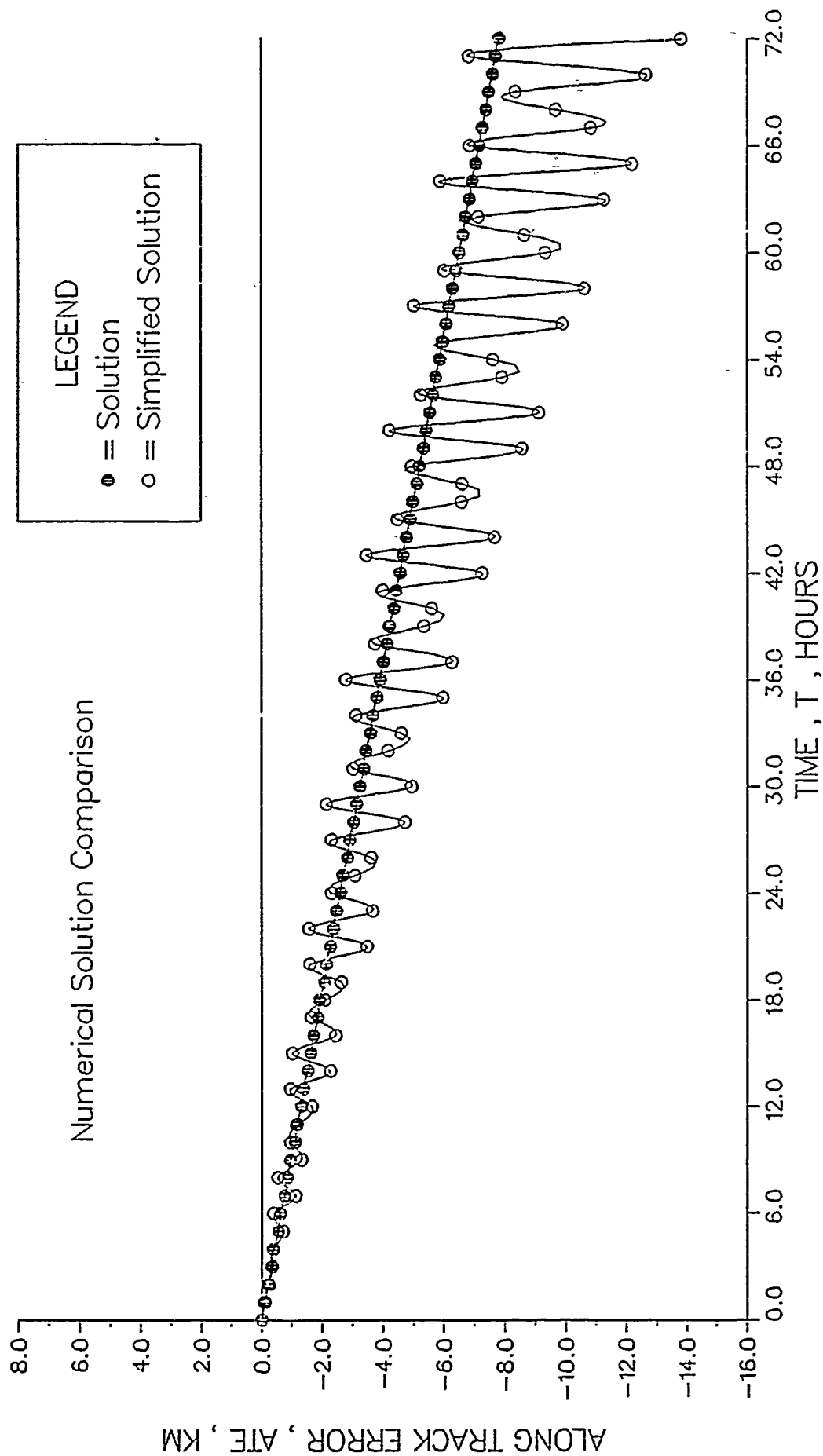


Figure 29. Along track error (3 days)

CROSS TRACK ERROR

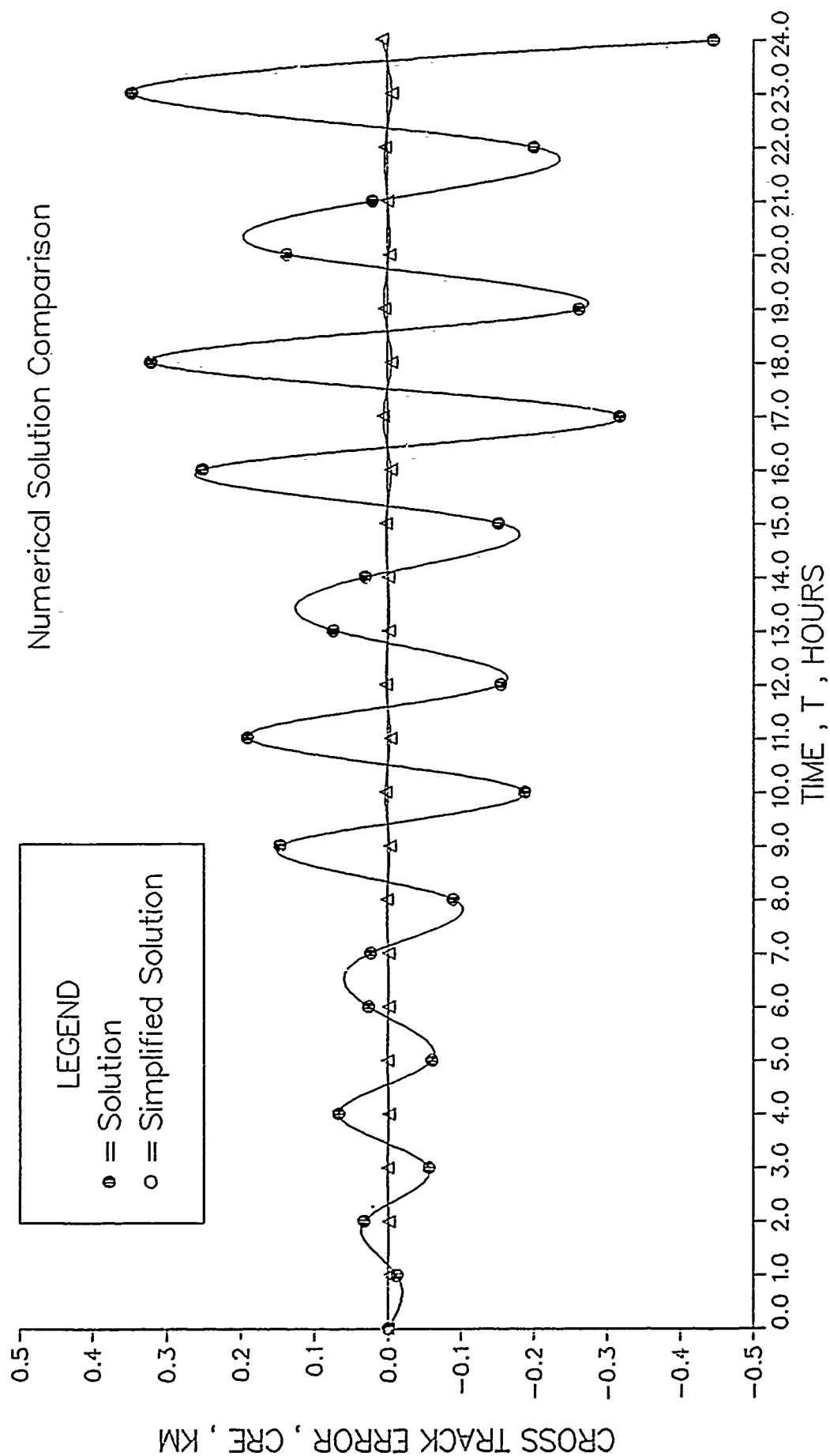


Figure 30. Cross track error (1 day)

CROSS TRACK ERROR

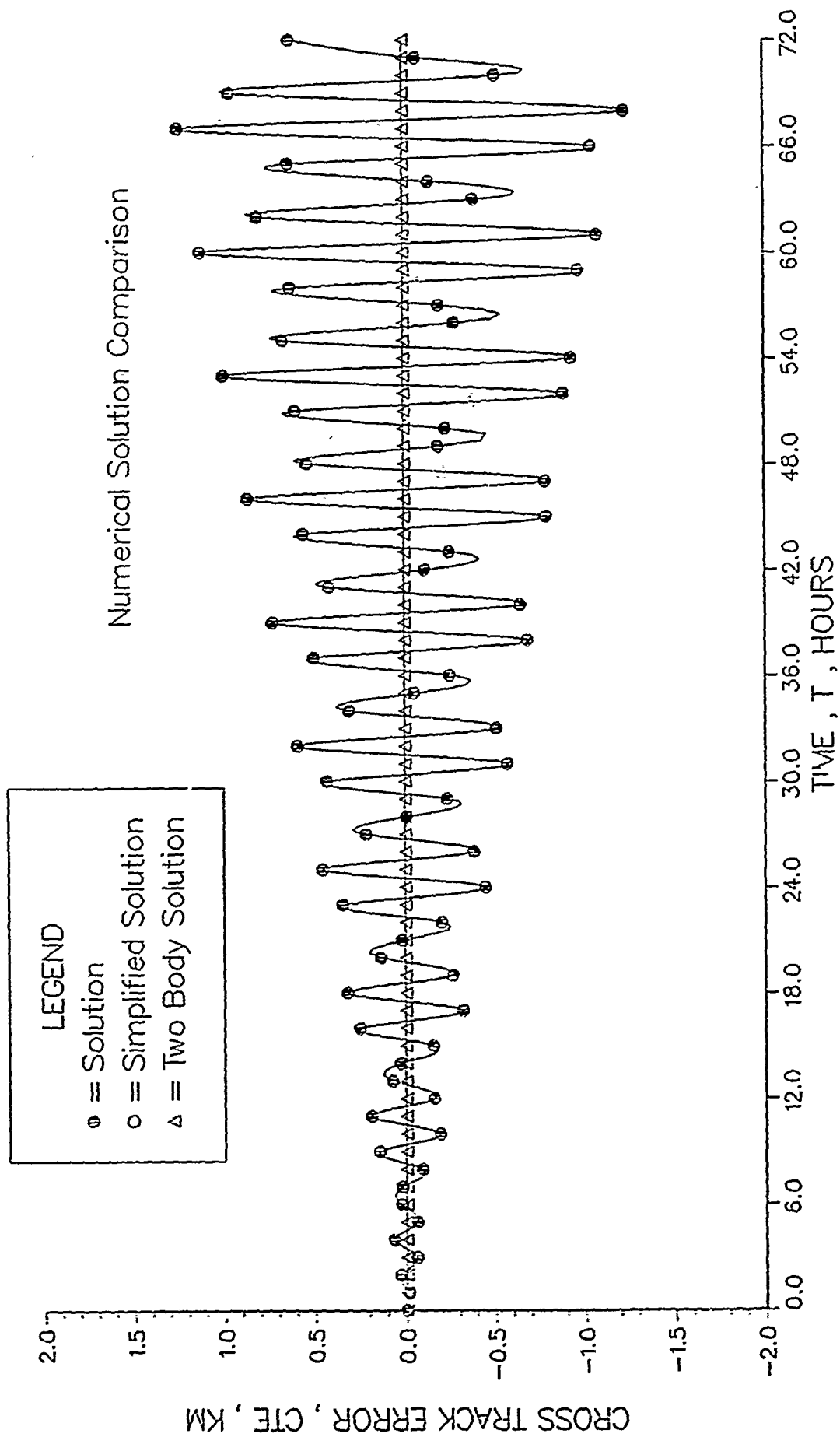


Figure 31. Cross track error (3 days)

APPENDIX B. NEAR EARTH ORBIT COMPARISON RESULTS

DELTA RADIUS VECTOR

Measured Data Comparison

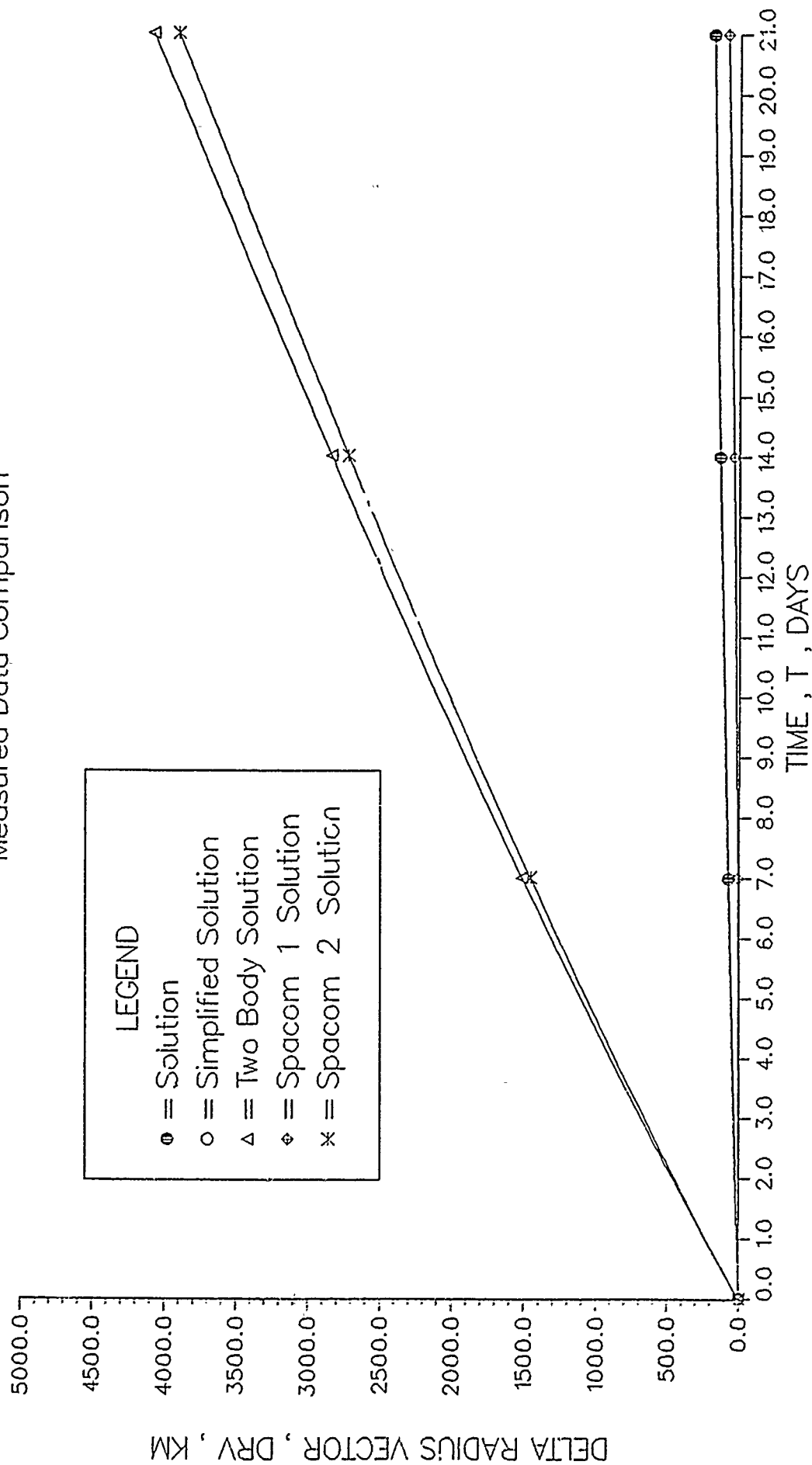


Figure 32. Delta radius vector (21 days)

EARTH ARC ANGLE

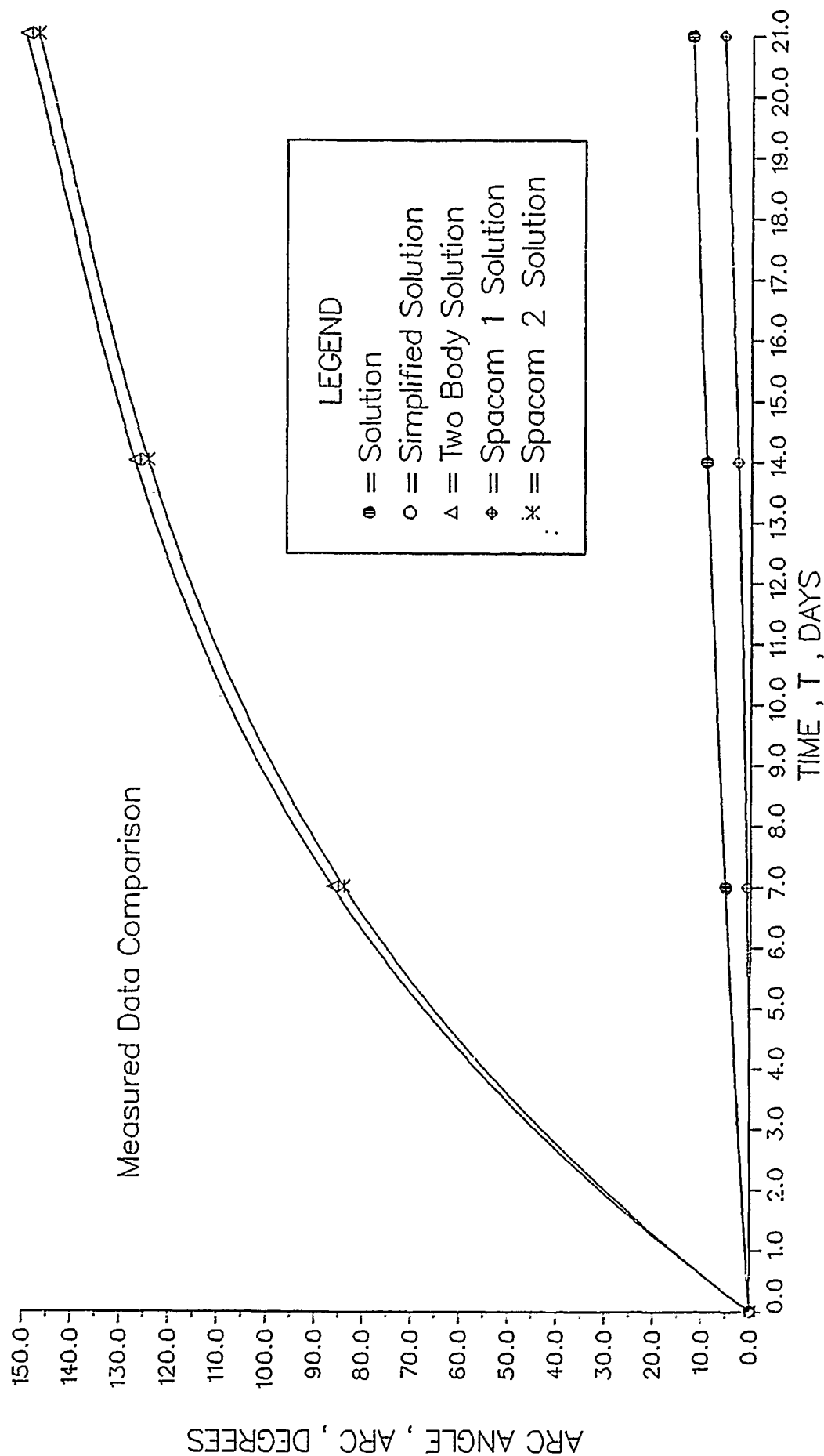


Figure 33. Earth arc angle (21 days)

DELTA OMEGA

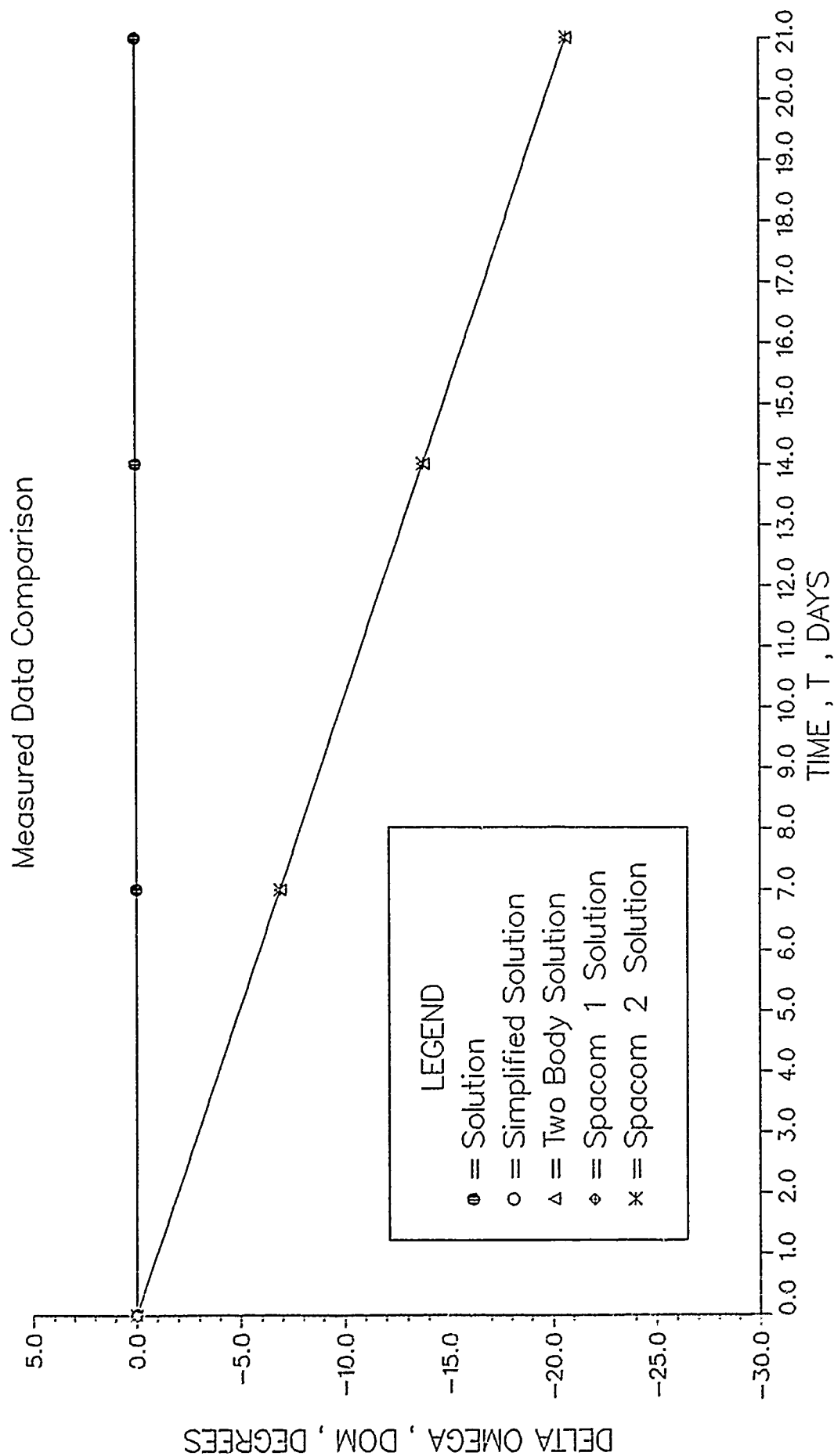


Figure 34. Delta omega (21 days)

DELTA OMEGA

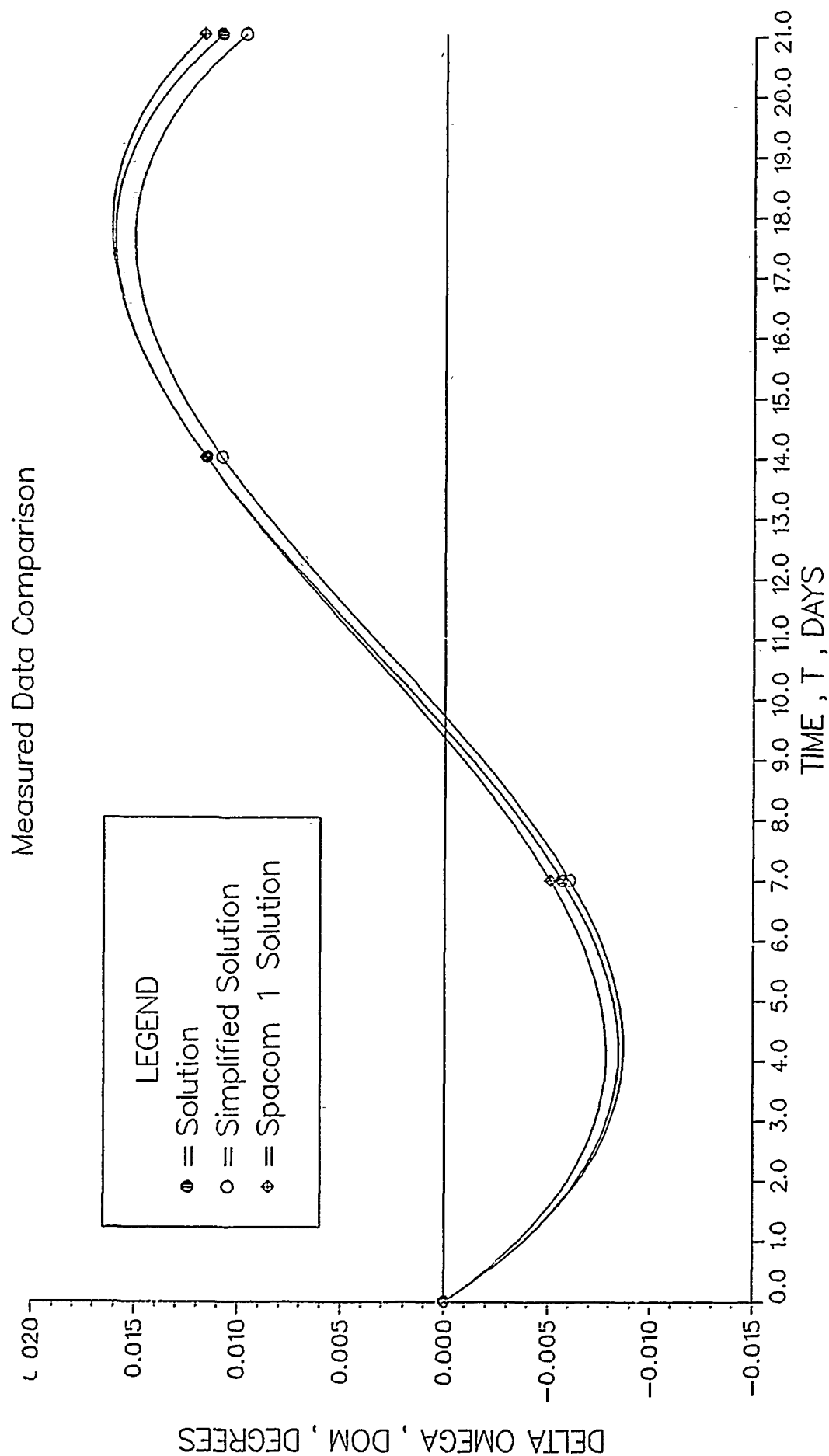


Figure 35. ,Delta omega (21 days)

DELTA INCLINATION

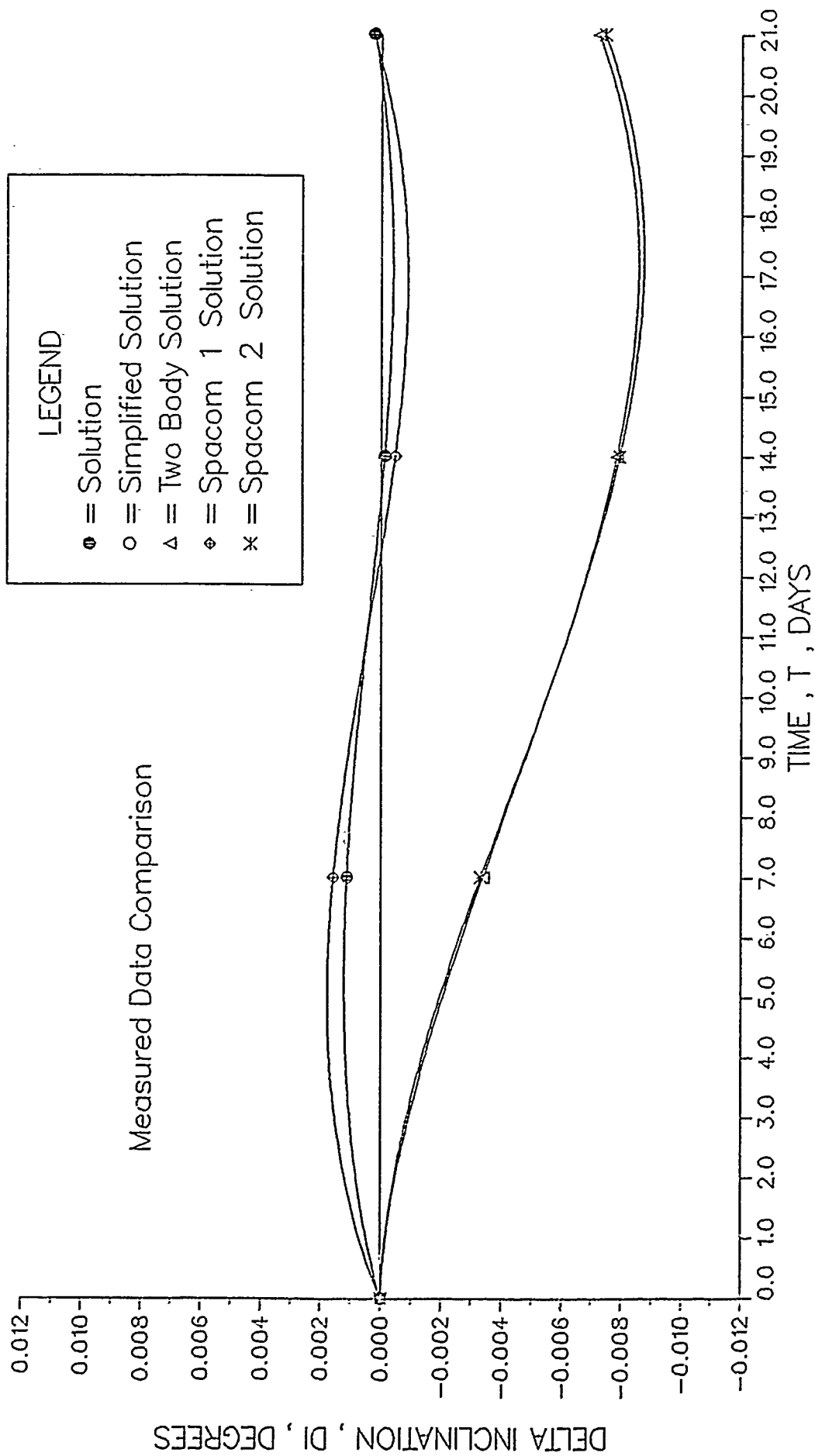


Figure 36. Delta inclination (21 days)

DELTA THETA

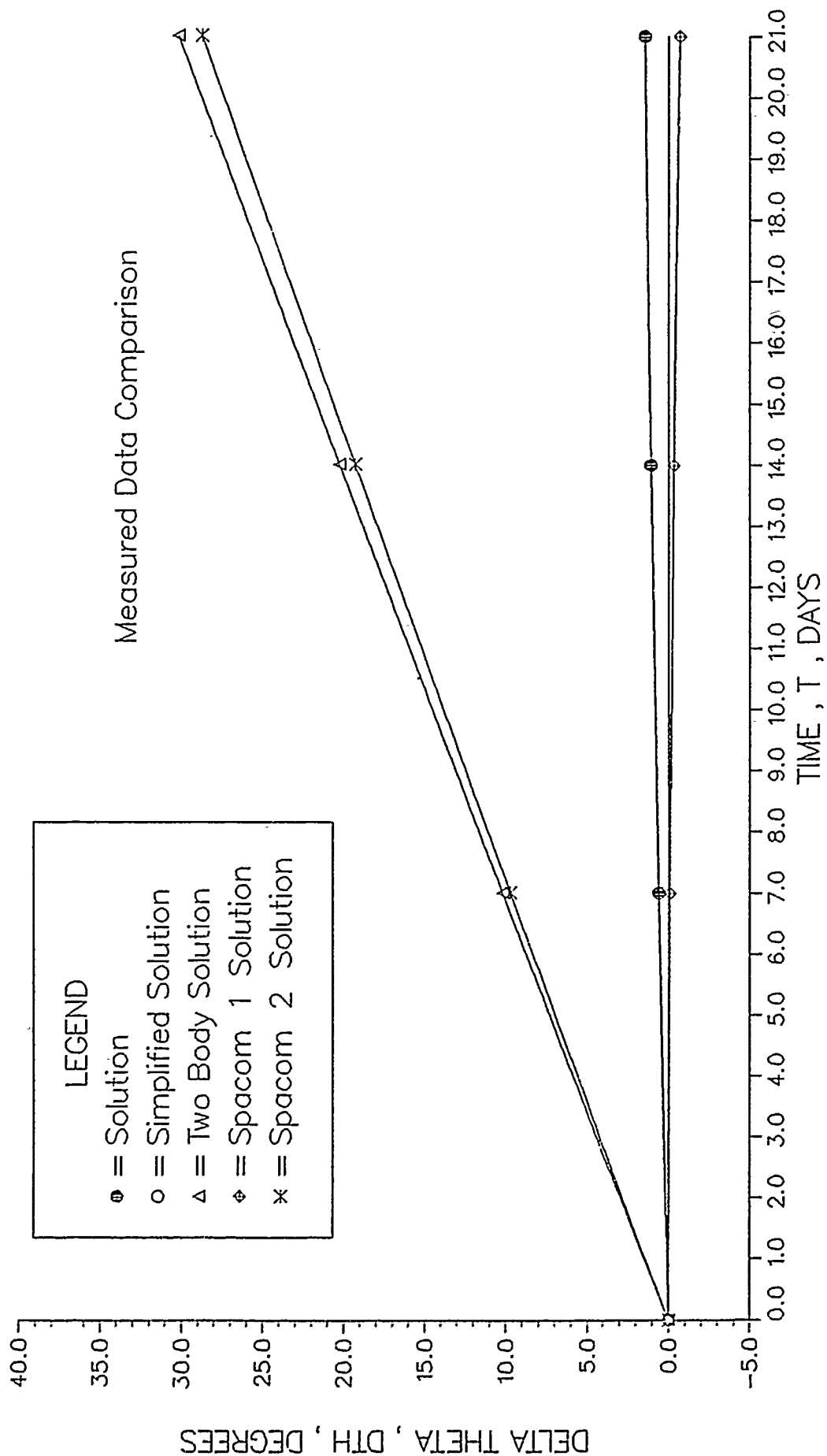


Figure 37. Delta theta (21 days)

DELTA THETA RELATIVE ERROR

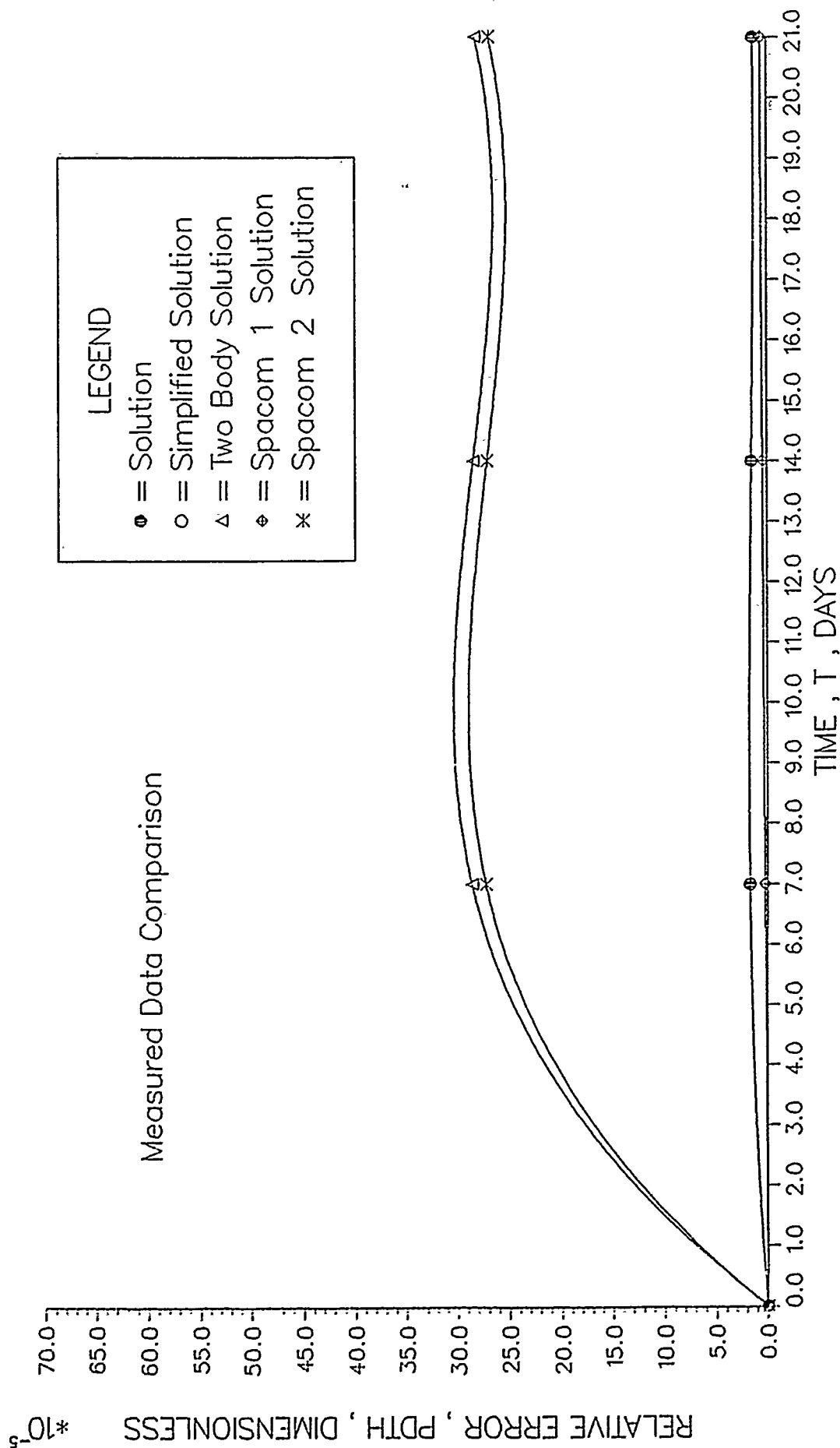


Figure 38. Delta theta relative error (21 days)

DELTA RADIUS RELATIVE ERROR

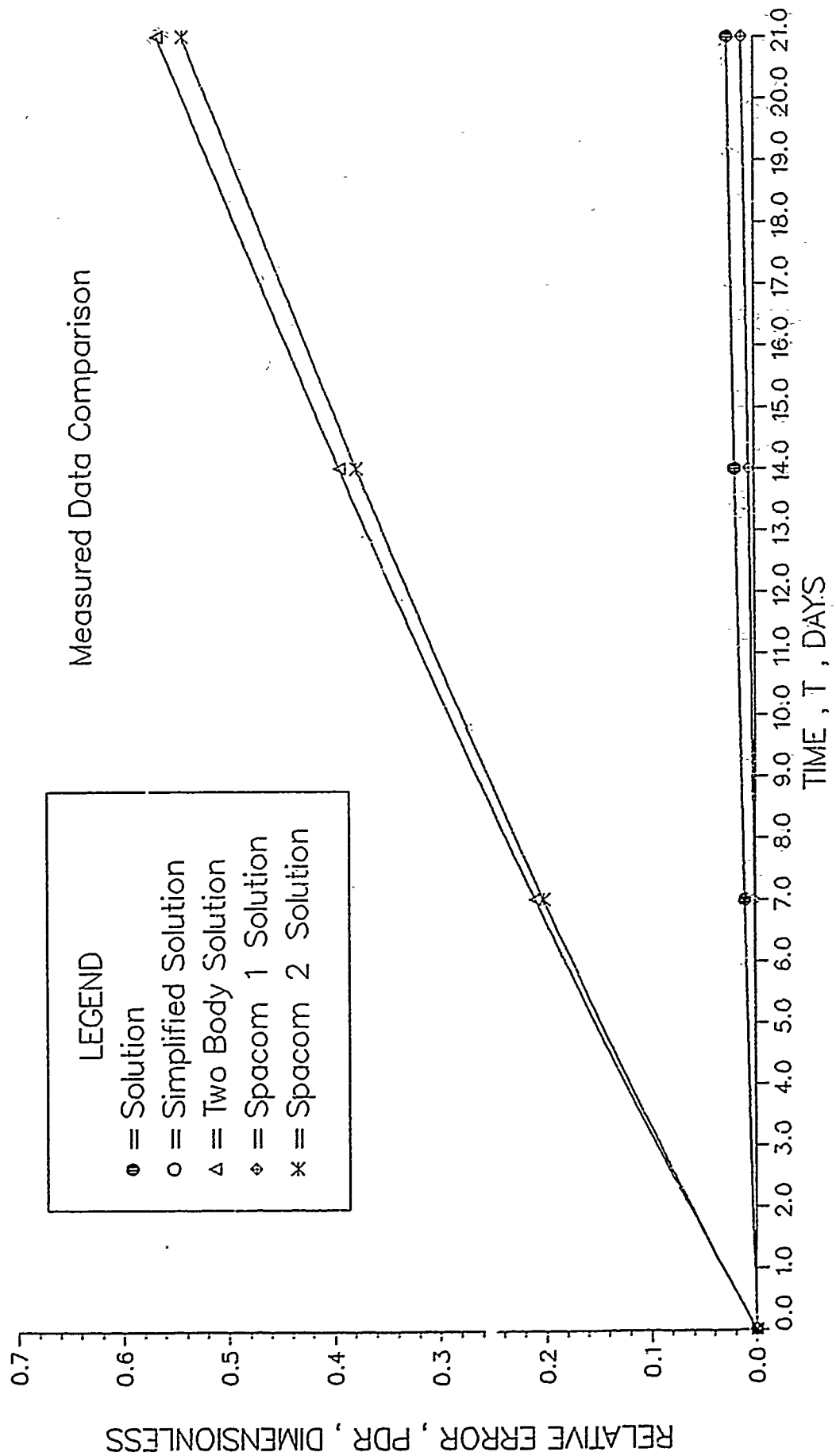


Figure 39. Delta radius relative error (21 days)

RADIAL TRACK ERROR

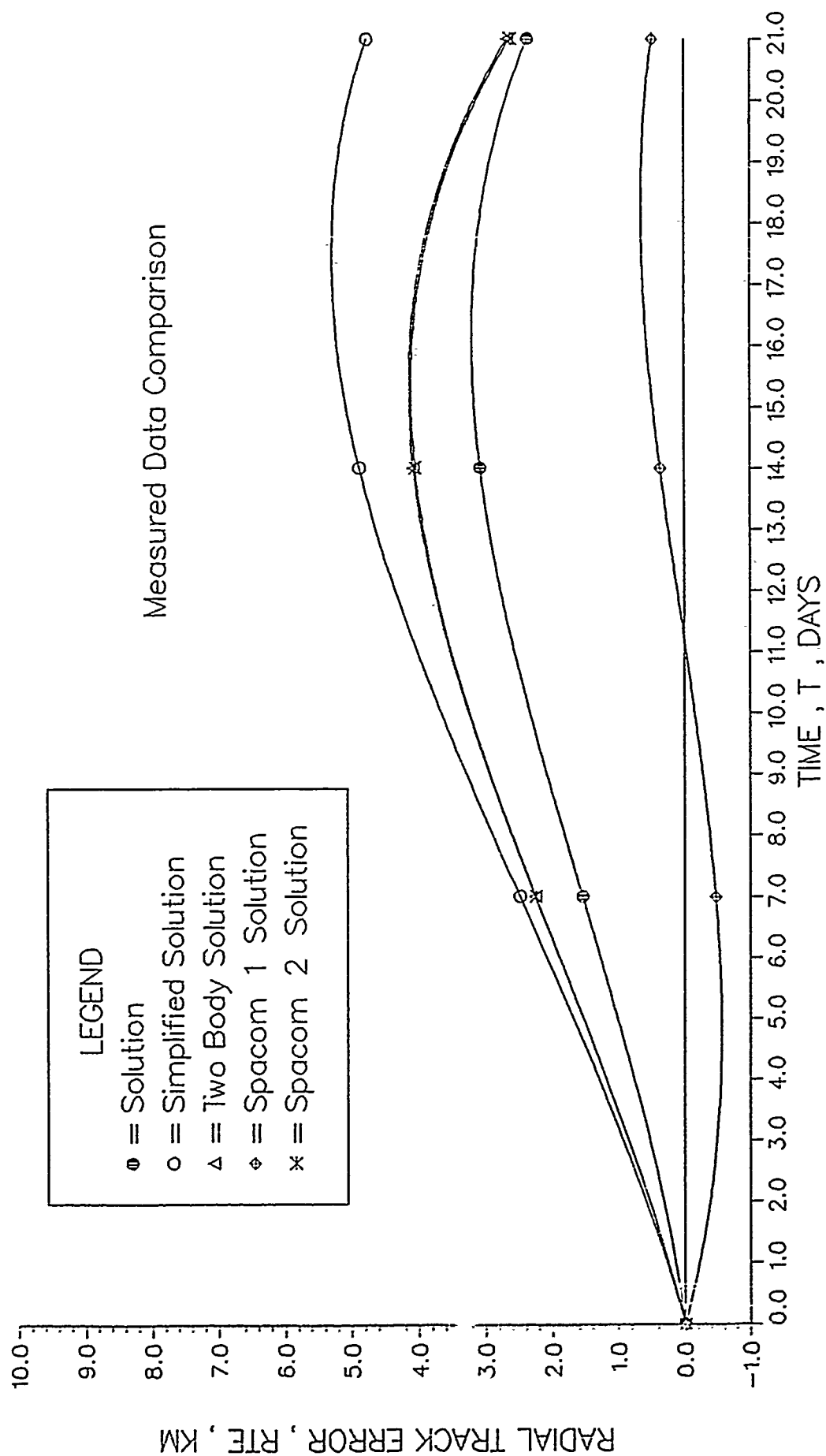


Figure 40. Radial track error (21 days)

ALONG TRACK ERROR

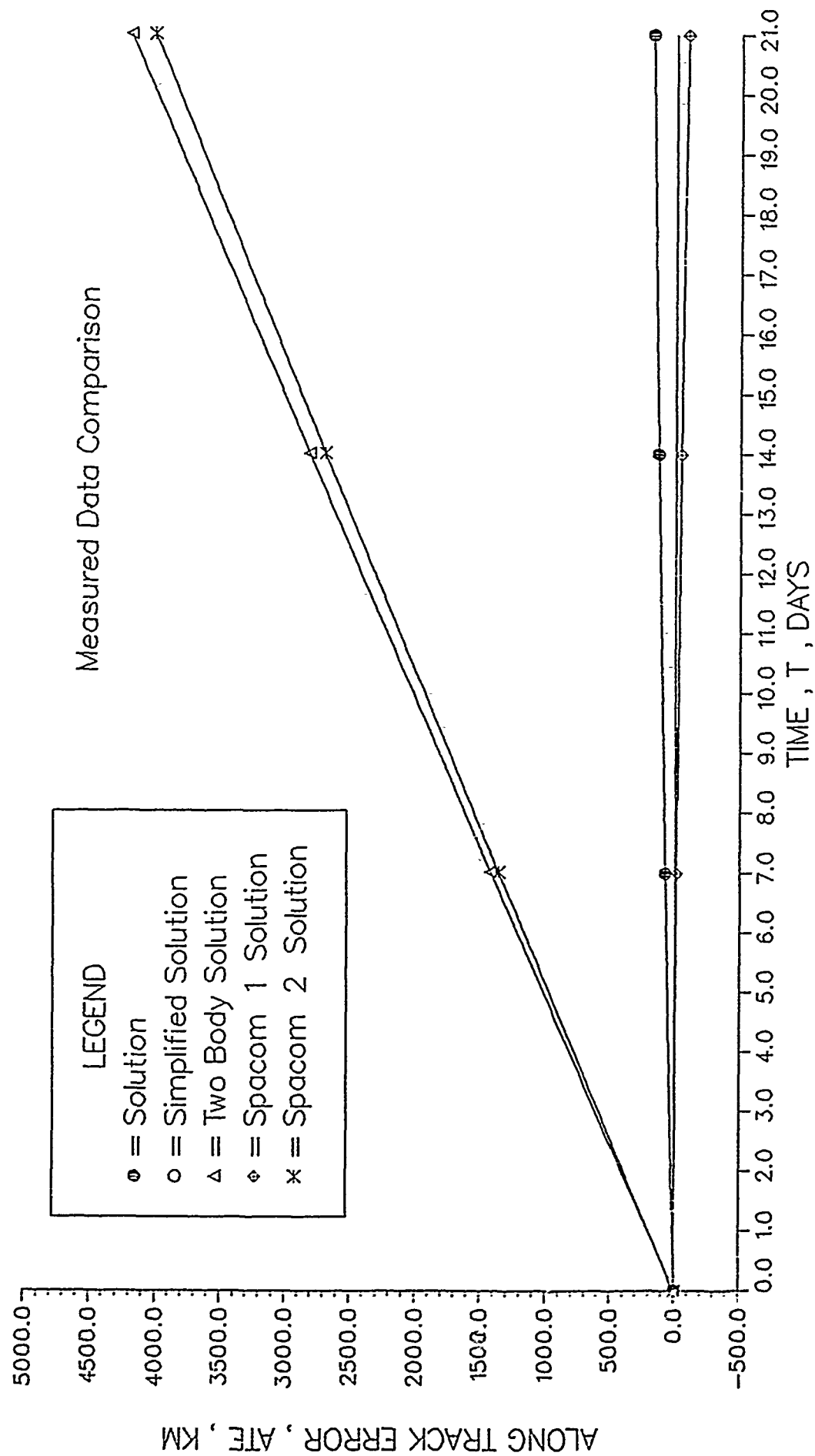


Figure 41. Along track error (21 days)

CROSS TRACK ERROR

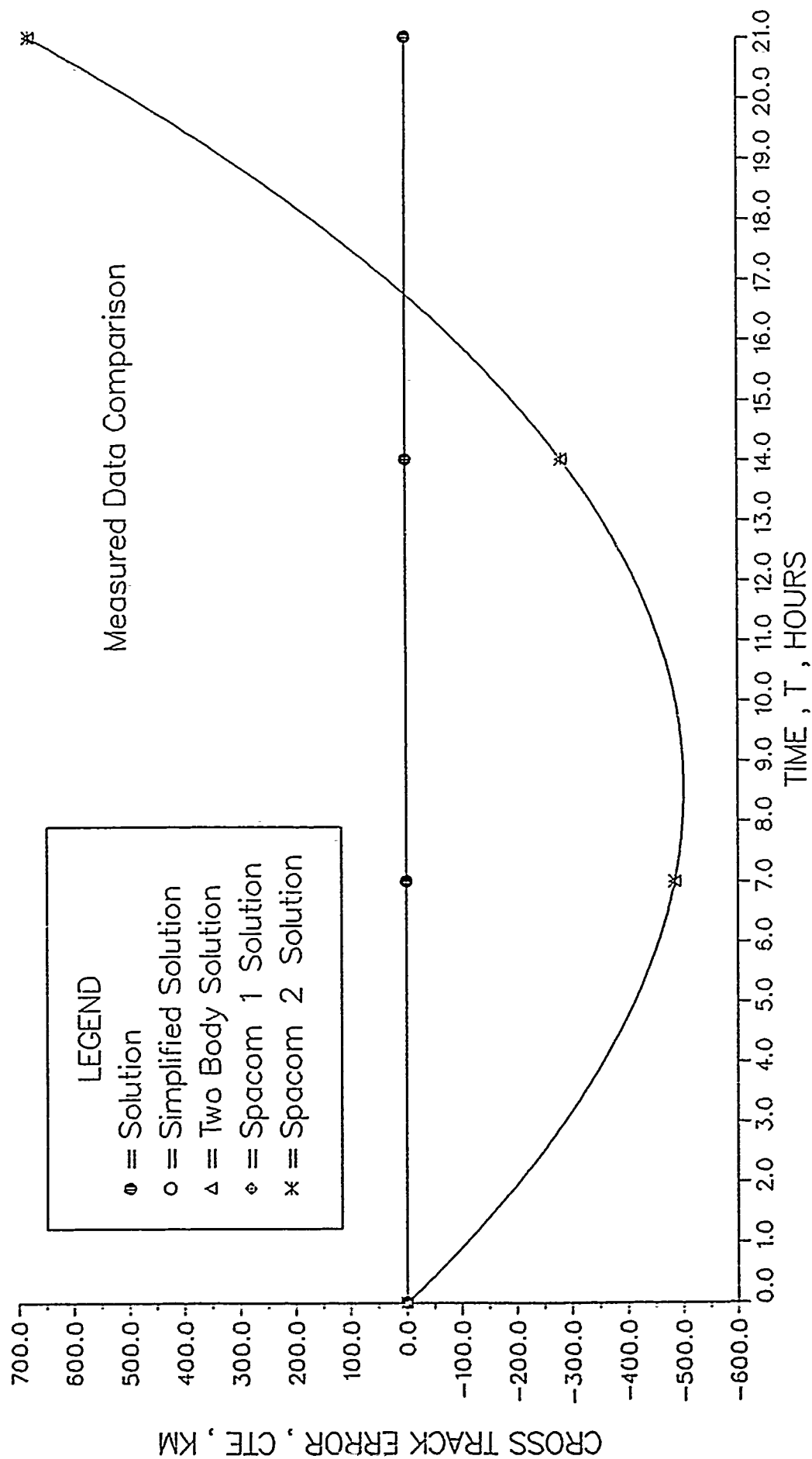


Figure 42. Cross track error (21 days)

CROSS TRACK ERROR

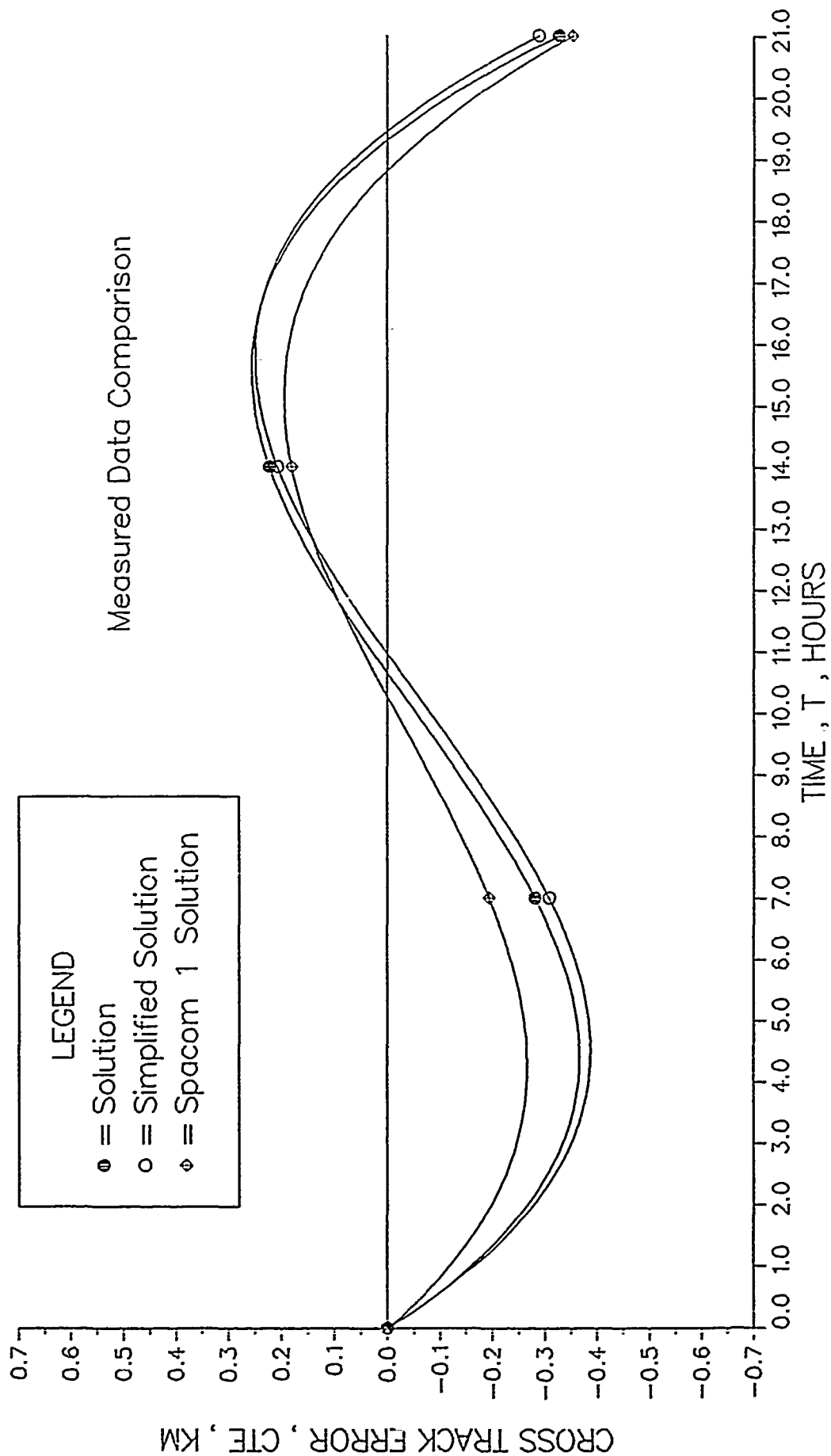


Figure 43. Cross track error (21 days)

APPENDIX C. SEMISYNCHRONOUS ORBIT COMPARISON RESULTS

DELTA RADIUS VECTOR

Measured Data Comparison

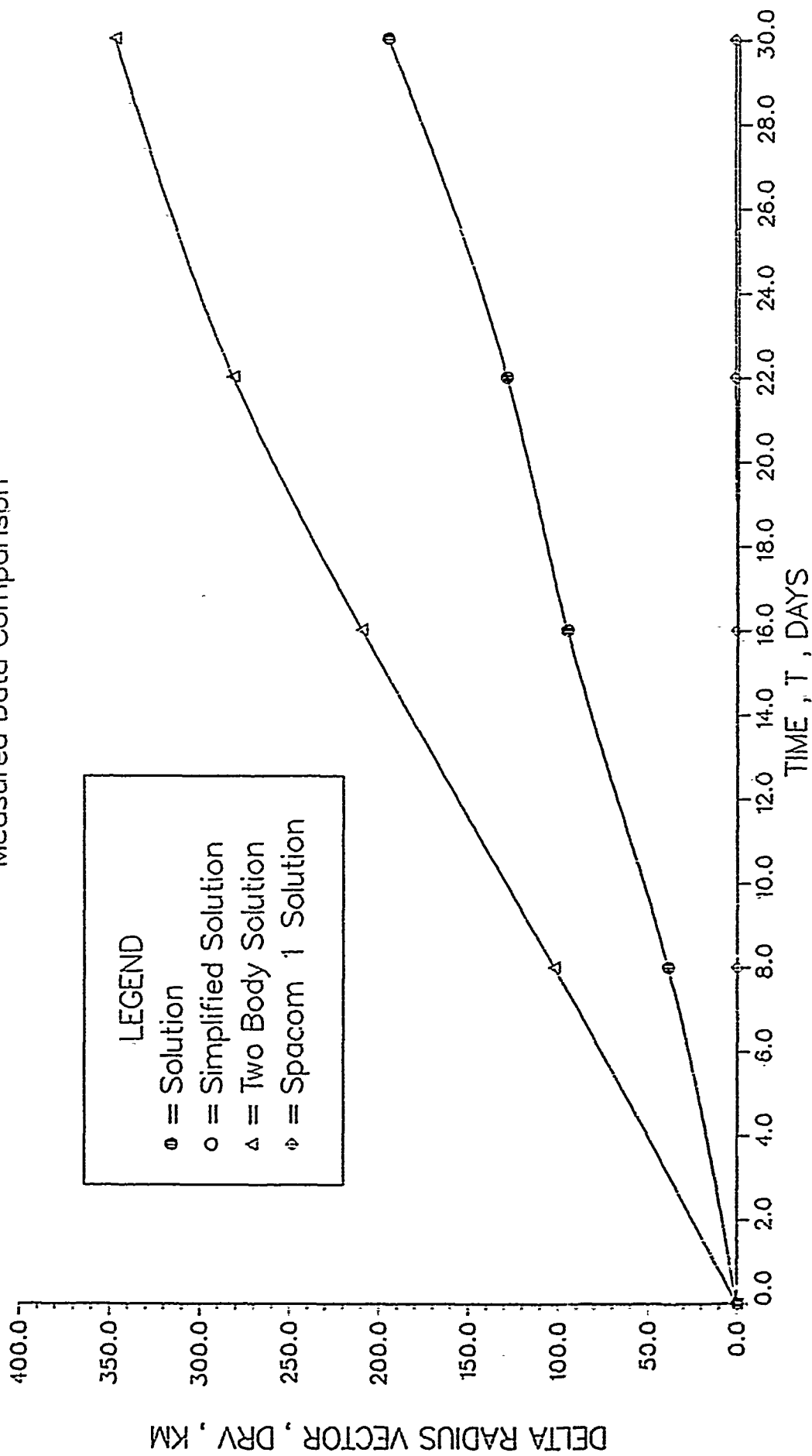


Figure 44. Delta radius vector (30 days)

EARTH ARC ANGLE

Measured Data Comparison

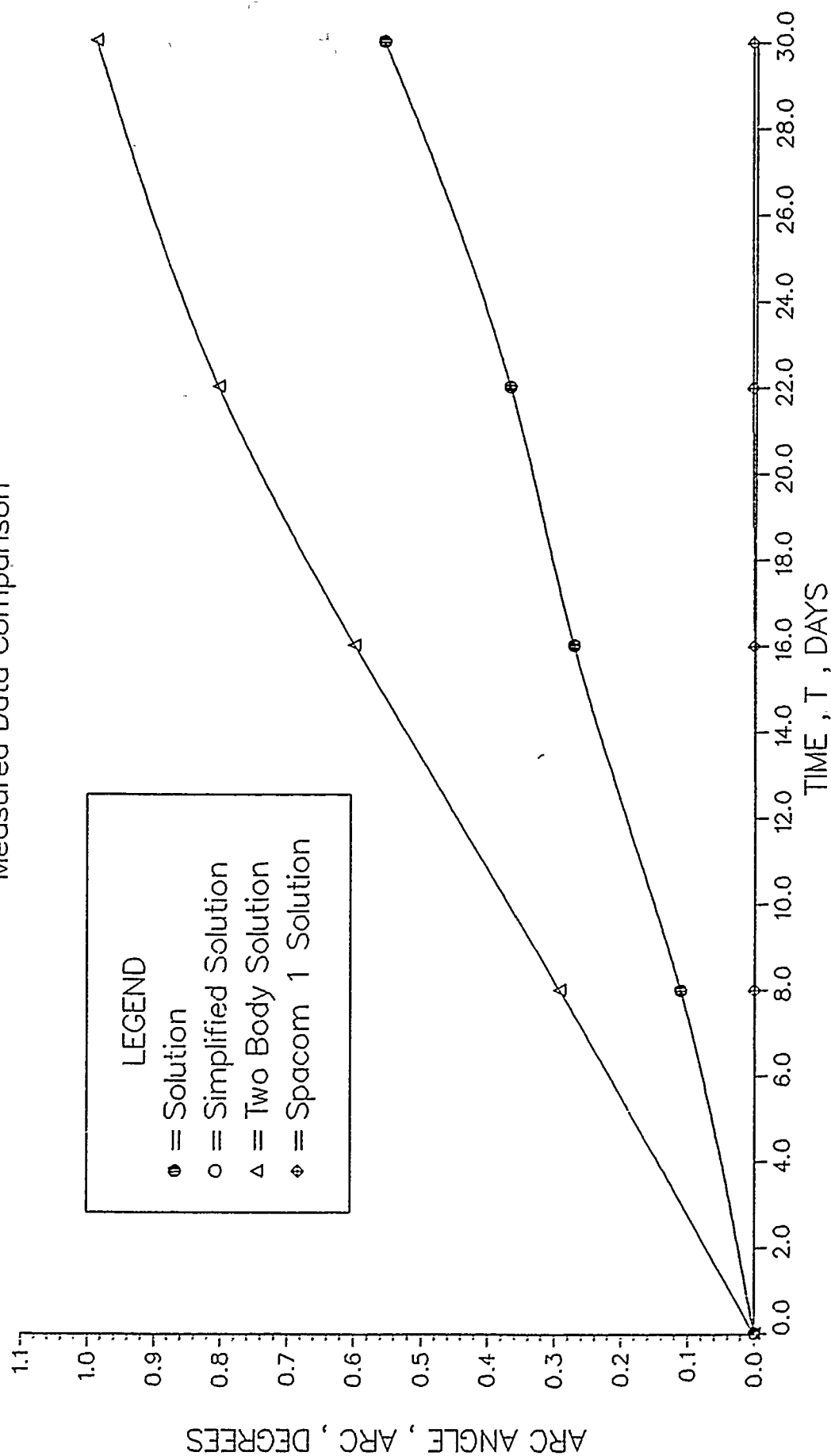


Figure 45. Earth arc angle (30 days)

DELTA OMEGA

Measured Data Comparison

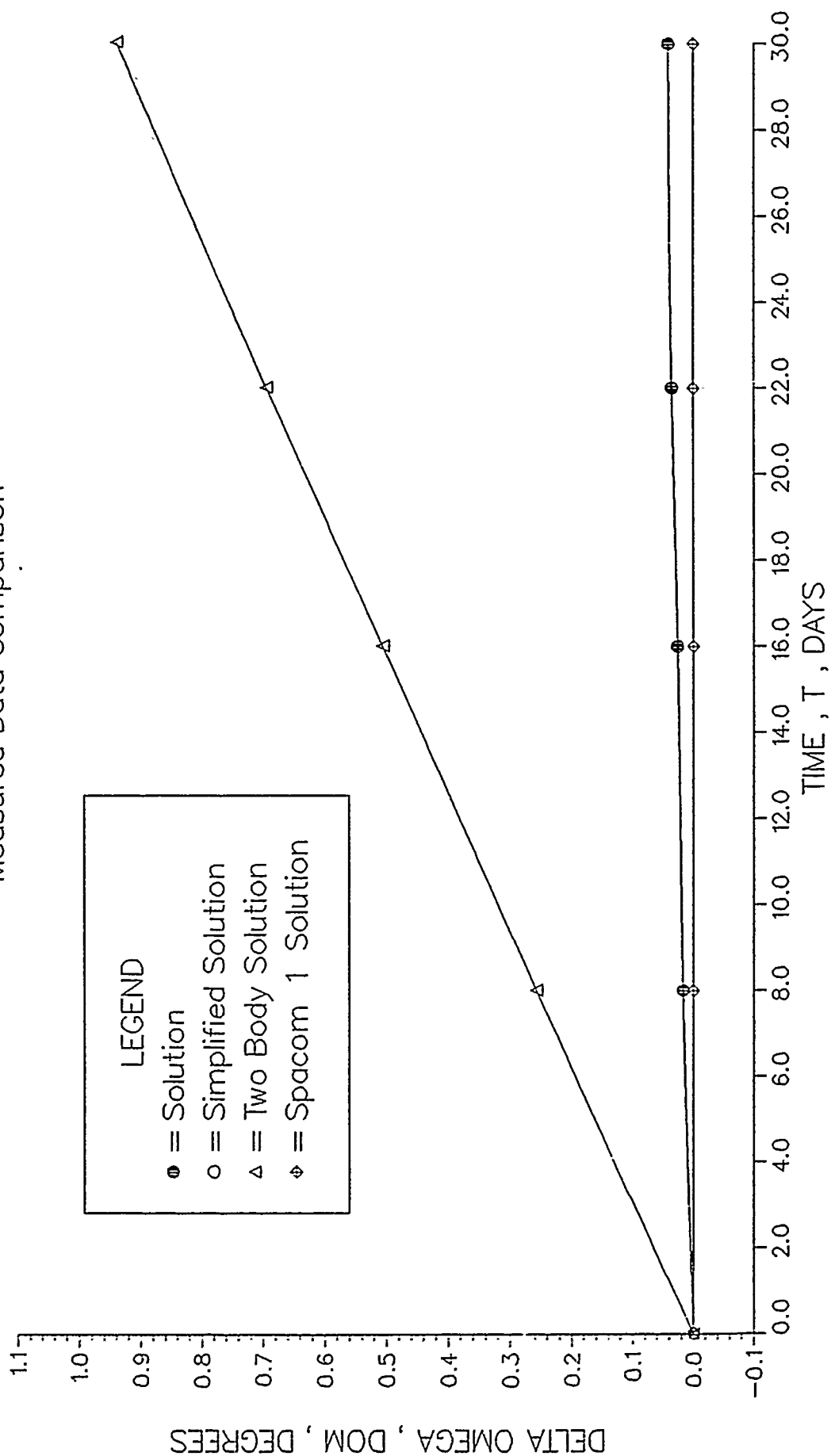


Figure 46, Delta omega (30 days)

DELTA INCLINATION

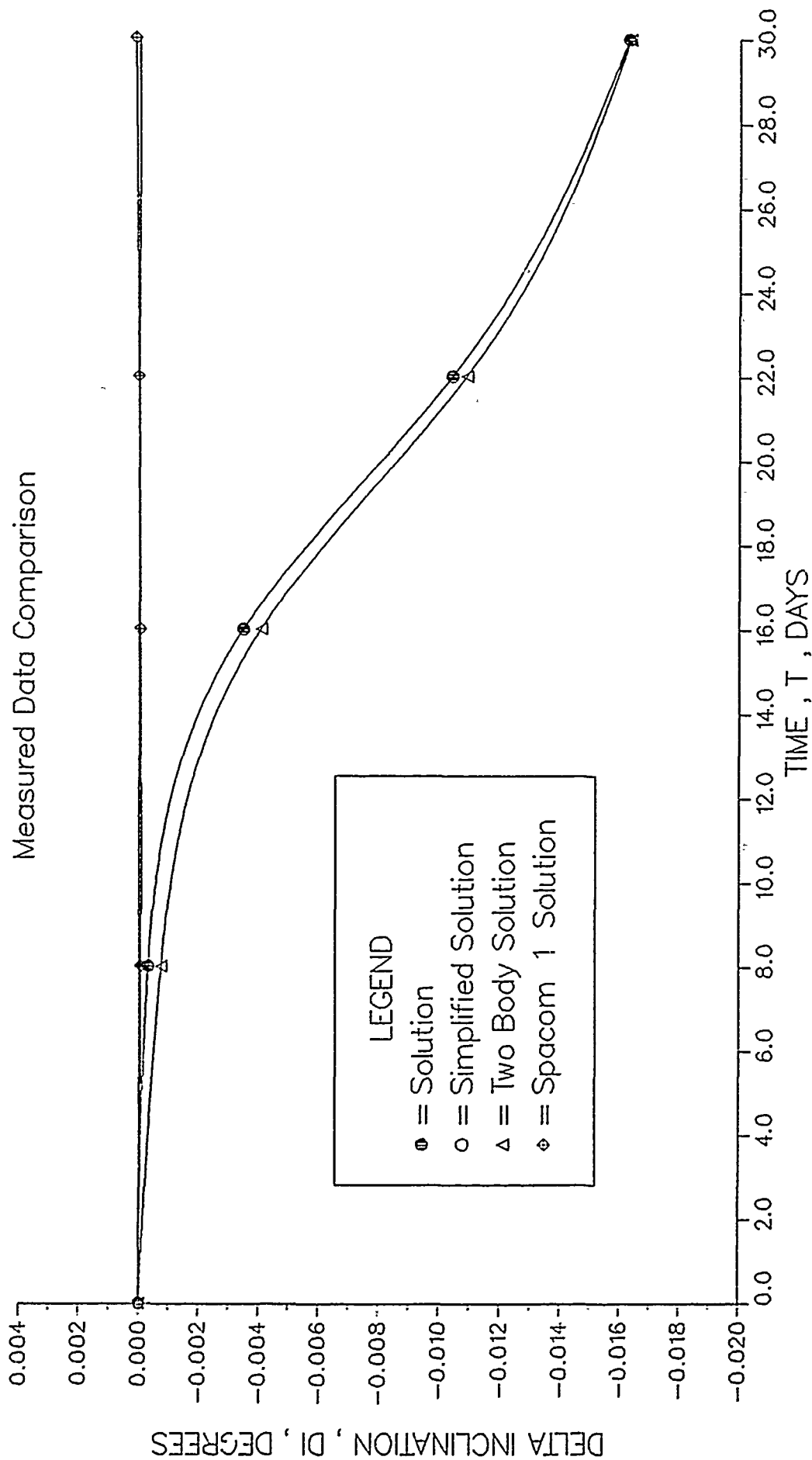


Figure 47. Delta inclination (30 days)

DELTA THETA

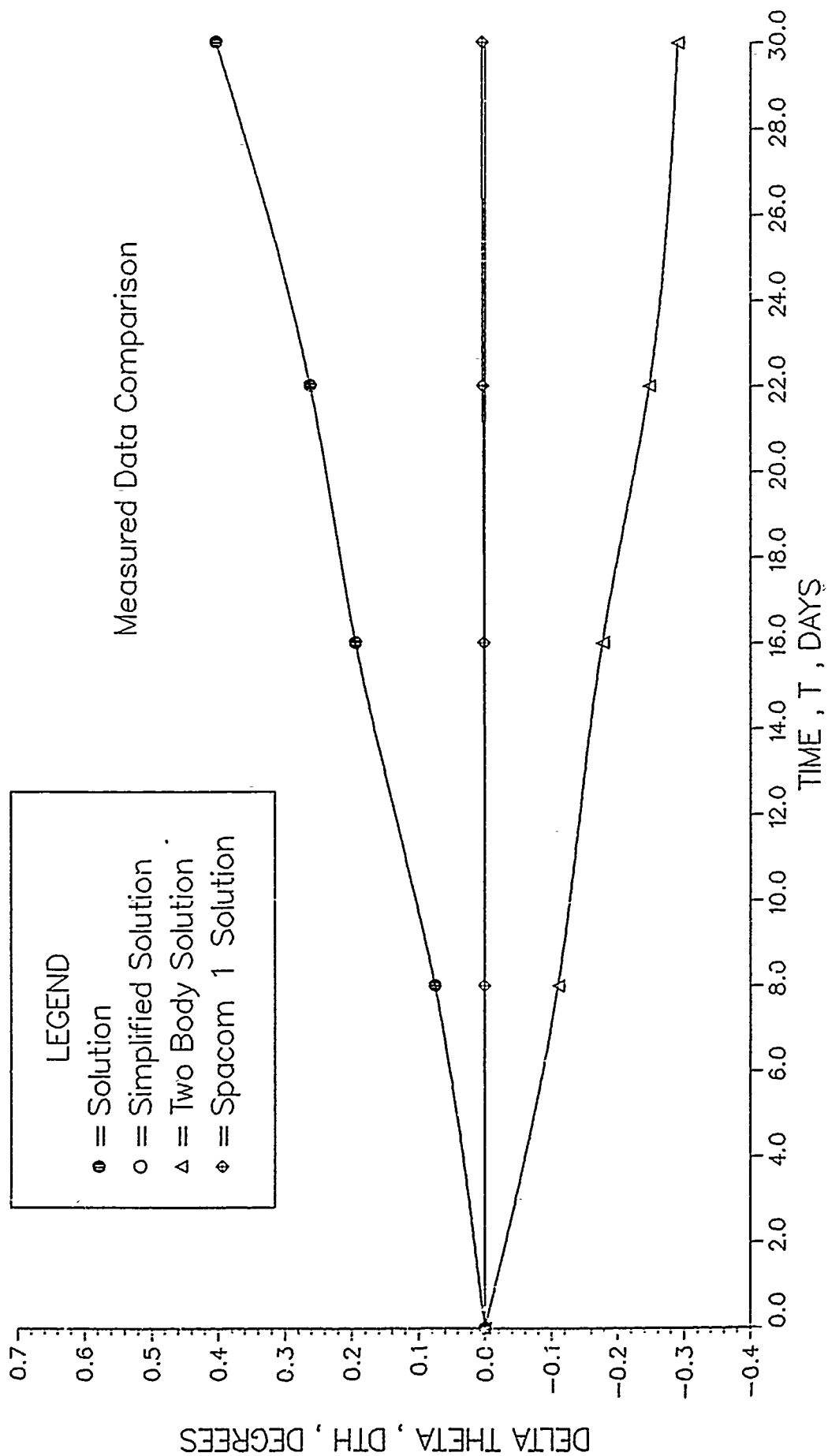


Figure 48. Delta theta (30 days)

DELTA THETA RELATIVE ERROR

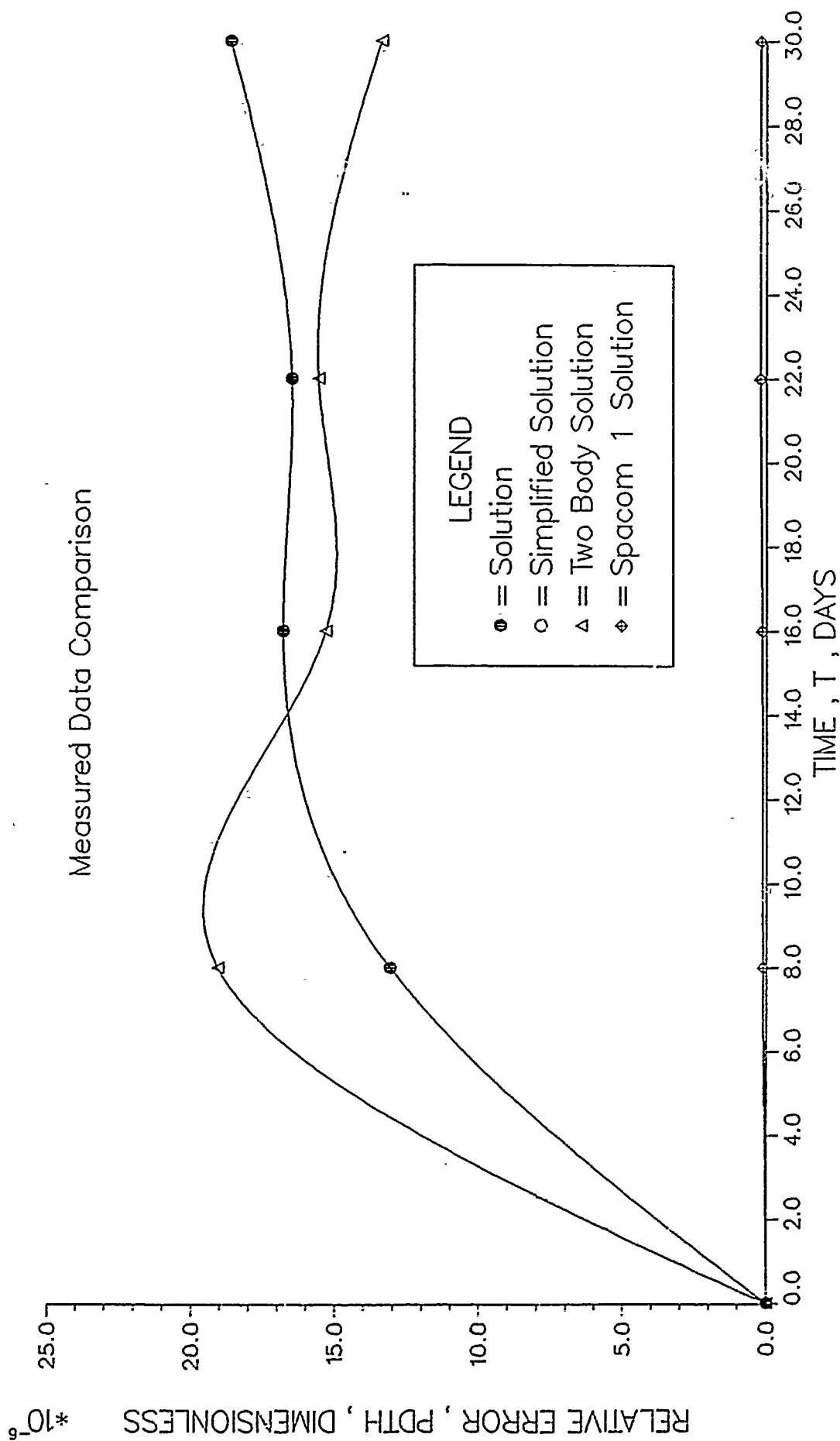


Figure 49. Delta theta relative error (30 days)

DELTA RADIUS RELATIVE ERROR

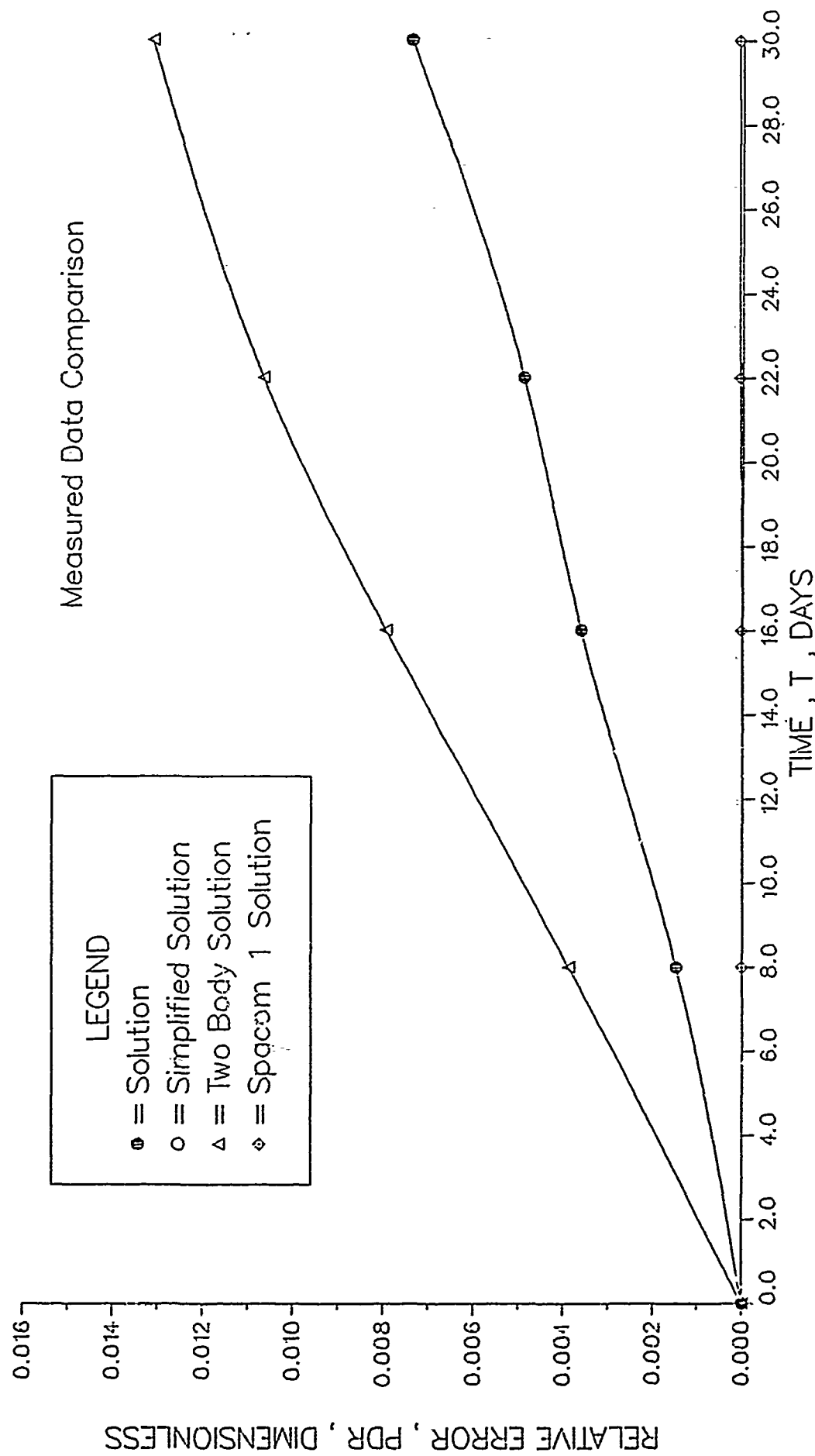


Figure 50. Delta radius relative error (30 days)

ALONG TRACK ERROR

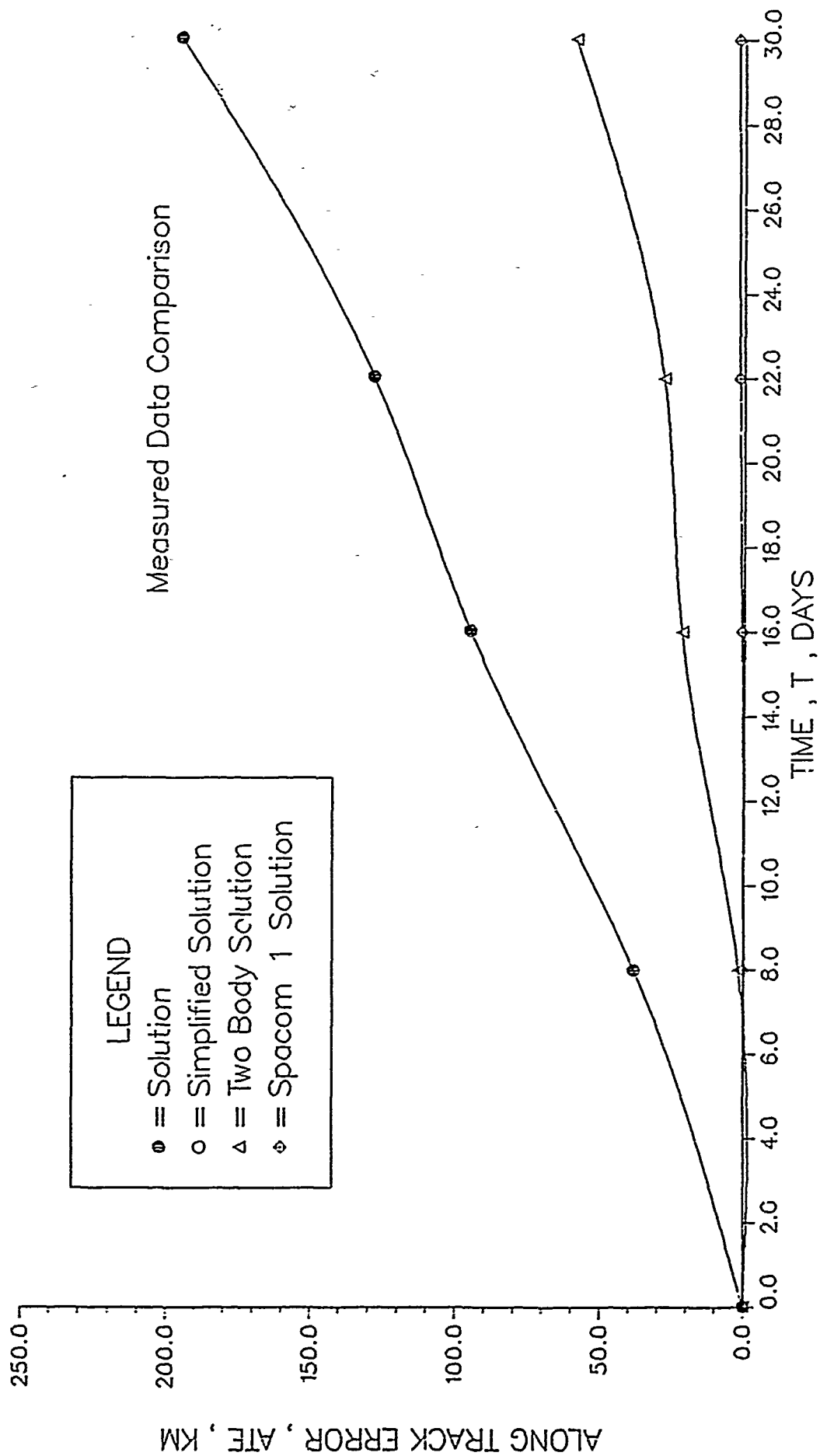


Figure 52. . Along track error (30 days)

CROSS TRACK ERROR

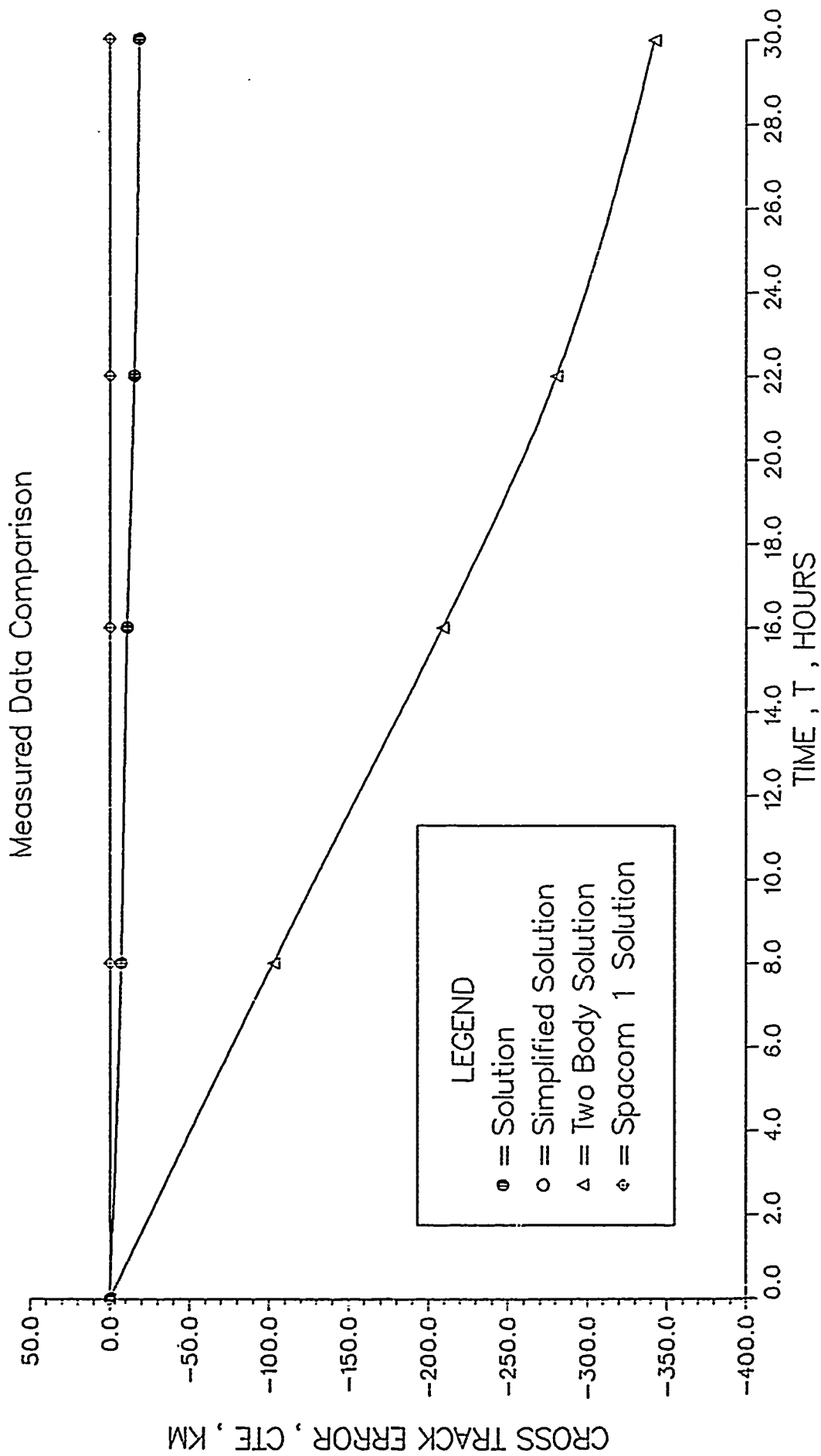


Figure 53. Cross track error (30 days)

APPENDIX D. GEOSYNCHRONOUS ORBIT COMPARISON RESULTS

DELTA RADIUS VECTOR

Measured Data Comparison

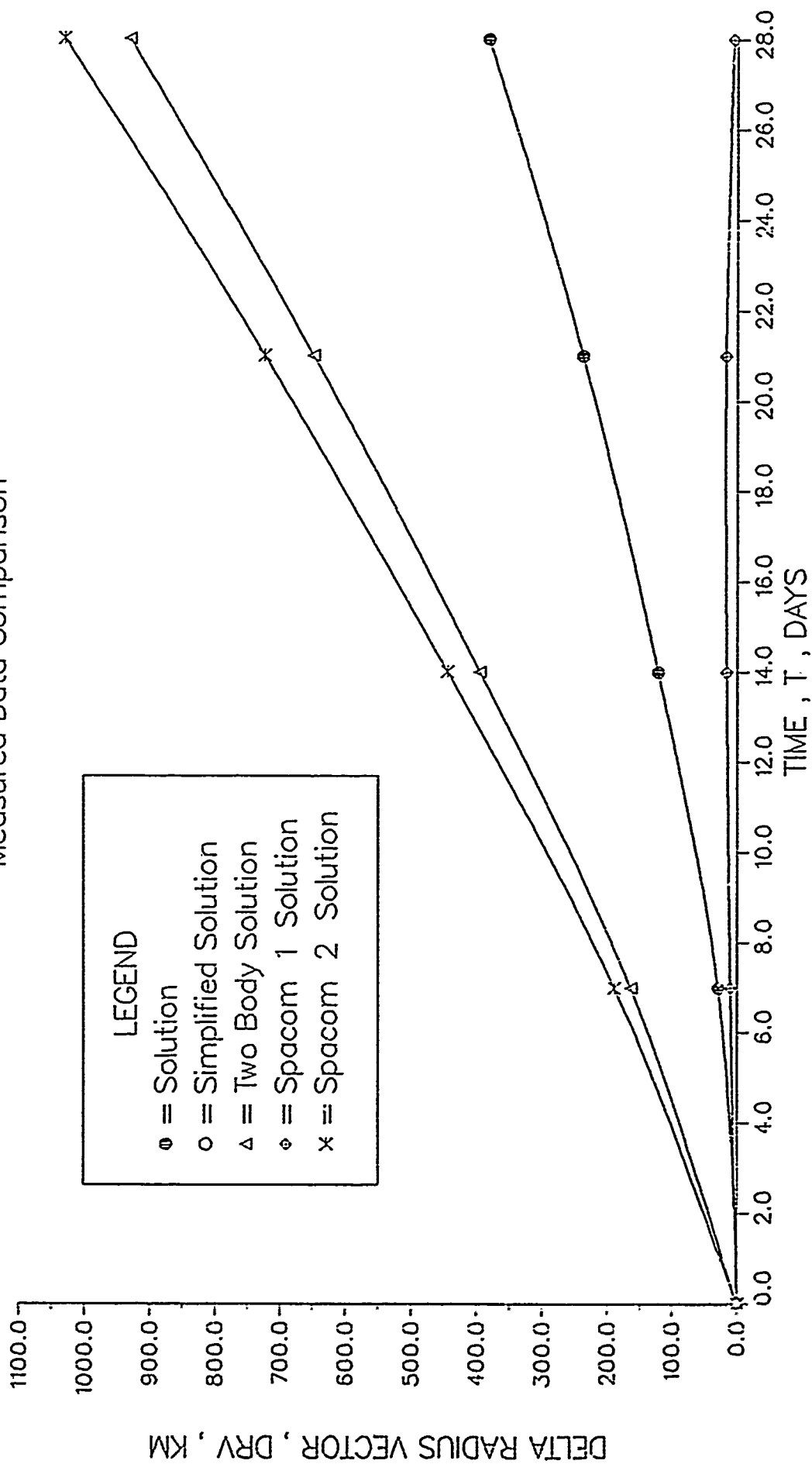


Figure 54. Delta radius vector (28 days)

EARTH ARC ANGLE

Measured Data Comparison

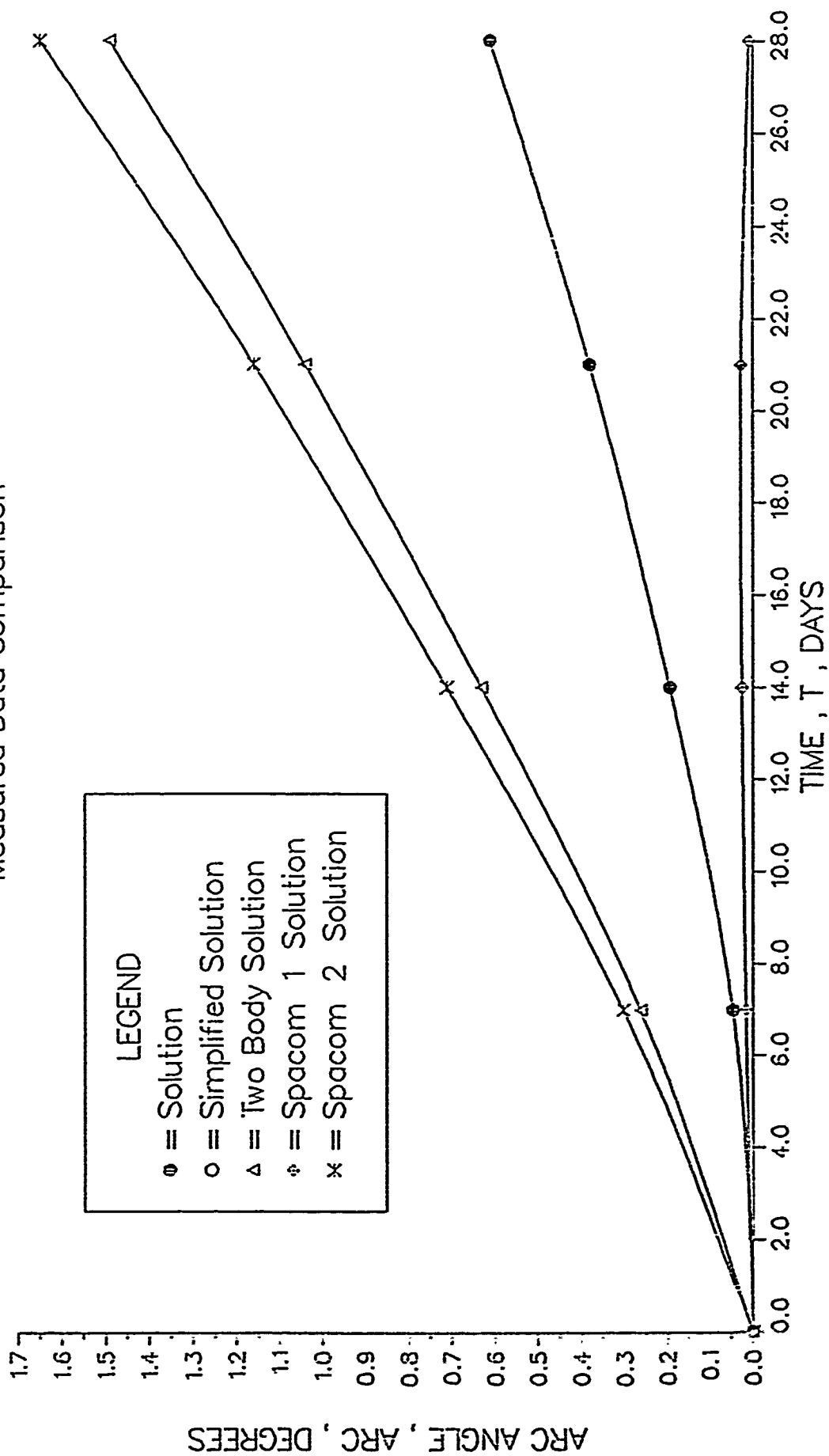


Figure 55. Earth arc angle (28 days)

DELTA OMEGA

Measured Data Comparison

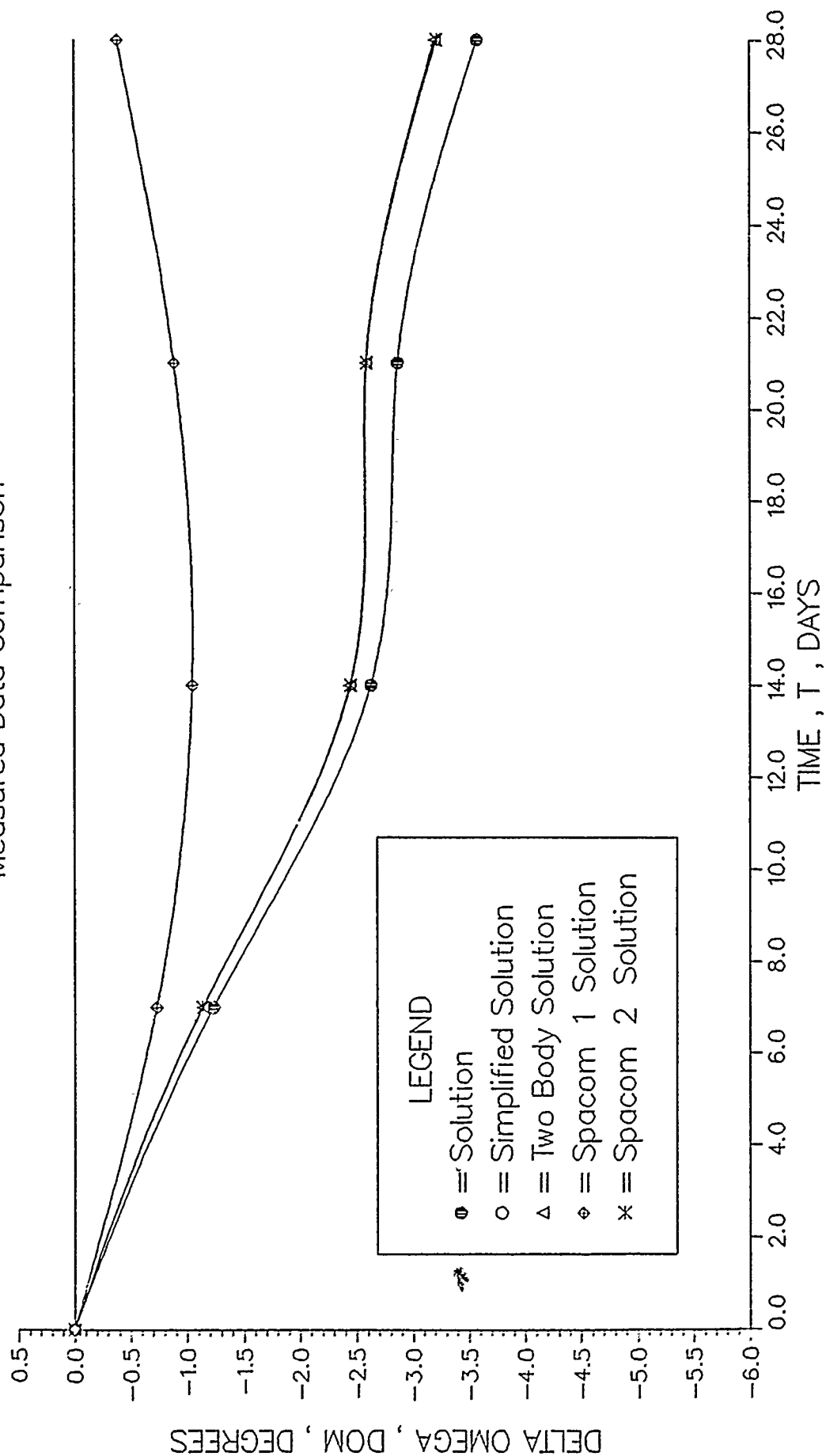


Figure 56. Delta omega (28 days)

DELTA INCLINATION

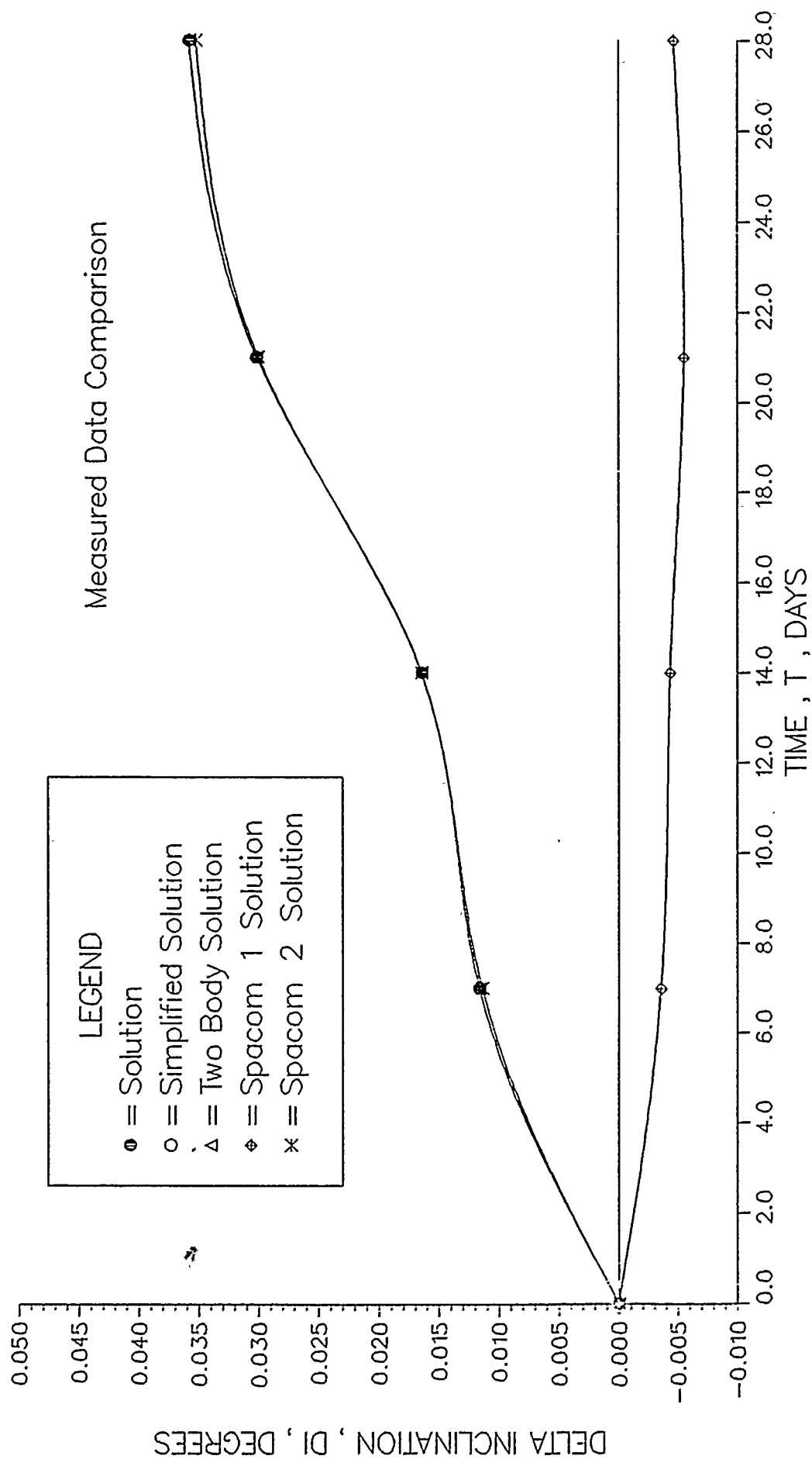


Figure 57. Delta inclination (28 days)

DELTA THETA

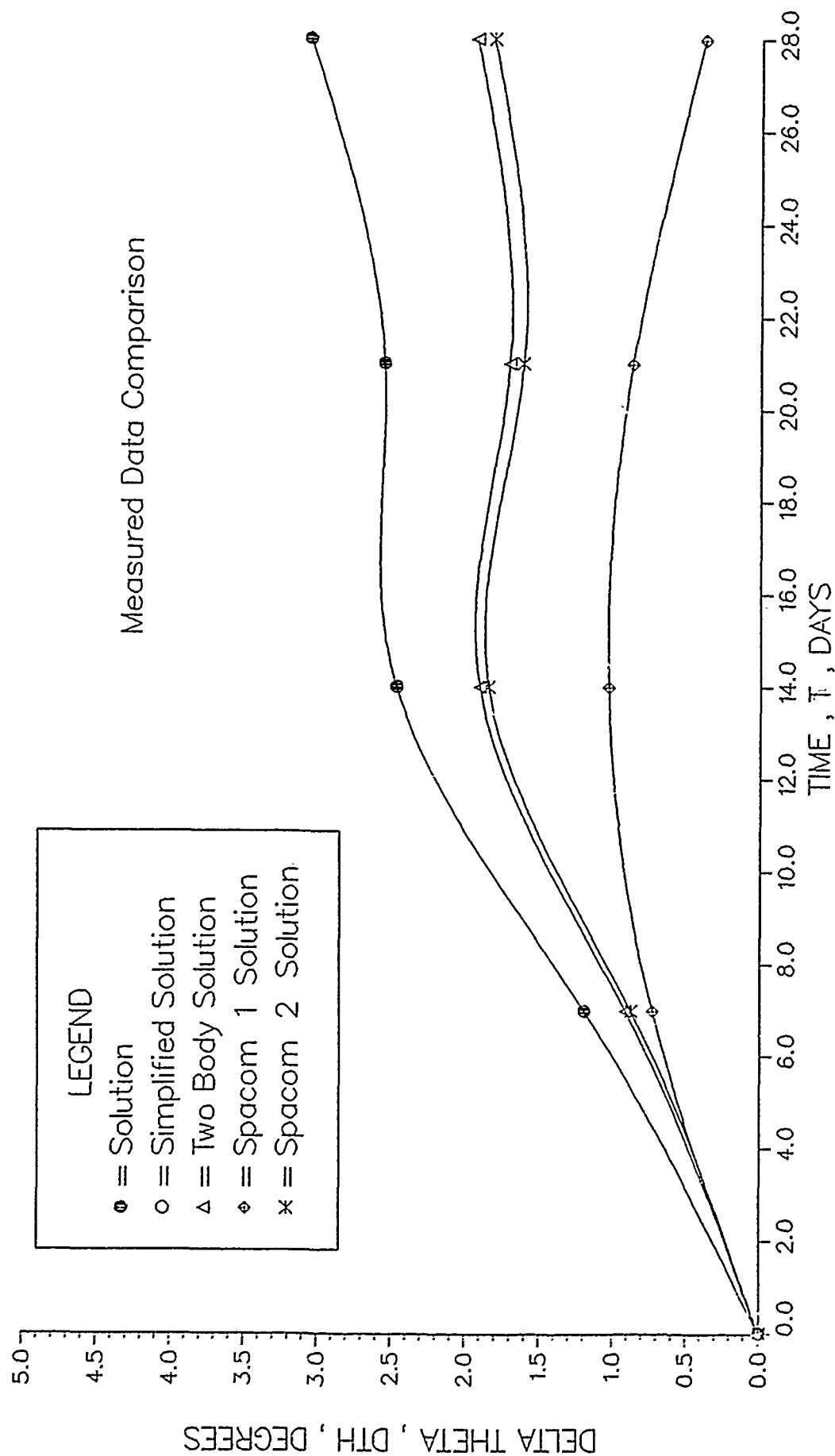


Figure 58. Delta theta (28 days)

DELTA THETA RELATIVE ERROR

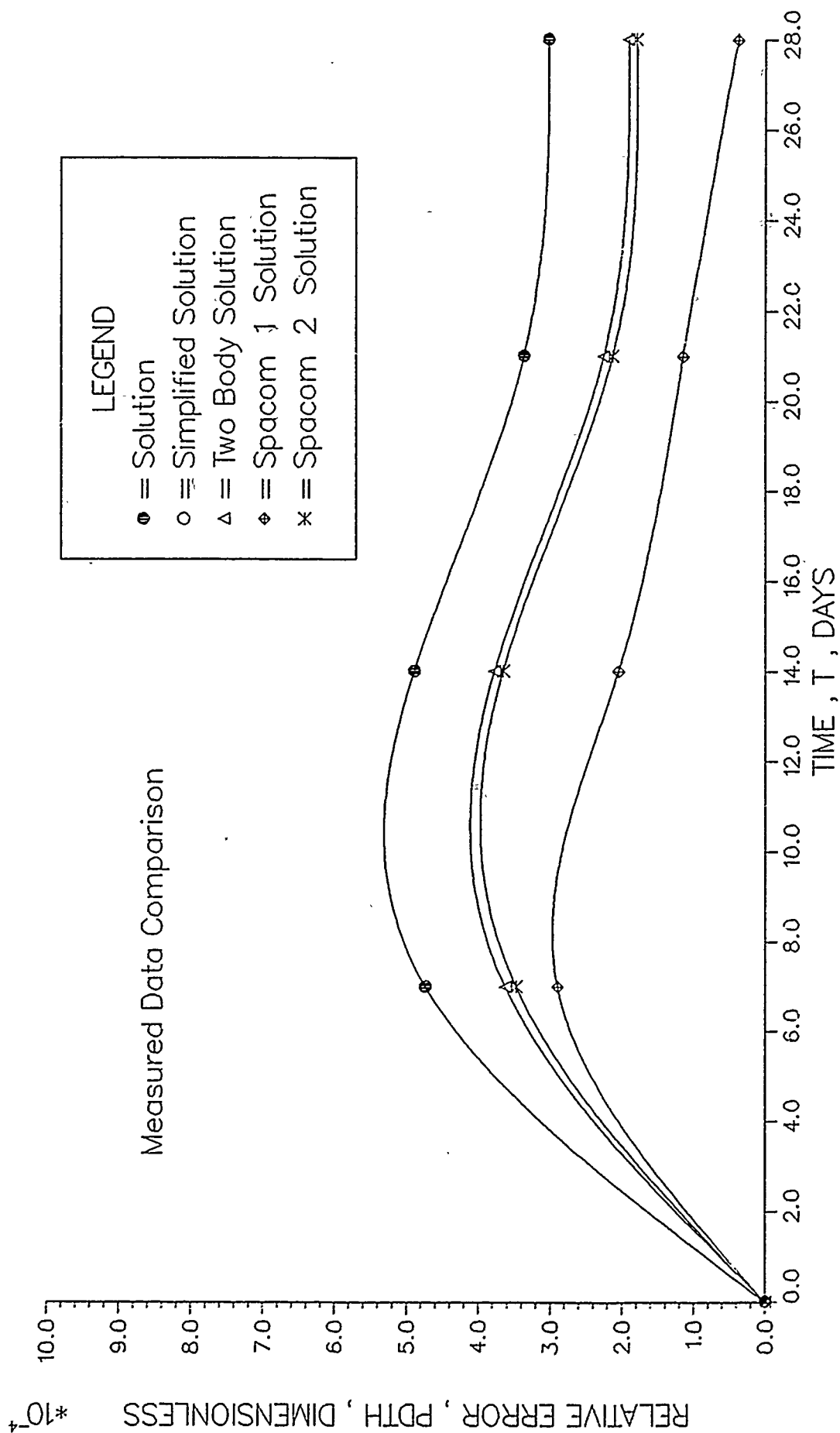


Figure 59. Delta theta relative error (28 days)

DELTA RADIUS RELATIVE ERROR

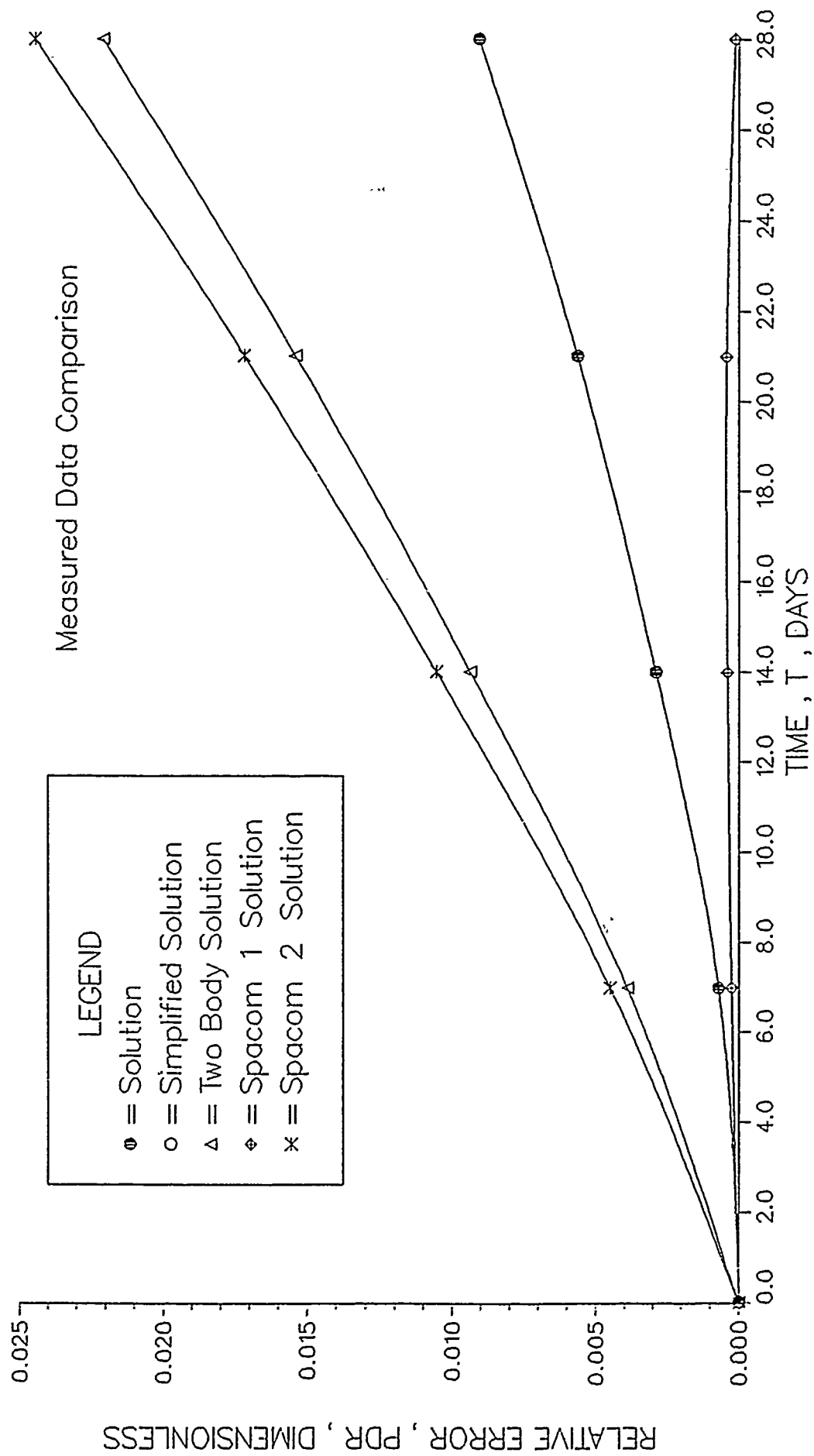


Figure 60. Delta radius relative error (28 days)

RADIAL TRACK ERROR

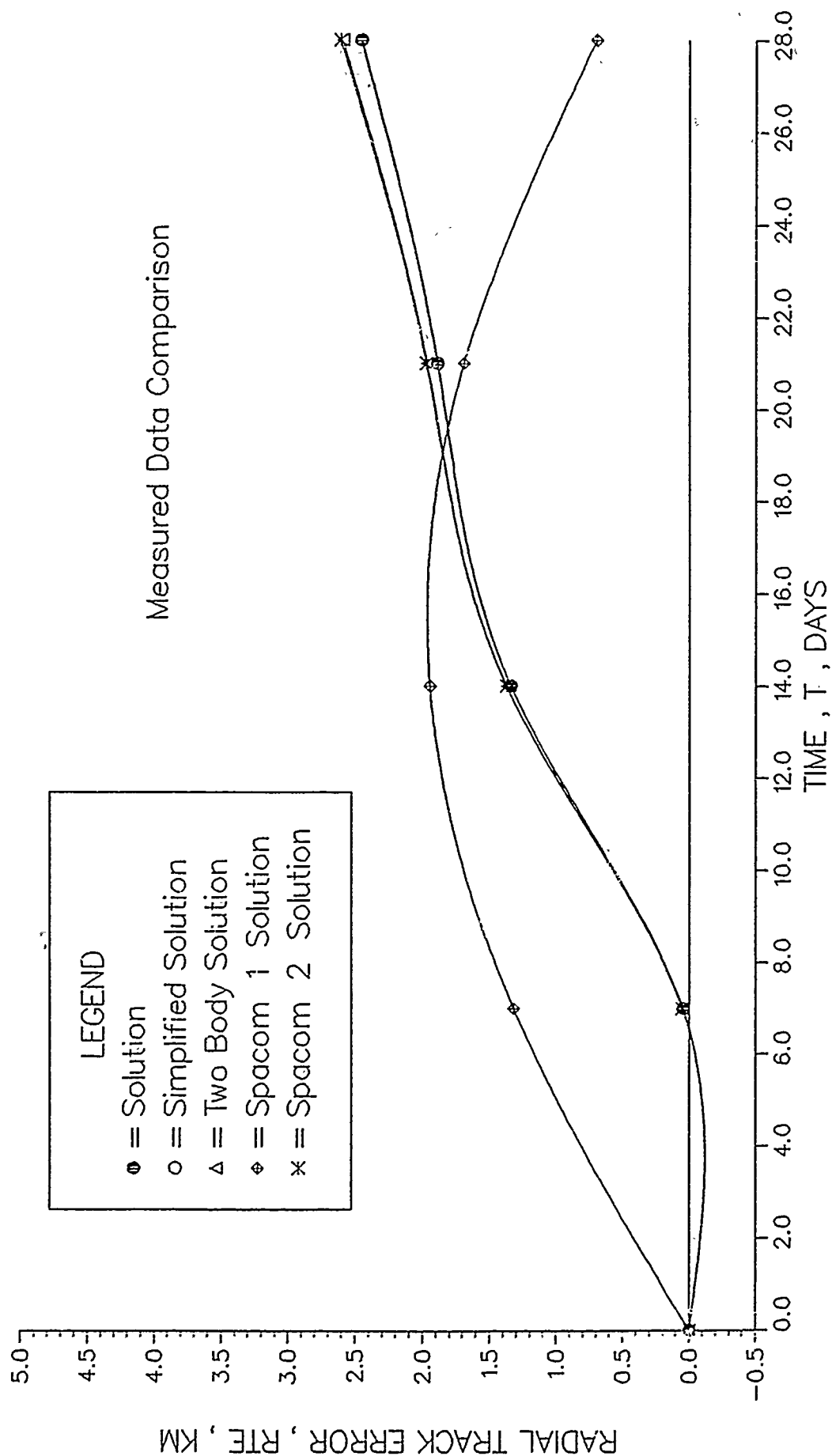


Figure 61. Radial track error (28 days)

ALONG TRACK ERROR

Measured Data Comparison

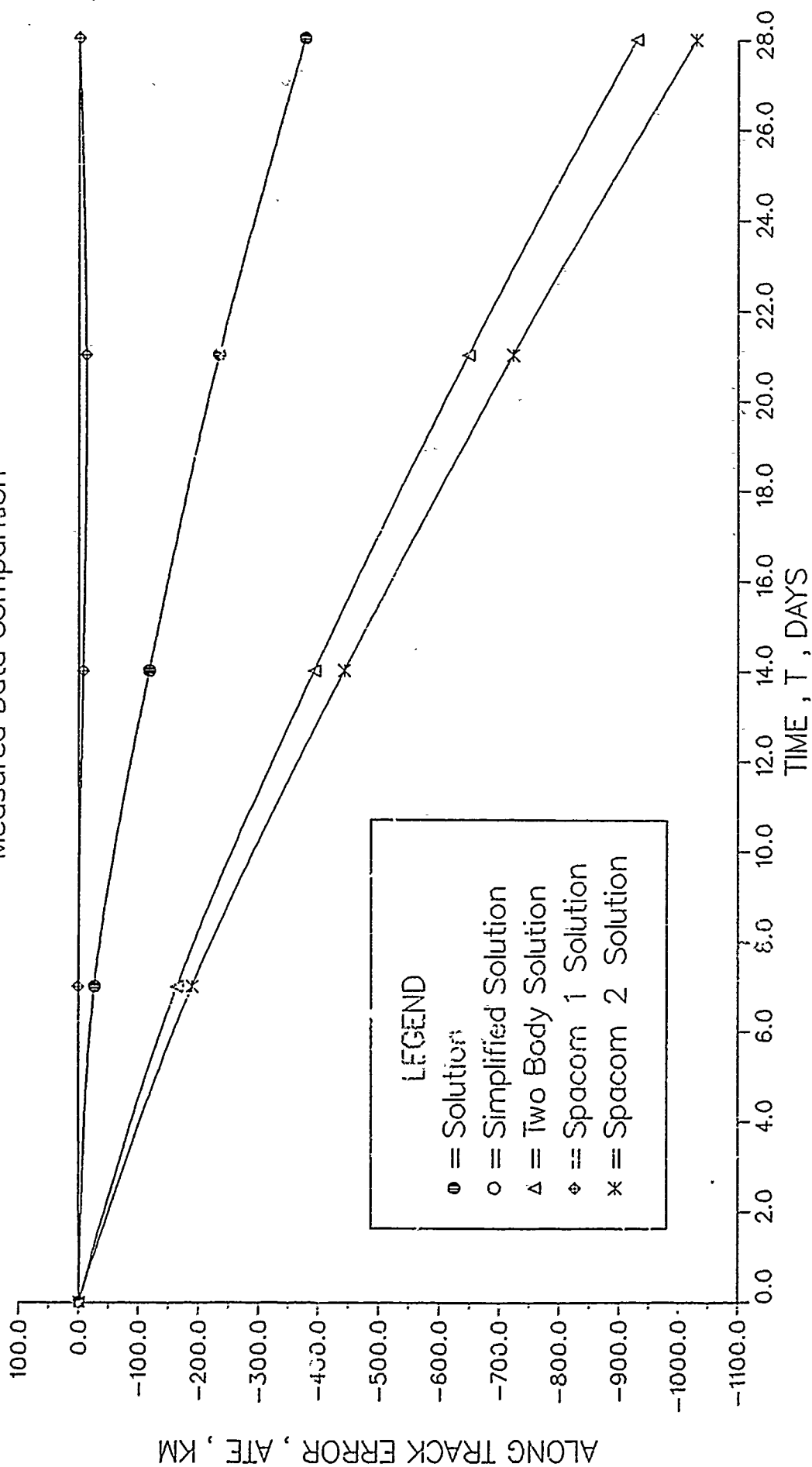


Figure 62. Along track error (28 days)

CROSS TRACK ERROR

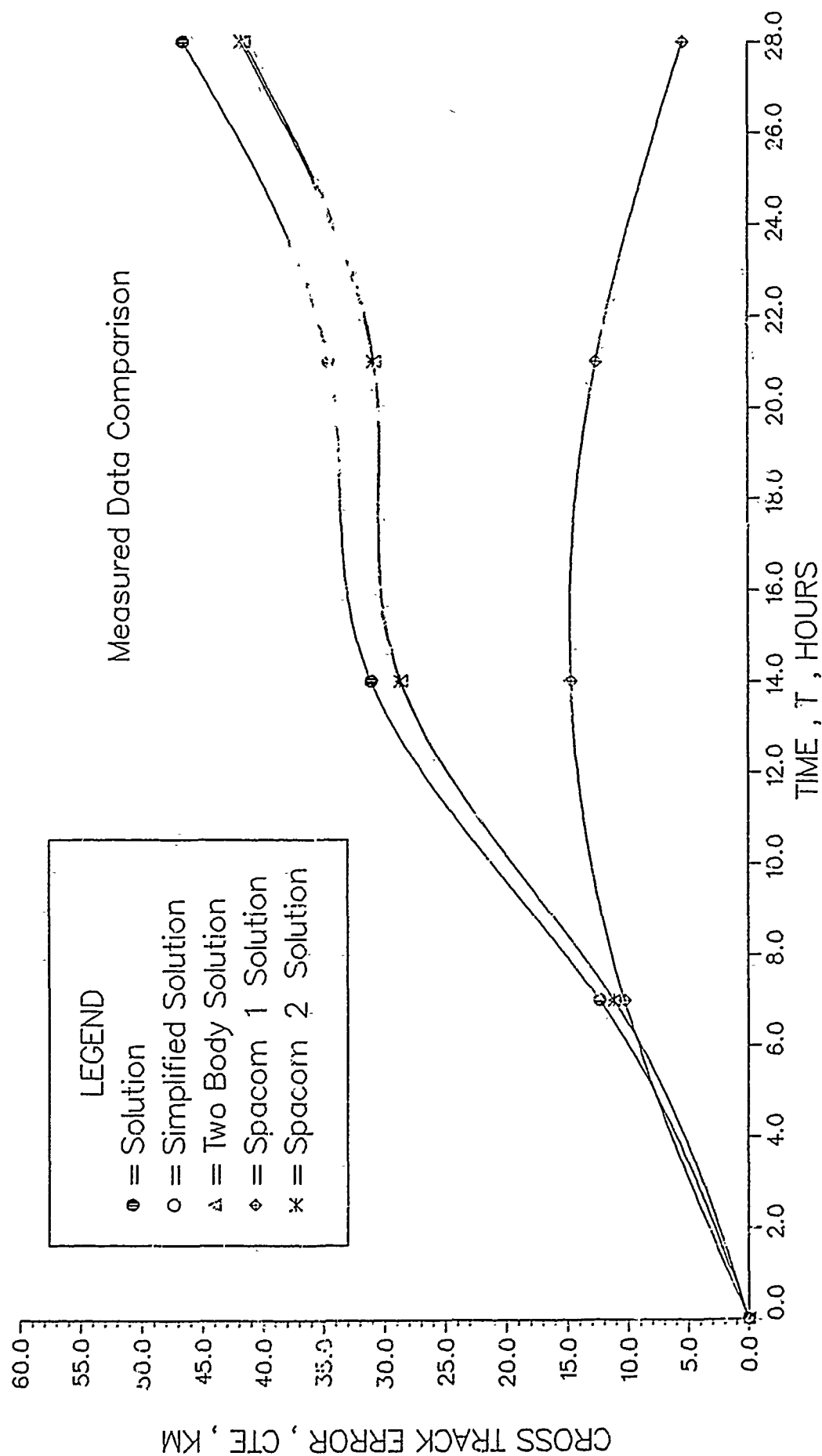


Figure 63. Cross track error (28 days)

APPENDIX E. COMPUTER PROGRAM

```

C      PROGRAM COLO2
C
C      *****
C      *
C      *      MAIN PROGRAM
C      *
C      *****
C
C      IMPLICIT DOUBLE PRECISION (A-I,M-Z)
C      CHARACTER*20 LINE
C      DIMENSION M(100),MD(100),E(100),W(100),WD(100),OM(100),OMD(100)
C      DIMENSION I(100),ID(100),F(100),FD(100),EC(100),ECD(100),A(100)
C      DIMENSION R(100),H(100),N(100),TH(100),THD(100)
C      DIMENSION RF(100),IF(100),IFD(100),OMF(100),OMFD(100),THF(100)
C      DIMENSION THFD(100),P(100),JORBIT(100),DR(100),DID(100),DTHD(100)
C      DIMENSION DOMD(100),RX(100),RY(100),RZ(100),RFX(100),RFY(100)
C      DIMENSION RFZ(100),DRV(100),ARC(100),ARCD(100),DAY(100),HX(100)
C      DIMENSION HY(100),HZ(100),VX(100),VY(100),VZ(100),DT(100),NX(100)
C      DIMENSION NY(100),NZ(100),RDV(100),EX(100),EY(100),EZ(100)
C      DIMENSION NDE(100),EDR(100),V(100),HT(100),RDRF(100),INTA(100)
C      DIMENSION ROMA(100),THJO(100),ATE(100),CTE(100)
C      COMMON/OBLATE1/DAY,RX,RY,RZ,VX,VY,VZ,DT,HX,HY,HZ,NX,NY,NZ,K,KK
C      COMMON/OBLATE2/RDV,R,V,EX,F,EZ,MU,NDE,EDR,H,N,E,P,I,OM,W,F
C      COMMON/OBLATE3/PI,EC,M,A,HT,ER,TH,THD,RTD,MD,WD,OMD,ID,ECD
C      COMMON/OBLATE4/FD,LINE,I,THF,THFD,IF,IFD,OMF,OMFD,RF,INT,ROM
C      COMMON/OBLATE5/RJ,DR,DID,DTHD,DOMD,ESTERR,ACTERR,TERROR,JVER
C      COMMON/OBLATE6/RFX,RFY,RFZ,ARC,ARCD,RDRF,DRV,RJ2,JN,JORBIT
C      COMMON/OBLATE7/INTA,ROMA,THJO,ATE,CTE
C
C      10 PRINT*, 'ENTER VERSION ( SOLUTION = 1, SIMPLE = 2, TWO BODY = 3 )'
C      READ*, JVER
C      IF(JVER.EQ. 1. OR. JVER.EQ. 2. OR. JVER.EQ. 3) THEN
C          GOTO 20
C      ELSE
C          GOTO 10
C      ENDIF
C
C      20 PRINT*, 'ENTER FIRST POINT'
C      READ*, K
C      PRINT*, 'ENTER FINAL POINT'
C      READ*, KK
C
C      PRINT*, 'ENTER RJ2'
C      READ*, RJ2
C      IF(RJ2.EQ. 1. OD0) THEN
C          RJ2=0.00108263D0
C      ENDIF
C
C      LINE='-----'
C      PI=3.141592653589793238462643D0
C      RTD=180.0D0/PI
C      ER=6378.137D0
C      HTS=1.0D0/806.812D0
C      MU=3.98600436D5
C
C      OPEN(UNIT=2, STATUS='OLD', FILE='/COLO2 OUT A')

```

```

OPEN(UNIT=3, STATUS='OLD', FILE='/COLO2 DSS A')
OPEN(UNIT=4, STATUS='OLD', FILE='/COLO20 DSS B')

C
CALL DATA
CALL ELEMENTS
CALL PINITIAL

C
J=1
WRITE(6,6000) 'POINT = ',J
WRITE(6,6000) 'INTEGRATE COMPLETED'
WRITE(6,6000) 'FORMULA COMPLETED'
WRITE(6,6000) 'INERTIAL COMPLETED'

C
DO 30 J = K, KK
  WRITE(6,6000) 'POINT = ',J
  CALL INTEGRATE
  WRITE(6,6000) 'INTEGRATE COMPLETED'
  CALL FORMULA
  WRITE(6,6000) 'FORMULA COMPLETED'
  CALL INERTIAL
  WRITE(6,6000) 'INERTIAL COMPLETED'
30 CONTINUE
CALL RESULTS

C
CLOSE(UNIT=2)
CLOSE(UNIT=3)
CLOSE(UNIT=4)

C
6000 FORMAT(3X,A,I3)
STOP
END

C
C *****
C *
C *      SUBROUTINE DATA      *
C *
C *****
C

SUBROUTINE DATA
IMPLICIT DOUBLE PRECISION (A-I,M-Z)
CHARACTER*20 LINE
DIMENSION M(100),MD(100),E(100),W(100),WD(100),OM(100),OMD(100)
DIMENSION I(100),ID(100),F(100),FD(100),EC(100),ECD(100),A(100)
DIMENSION R(100),H(100),N(100),TH(100),THD(100)
DIMENSION RF(100),IF(100),IFD(100),OMF(100),OMFD(100),THF(100)
DIMENSION THFD(100),P(100),JORBIT(100),DR(100),DID(100),DTHD(100)
DIMENSION DOMD(100),RX(100),RY(100),RZ(100),RFX(100),RFY(100)
DIMENSION RFZ(100),DRV(100),ARC(100),ARCD(100),DAY(100),HX(100)
DIMENSION HY(100),HZ(100),VX(100),VY(100),VZ(100),DT(100),NX(100)
DIMENSION NY(100),NZ(100),RDV(100),EX(100),EY(100),EZ(100)
DIMENSION NDE(100),EDR(100),V(100),HT(100),RDRF(100),INTA(100)
DIMENSION MONTH(100),DATE(100),HOUR(100),MIN(100),SEC(100)
DIMENSION ROMA(100),THJO(100),ATE(100),CTE(100)
COMMON/OBLATE1/DAY,RX,RY,RZ,VX,VY,VZ,DT,HX,HY,HZ,NX,NY,NZ,K,KK
COMMON/OBLATE2/RDV,R,V,EX,EY,EZ,MU,NDE,EDR,H,N,E,P,I,OM,W,F
COMMON/OBLATE3/PI,EC,M,A,HT,ER,TH,THD,RTD,MD,WD,OMD,ID,ECD

```

[illegible]

```
OPEN(UNIT=1, STATUS='OLD', FILE='/COLO2 DAT', ACTION='READ')
```

```
DO 10 J = 1, KK
  READ(1,*) MONTH(J),DATE(J),HOUR(J),MIN(J),SEC(J)
  READ(1,*) RX(J),RY(J),RZ(J)
  RX(J)=RX(J)/1000.0D0
  RY(J)=RY(J)/1000.0D0
  RZ(J)=RZ(J)/1000.0D0
  READ(1,*) VX(J),VY(J),VZ(J)
  VX(J)=VX(J)/1000.0D0
  VY(J)=VY(J)/1000.0D0
  VZ(J)=VZ(J)/1000.0D0
```

CONVERT PARAMETERS

```
DO 20 J = 1, KK
  DAY(J)=DATE(J)+((3600.000*HOUR(J)+
    (60.000*MIN(J)+SEC(J))))/86400.000
  DT(J)=(DAY(J)-DAY(1))*24.000*3600.000
```

CLOSE(UNIT=1)

RETURN
END

```

*****
**                                     **
**          SUBROUTINE ELEMENTS      **
**                                     **
*****

```

IMPLICIT DOUBLE PRECISION (A-I,M-Z)

```

DIMENSION M(100),MD(100),E(100),W(100),WD(100),OM(100),OMD(100)
DIMENSION I(100),ID(100),F(100),FD(100),EC(100),ECD(100),A(100)
DIMENSION R(100),H(100),N(100),TH(100),THD(100)
DIMENSION RF(100),IF(100),IFD(100),OMF(100),OMFD(100),THF(100)
DIMENSION THFD(100),P(100),JORBIT(100),DR(100),DID(100),DTHD(100)
DIMENSION DOMD(100),RX(100),RY(100),RZ(100),REFX(100),RFY(100)
DIMENSION RFZ(100),DRV(100),ARC(100),ARCD(100),DAY(100),HX(100)
DIMENSION HY(100),HZ(100),VX(100),VY(100),VZ(100),DT(100),NX(100)
DIMENSION NY(100),NZ(100),RDV(100),EX(100),EY(100),EZ(100)
DIMENSION NDE(100),EDR(100),V(100),HT(100),RDRF(100),INTA(100)
DIMENSION ROMA(100),THJO(100),ATE(100),CTE(100)
COMMON/OBLATE1/DAY,RX,RY,RZ,VX,VY,VZ,DT,HX,HY,HZ,NX,NY,NZ,K,KK
COMMON/OBLATE2/RDV,R,V,EX,EY,EZ,MU,NDE,EDR,H,N,E,P,I,OM,W,F

```



```

COMMON/OBLATE3/PI,EC,M,A,HT,ER,TH,THD,RTD,MD,WD,OMD,ID,ECD
COMMON/OBLATE4/FD,LINE,J,THF,THFD,IF,IFD,OMF,OMFD,RF,INT,ROM
COMMON/OBLATE5/RJ,DR,DID,DTHD,DOMD,ESTERR,ACTERR,TERROR,JVER
COMMON/OBLATE6/RFX,RFY,RFZ,ARC,ARCD,RDRF,DRV,RJ2,JN,JORBIT
COMMON/OBLATE7/INTA,ROMA,THJO,ATE,CTE

```

C
C
C

```

CALCULATE R,V,E,H,N,P,I,OM,W,F,EC,M,HT,TH

```

```

DO 10 J = 1, KK
  CALL CROSS(RX(J),RY(J),RZ(J),VX(J),VY(J),VZ(J),HX(J),HY(J),
+      HZ(J))
  CALL CROSS(0.0D0,0.0D0,1.0D0,HX(J),HY(J),HZ(J),NX(J),NY(J),
+      NZ(J))
  CALL DOT(RX(J),RY(J),RZ(J),VX(J),VY(J),VZ(J),RDV(J))
  R(J)=DSQRT(RX(J)*RX(J)+RY(J)*RY(J)+RZ(J)*RZ(J))
  V(J)=DSQRT(VX(J)*VX(J)+VY(J)*VY(J)+VZ(J)*VZ(J))
  EX(J)=((V(J)*V(J)-MU/R(J))*RX(J)-RDV(J)*VX(J))/MU
  EY(J)=((V(J)*V(J)-MU/R(J))*RY(J)-RDV(J)*VY(J))/MU
  EZ(J)=((V(J)*V(J)-MU/R(J))*RZ(J)-RDV(J)*VZ(J))/MU
  CALL DOT(NX(J),NY(J),NZ(J),EX(J),EY(J),EZ(J),NDE(J))
  CALL DOT(EX(J),EY(J),EZ(J),RX(J),RY(J),RZ(J),EDR(J))
  H(J)=DSQRT(HX(J)*HX(J)+HY(J)*HY(J)+HZ(J)*HZ(J))
  N(J)=DSQRT(NX(J)*NX(J)+NY(J)*NY(J)+NZ(J)*NZ(J))
  E(J)=DSQRT(EX(J)*EX(J)+EY(J)*EY(J)+EZ(J)*EZ(J))
  P(J)=H(J)*H(J)/MU
  I(J)=DACOS(HZ(J)/H(J))
  OM(J)=DACOS(NX(J)/N(J))
  W(J)=DACOS(NDE(J)/(N(J)*E(J)))
  F(J)=DACOS(EDR(J)/(E(J)*R(J)))
  IF(NY(J).LE.0.0D0)THEN
    OM(J)=2.0D0*PI-OM(J)
  ENDIF
  IF(EZ(J).LE.0.0D0)THEN
    W(J)=2.0D0*PI-W(J)
  ENDIF
  IF(RDV(J).LE.0.0D0)THEN
    F(J)=2.0D0*PI-F(J)
  ENDIF
  EC(J)=DACOS((E(J)+DCOS(F(J)))/(1.0D0+E(J)*DCOS(F(J))))
  IF(F(J).GE.PI)THEN
    EC(J)=2.0D0*PI-EC(J)
  ENDIF
  M(J)=EC(J)-E(J)*DSIN(EC(J))
  A(J)=P(J)/(1-E(J)*E(J))
  AT=(MU/(N(1)*N(1)))*(1.0D0/3.0D0)
  HT(J)=R(J)-ER
  RJ=3.0D0*RJ2*ER*ER/(2.0D0*P(1)*P(1))
  TH(J)=F(J)+W(J)
  THD(J)=TH(J)*RTD
20  IF(THD(J).GT.360.0D0)THEN
    THD(J)=THD(J)-360.0D0
    GOTO 20
  END IF
  TH(J)=THD(J)/RTD

```

20

C

```

C      CONVERT ORBITAL ELEMENTS TO DEGREES
C
      MD(J)=M(J)*RTD
      WD(J)=W(J)*RTD
      OMD(J)=OM(J)*RTD
      ID(J)=I(J)*RTD
      ECD(J)=EC(J)*RTD
      FD(J)=F(J)*RTD
      THD(J)=TH(J)*RTD
10     CONTINUE
      RETURN
      END

C
C      *****
C      *
C      *      SUBROUTINE CROSS      *
C      *
C      *****
C
      SUBROUTINE CROSS(AX,AY,AZ,BX,BY,BZ,CX,CY,CZ)
      IMPLICIT DOUBLE PRECISION (A-I,M-Z)

C
C      CALCULATE THE CROSS PRODUCT OF TWO VECTORS A AND B
C
      CX=AY*BZ-AZ*BY
      CY=AZ*BX-AX*BZ
      CZ=AX*BY-AY*BX

C
      RETURN
      END

C
C      *****
C      *
C      *      SUBROUTINE DOT      *
C      *
C      *****
C
      SUBROUTINE DOT(AX,AY,AZ,BX,BY,BZ,ADB)
      IMPLICIT DOUBLE PRECISION (A-I,M-Z)

C
C      CALCULATE THE DOT PRODUCT OF TWO VECTORS A AND B
C
      ADB=AX*BX+AY*BY+AZ*BZ

C
      RETURN
      END

C
C      *****
C      *
C      *      SUBROUTINE PINITIAL      *
C      *
C      *****
C
      SUBROUTINE PINITIAL
      IMPLICIT DOUBLE PRECISION (A-I,M-Z)
      CHARACTER*20 LINE

```

C
C
C

C

C

C

C

C

C

C
C

CC

22

2

```

DIMENSION R(100),H(100),N(100),TH(100),THD(100)
DIMENSION RF(100),IF(100),IFD(100),OMF(100),OMFD(100),THF(100)
DIMENSION THFD(100),P(100),JORBIT(100),DR(100),DID(100),DTHD(100)
DIMENSION DOME(100),RX(100),RY(100),RZ(100),RFX(100),RFY(100)
DIMENSION RFZ(100),DRV(100),ARC(100),ARCD(100),DAY(100),HX(100)
DIMENSION HY(100),HZ(100),VX(100),VY(100),VZ(100),DT(100),NX(100)
DIMENSION NY(100),NZ(100),RDV(100),EX(100),EY(100),EZ(100)
DIMENSION NDE(100),EDR(100),V(100),HT(100),RDRF(100),INTA(100)
DIMENSION ROMA(100),THJO(100),ATE(100),CTE(100)
COMMON/OBLATE1/DAY,RX,RY,RZ,VX,VY,VZ,DT,HX,HY,HZ,NX,NY,NZ,K,KK
COMMON/OBLATE2/RDV,R,V,EX,EY,EZ,MU,NDE,EDR,H,N,E,P,I,OM,W,F
COMMON/OBLATE3/PI,EC,M,A,HT,ER,TH,THD,RTD,MD,WD,OMD,ID,ECD
COMMON/OBLATE4/FD,LINE,J,THF,THFD,IF,IFD,OMF,OMFD,RF,INT,ROM
COMMON/OBLATE5/RJ,DR,DID,DTHD,DOMD,ESTERR,ACTERR,TERROR,JVER
COMMON/OBLATE6/RFX,RFY,RFZ,ARC,ARCD,RDRF,DRV,RJ2,JN,JORBIT
COMMON/OBLATE7/INTA,ROMA,THJO,ATE,CTE

C
C
C
EQUATE INITIAL VALUES

THF(1)=TH(1)
THFD(1)=THD(1)
IF(1)=I(1)
IFD(1)=ID(1)
OMF(1)=OM(1)
OMFD(1)=OMD(1)
RF(1)=R(1)

C
C
C
ESTIMATE UPPER BOUND OF THETA

THF(J)=TH(J)+(J-1)*0.57D0*2.0D0*PI
ROM00080

C
C
C
INITIALIZE

(1X10)-12
ESTERR=0.000000000001D0
INT=DT(J)*H(1)
DTHF=0.1745329251994
(1X10)-10
TERROR=0.0000000001D0

C
C
10
CALL ROMBERG
ACTERR=INT-ROM
IF(ACTERR.LT.0.0D0)THEN
    THF(J)=THF(J)-DTHF
    GOTO 10
ENDIF
TEMPHOF=THF(J)
GOTO 20

C
30
CALL ROMBERG
ACTERR=INT-ROM
20
IF(ACTERR.GE.0.0D0)THEN
    IF((ACTERR/INT).LE.ESTERR)THEN
        GOTO 40
    ELSE
        TEMPHOF=THF(J)

```

```

      THF(J)=THF(J)+DTHF
      GOTO 30
    ENDIF
ELSE
  DTHF=DTHF/2.0D0
  THF(J)=TEMPTHF+DTHF
  GOTO 30
END IF

C
40 INTA(J)=INT
   ROMA(J)=ROM
   RETURN
   END

C
C *****
C *
C *      SUBROUTINE ROMBERG
C *
C *****
C

SUBROUTINE ROMBERG
IMPLICIT DOUBLE PRECISION (A-I,M-Z)
CHARACTER*20 LINE
DIMENSION M(100),MD(100),E(100),W(100),WD(100),OM(100),OMD(100)
DIMENSION I(100),ID(100),F(100),FD(100),EC(100),ECD(100),A(100)
DIMENSION R(100),H(100),N(100),TH(100),THD(100)
DIMENSION RF(100),IF(100),IFD(100),OMF(100),OMFD(100),THF(100)
DIMENSION THFD(100),P(100),JORBIT(100),DR(100),DID(100),DTHD(100)
DIMENSION DOMD(100),RX(100),RY(100),RZ(100),RFX(100),RFY(100)
DIMENSION RFZ(100),DRV(100),ARC(100),ARCD(100),DAY(100),HX(100)
DIMENSION HY(100),HZ(100),VX(100),VY(100),VZ(100),DT(100),NX(100)
DIMENSION NY(100),NZ(100),RDV(100),EX(100),EY(100),EZ(100)
DIMENSION NDE(100),EDR(100),V(100),HT(100),RDRF(100),INTA(100)
DIMENSION ROMA(100),THJO(100),ATE(100),CTE(100)
COMMON/OBLATE1/DAY,RX,RY,RZ,VX,VY,VZ,DT,HX,HY,HZ,NX,NY,NZ,K,KK
COMMON/OBLATE2/RDV,R,V,EX,EY,EZ,MU,NDE,EDR,H,N,E,P,I,OM,W,F
COMMON/OBLATE3/PI,EC,M,A,HT,ER,TH,THD,RTD,MD,WD,OMD,ID,ECD
COMMON/OBLATE4/FD,LINE,J,THF,THFD,IF,IFD,OMF,OMFD,RF,INT,ROM
COMMON/OBLATE5/RJ,DR,DID,DTHD,DOMD,ESTERR,ACTERR,TERROR,JVER
COMMON/OBLATE6/RFX,RFY,RFZ,ARC,ARCD,RDRF,DRV,RJ2,JN,JORBIT
COMMON/OBLATE7/INTA,ROMA,THJO,ATE,CTE

C
EXTERNAL FUNC
C
C INITIALIZE VARIABLES
C
HS=THF(J)-THF(1)
FUNCA=FUNC(RJ,A(1),I(1),E(1),W(1),TH(1),THF(1),JVER)
FUNCB=FUNC(RJ,A(1),I(1),E(1),W(1),TH(1),THF(J),JVER)
P(1)=HS*(FUNCA+FUNCB)/2.0D0
JM=1

C
C BEGIN THE ROMBERG LOOP.
C
DO 10 JN = 1, 100
  OLDINT=P(1)

```

ROM00190

ROM00460

ROM00560

ROM00570

ROM00580

ROM00590

ROM00610

ROM00620

ROM00630

ROM00640

	HH=HS	ROM00670
	SS=0.0D0	ROM00680
	TT=THF(1)+HH/2.0D0	ROM00690
	DO 20 L = 1, JM	ROM00720
	T=TT	ROM00730
	SS=SS+FUNC(RJ,A(1),I(1),E(1),W(1),TH(1),T,JVER)	ROM00740
	TT=TT+HH	ROM00750
20	CONTINUE	ROM00760
	SUM=HH*SS	ROM00780
	P(JN+1)=(P(JN)+SUM)/2.0D0	ROM00800
	D=1.0D0	ROM00830
	DO 30 JK = JN, 1, -1	ROM00840
	D=4.0D0*D	ROM00850
	P(JK)=P(JK+1)+(P(JK+1)-P(JK))/(D-1.0D0)	ROM00860
30	CONTINUE	ROM00870
	ERROR=(P(1)-OLDINT)	ROM00900
	IF (JN. GE. 10) THEN	
	IF (DABS(ERROR/OLDINT). LE. TERROR) THEN	ROM00930
	GOTO 40	
	ENDIF	
	ENDIF	
	HS=HS/2.0D0	ROM00940
	JM=JM*2	ROM00950
10	CONTINUE	ROM00960
40	ROM=P(1):	ROM00970
	RETURN	
	END	
C		
C	*****	
C	*	*
C	* FUNCTION FUNC *	
C	*	*
C	*****	
C		
	FUNCTION FUNC(RJ,A1,I1,E1,W1,TH1,THFJ,JVER)	
	IMPLICIT DOUBLE PRECISION (A-I,O-Z)	ROM00030
C		
	EXTERNAL RADIUS	
C		
	S=DSIN(I1)	
	S2=S*S	
	S4=S2*S2	
	S6=S4*S2	
	E2=E1*E1	
C		
	RAD=RADIUS(RJ,A1,I1,E1,W1,TH1,THFJ,JVER)	
C		
C	F (SOLUTION)	
C		
	IF(JVER. EQ. 1) THEN	
C		
	Y1=112.0D0-75.0D0*S6+260.0D0*S4-296.0D0*S2	
	Y2=RJ*THFJ*(2.5D0*S2-2.0D0)	
	Y3=2.0D0*W1-Y2	
	Y4=24.0D0*(5.0D0*S2-4.0D0)*(5.0D0*S2-4.0D0)	
	Y5=E2*S2*(14.0D0-15.0D0*S2)*(15.0D0*S2-13.0D0)	

```

Y6=9.0D0*E2+34.0D0
Y9=12.0D0*(5.0D0*S2-4.0D0)
Y12=9.0D0*E2-34.0D0
C
YF=(2.5D0*S2-2.0D0)*(THFJ-TH1)+E2*Y1*DSIN(Y2)*DCOS(Y3)/Y4
C
YS=Y5*DCOS(2.0D0*W1)/(2.0D0*Y9)+
+ E1*S2*(15.0D0*S2-13.0D0)*DCOS(TH1+W1)/2.0D0+
+ E1*S2*(15.0D0*S2-13.0D0)*DCOS(3.0D0*TH1-W1)/6.0D0+
+ S2*(15.0D0*S2-13.0D0)*DCOS(2.0D0*TH1)/2.0D0+
+ (5.0D0*Y6*S4+4.0D0*Y12*S2-56.0D0*E2)/96.0D0
C
Y=THFJ-W1+RJ*YF+RJ*YJ*THFJ*YS
C
F=(2.0D0-3.0D0*S2)*DCOS(2.0D0*THFJ)/2.0D0+
+ E1*(S2-1)*DCOS(Y)+E1*(3.0D0-4.0D0*S2)*DCOS(Y+2.0D0*THFJ)/6.0D0+
+ E1*(1.0D0-2.0D0*S2)*DCOS(Y-2.0D0*THFJ)/2.0D0+S2-1.0D0+
+ E2*S2*(15.0D0*S2-14.0D0)*DSIN(Y2)*DSIN(Y3)/Y9+
+ S2*DCOS(2.0D0*TH1)/2.0D0+E1*S2*DCOS(3.0D0*TH1-W1)/6.0D0+
+ E1*S2*DCOS(TH1+W1)/2.0D0
C
ENDIF
C
F ( SIMPLIFIED SOLUTION )
C
IF(JVER.EQ.2)THEN
C
F=(2.0D0-3.0D0*S2)*DCOS(2.0D0*THFJ)/2.0D0+
+ E1*(S2-1)*DCOS(THFJ-W1)+
+ E1*(3.0D0-4.0D0*S2)*DCOS(3.0D0*THFJ-W1)/6.0D0+
+ E1*(1.0D0-2.0D0*S2)*DCOS(THFJ+W1)/2.0D0+S2-1.0D0+
+ S2*DCOS(2.0D0*TH1)/2.0D0+E1*S2*DCOS(3.0D0*TH1-W1)/6.0D0+
+ E1*S2*DCOS(TH1+W1)/2.0D0
C
ENDIF
C
F ( TWO BODY SOLUTION )
C
IF(JVER.EQ.3)THEN
F=0.0D0
ENDIF
C
FUNCTION
C
FUNC=RAD*RAD*(1.0D0+RJ*F)
C
RETURN
END
C
*****
C
*
C
* FUNCTION RADIUS
C
*
C
*****
C
FUNCTION RADIUS(RJ,A1,I1,E1,W1,TH1,TFJ,JVER)

```

IMPLICIT DOUBLE PRECISION (A-I,O-Z)

ROM00030

C
C
C

CALCULATE E, SINE, AND COSINE FUNCTIONS

S=DSIN(I1)
S2=S*S
S4=S2*S2
S6=S4*S2
C=DCOS(I1)
C2=C*C
SC=DSIN(I1)*DCOS(I1)
E2=E1*E1
P0=A1*(1.0D0-E2)

C
C
C

RADIUS BOTTOM (SOLUTION)

IF(JVER.EQ.1)THEN

C

Y1=112.0D0-75.0D0*S6+260.0D0*S4-296.0D0*S2
Y2=RJ*TFJ*(2.5D0*S2-2.0D0)
Y3=2.0D0*W1-Y2
Y4=24.0D0*(5.0D0*S2-4.0D0)*(5.0D0*S2-4.0D0)
Y5=E2*S2*(14.0D0-15.0D0*S2)*(15.0D0*S2-13.0D0)
Y6=9.0D0*E2+34.0D0
Y9=12.0D0*(5.0D0*S2-4.0D0)

C

Y11=15.0D0*(2.0D0+E2)*S4-14.0D0*(4.0D0+E2)*S2+24.0D0

C

Y12=9.0D0*E2-34.0D0

C

YF=(2.5D0*S2-2.0D0)*(TFJ-TH1)+E2*Y1*DSIN(Y2)*DCOS(Y3)/Y4

C

YS=Y5*DCOS(2.0D0*W1)/(2.0D0*Y9)+
+ E1*S2*(15.0D0*S2-13.0D0)*DCOS(TH1+W1)/2.0D0+
+ E1*S2*(15.0D0*S2-13.0D0)*DCOS(3.0D0*TH1-W1)/6.0D0+
+ S2*(15.0D0*S2-13.0D0)*DCOS(2.0D0*TH1)/2.0D0+
+ (5.0D0*Y6*S4+4.0D0*Y12*S2-56.0D0*E2)/96.0D0

C

Y=TFJ-W1+RJ*YF+RJ*YF*TFJ*YS

C

RF1=1.0D0-1.5D0*S2+E2*(1.0D0-1.25D0*S2)-
+ ((2.0D0+5.0D0*E2)*S2-2.0D0*E2)*DCOS(2.0D0*TFJ)/12.0D0+
+ E2*(9.0D0*S2-8.0D0)*DCOS(2.0D0*Y)/12.0D0+
+ E1*(-11.0D0*S2+6.0D0)*DCOS(Y+2.0D0*TFJ)/24.0D0+
+ E2*(-3.0D0*S2+2.0D0)*DCOS(2.0D0*Y+2.0D0*TFJ)/24.0D0+
+ E2*(3.0D0*S2-2.0D0)*DCOS(2.0D0*Y-2.0D0*TFJ)/8.0D0+
+ E1*Y11*DSIN(Y2)*DSIN(TFJ+W1)/Y9

C

RF2=E2*S2*(15.0D0*S2-14.0D0)*DSIN(Y2)*DSIN(Y3)/(0.5D0*Y9)-
+ E2*S2*DCOS(Y-TH1+3.0D0*W1)/16.0D0+
+ E2*(3.0D0*S2-2.0D0)*DCOS(Y-3.0D0*TH1+3.0D0*W1)/24.0D0-
+ E2*S2*DCOS(Y-5.0D0*TH1+3.0D0*W1)/16.0D0+
+ E1*(3.0D0*S2-2.0D0)*DCOS(Y-2.0D0*TH1+2.0D0*W1)/4.0D0-
+ 3.0D0*E1*S2*DCOS(Y-4.0D0*TH1+2.0D0*W1)/8.0D0-
+ E1*(S2+1.0D0)*DCOS(Y+2.0D0*W1)/4.0D0

C


```

      RF3=((5.0D0*E2-2.0D0)*S2-2.0D0*E2)*DCOS(Y+TH1+W1)/8.0D0+
+      ((5.0D0*E2+6.0D0)*S2-4.0D0*(E2+1.0D0))*DCOS(Y-TH1+W1)/4.0D0+
+      (2.0D0*E2-S2*(5.0D0*E2+14.0D0))*DCOS(Y-3.0D0*TH1+W1)/24.0D0+
+      E2*(9.0D0*S2-4.0D0)*DCOS(Y+3.0D0*TH1-W1)/48.0D0+
+      E2*(6.0D0-7.0D0*S2)*DCOS(Y+TH1-W1)/8.0D0+
+      E2*(4.0D0-5.0D0*S2)*DCOS(Y-TH1-W1)/16.0D0+
+      E1*(2.0D0*S2-1.0D0)*DCOS(Y+2.0D0*TH1)/4.0D0
C
      RF4=E1*(1.0D0-3.0D0*S2)*DCOS(Y-2.0D0*TH1)/4.0D0+
+      E1*(2.0D0-3.0D0*S2)*DCOS(Y)/4.0D0+
+      E1*S2*DCOS(TH1+W1)+S2*DCOS(2.0D0*TH1)+
+      E1*S2*DCOS(3.0D0*TH1-W1)/3.0D0
C
      RFB=1.0D0+E1*DCOS(Y)+RJ*(RF1+RF2+RF3+RF4)
C
      ENDIF
C
      RADIUS BOTTOM ( SIMPLIFIED SOLUTION )
C
      IF(JVER.EQ.2)THEN
C
      RF1=1.0D0-1.5D0*S2+E2*(1.0D0-1.25D0*S2)-
+      ((2.0D0+5.0D0*E2)*S2-2.0D0*E2)*DCOS(2.0D0*TFJ)/12.0D0+
+      E2*(9.0D0*S2-8.0D0)*DCOS(2.0D0*(TFJ-W1))/12.0D0+
+      E1*(-11.0D0*S2+6.0D0)*DCOS(3.0D0*TFJ-W1)/24.0D0+
+      E2*(-3.0D0*S2+2.0D0)*DCOS(4.0D0*TFJ-2.0D0*W1)/24.0D0+
+      E2*(3.0D0*S2-2.0D0)*DCOS(2.0D0*W1)/8.0D0-
+      E2*S2*DCOS(TFJ-TH1+2.0D0*W1)/16.0D0
C
      RF2=E2*(3.0D0*S2-2.0D0)*DCOS(TFJ-3.0D0*TH1+2.0D0*W1)/24.0D0-
+      E2*S2*DCOS(TFJ-5.0D0*TH1+2.0D0*W1)/16.0D0+
+      E1*(3.0D0*S2-2.0D0)*DCOS(TFJ-2.0D0*TH1+W1)/4.0D0-
+      3.0D0*E1*S2*DCOS(TFJ-4.0D0*TH1+W1)/8.0D0-
+      E1*(S2+1.0D0)*DCOS(TFJ+W1)/4.0D0+
+      ((5.0D0*E2-2.0D0)*S2-2.0D0*E2)*DCOS(TFJ+TH1)/8.0D0+
+      ((5.0D0*E2+6.0D0)*S2-4.0D0*(E2+1.0D0))*DCOS(TFJ-TH1)/4.0D0
C
      RF3=(2.0D0*E2-S2*(5.0D0*E2+14.0D0))*DCOS(TFJ-3.0D0*TH1)/24.0D0+
+      E2*(9.0D0*S2-4.0D0)*DCOS(TFJ+3.0D0*TH1-2.0D0*W1)/48.0D0+
+      E2*(6.0D0-7.0D0*S2)*DCOS(TFJ+TH1-2.0D0*W1)/8.0D0+
+      E2*(4.0D0-5.0D0*S2)*DCOS(TFJ-TH1-2.0D0*W1)/16.0D0+
+      E1*(2.0D0*S2-1.0D0)*DCOS(TFJ+2.0D0*TH1-W1)/4.0D0+
+      E1*(1.0D0-3.0D0*S2)*DCOS(TFJ-2.0D0*TH1-W1)/4.0D0+
+      E1*(2.0D0-3.0D0*S2)*DCOS(TFJ-W1)/4.0D0
C
      RF4=E1*S2*DCOS(TH1+W1)+S2*DCOS(2.0D0*TH1)+
+      E1*S2*DCOS(3.0D0*TH1-W1)/3.0D0
C
      RFB=E1*DCOS(TFJ-W1)+RJ*(TFJ-TH1)*(2.5D0*S2-2.0D0))+
+      1.0D0+RJ*(RF1+RF2+RF3+RF4)
C
      ENDIF
C
      RADIUS BOTTOM ( TWO BODY SOLUTION )
C
      IF(JVER.EQ.3)THEN

```

```

      RFB=1.0D0+E1*DCOS(TFJ-W1)
ENDIF
C
C
C  RADIUS
C
C  RADIUS=P0/RFB
C
C  RETURN
C
C  END
ROM00410
ROM00420
C
C *****
C *
C *      SUBROUTINE FORMULA
C *
C *****
C
C  SUBROUTINE FORMULA
C  IMPLICIT DOUBLE PRECISION (A-I,M-Z)
C  CHARACTER*20 LINE
C  DIMENSION M(100),MD(100),E(100),W(100),WD(100),OM(100),OMD(100)
C  DIMENSION I(100),ID(100),F(100),FD(100),EC(100),ECD(100),A(100)
C  DIMENSION R(100),H(100),N(100),TH(100),THD(100)
C  DIMENSION RF(100),IF(100),IFD(100),OMF(100),OMFD(100),THF(100)
C  DIMENSION THFD(100),P(100),JORBIT(100),DR(100),DID(100),DTHD(100)
C  DIMENSION DOMD(100),RX(100),RY(100),RZ(100),RFX(100),RFY(100)
C  DIMENSION RFZ(100),DRV(100),ARC(100),ARCD(100),DAY(100),HX(100)
C  DIMENSION HY(100),HZ(100),VX(100),VY(100),VZ(100),DT(100),NX(100)
C  DIMENSION NY(100),NZ(100),RDV(100),EX(100),EY(100),EZ(100)
C  DIMENSION NDE(100),EDR(100),V(100),HT(100),RDRF(100),INTA(100)
C  DIMENSION ROMA(100),THJO(100),ATE(100),CTE(100)
C  COMMON/OBLATE1/DAY,RX,RY,RZ,VX,VY,VZ,DT,HX,HY,HZ,NX,NY,NZ,K,KK
C  COMMON/OBLATE2/RDV,R,V,EX,EY,EZ,MU,NDE,EDR,H,N,E,P,I,OM,W,F
C  COMMON/OBLATE3/PI,EC,M,A,HT,ER,TH,THD,RTD,MD,WD,OMD,ID,ECD
C  COMMON/OBLATE4/LINE,J,THF,THFD,IF,IFD,OMF,OMFD,RF,INT,ROM
C  COMMON/OBLATE5/RJ,DR,DID,DTHD,DOMD,ESTERR,ACTERR,TERROR,JVER
C  COMMON/OBLATE6/RFX,RFY,RFZ,ARC,ARCD,RDRF,DRV,RJ2,JN,JORBIT
C  COMMON/OBLATE7/INTA,ROMA,THJO,ATE,CTE
C
C  EXTERNAL RADIUS
C
C  CALCULATE E, SINE, AND COSINE FUNCTIONS
C
C  S=DSIN(I(1))
C  S2=S*S
C  S4=S2*S2
C  S6=S4*S2
C  C=DCOS(I(1))
C  C2=C*C
C  SC=DSIN(I(1))*DCOS(I(1))
C  E2=E(1)*E(1)
C
C  FORMULA ( SOLUTION )
C
C  IF(JVER.EQ.1)THEN
C
C  Y1=112.0D0-75.0D0*S6+260.0D0*S4-296.0D0*S2

```

```

Y2=RJ*THF(J)*(2.5D0*S2-2.0D0)
Y3=2.0D0*W(1)-Y2
Y4=24.0D0*(5.0D0*S2-4.0D0)*(5.0D0*S2-4.0D0)
Y5=E2*S2*(14.0D0-15.0D0*S2)*(15.0D0*S2-13.0D0)
Y6=9.0D0*E2+34.0D0
Y7=15.0D0*S4-45.0D0*S2+28.0D0
Y8=6.0D0*(5.0D0*S2-4.0D0)*(5.0D0*S2-4.0D0)
Y9=12.0D0*(5.0D0*S2-4.0D0)

C
Y10=(6.0D0-S2)/12.0D0-E(1)*S2*DCOS(3.0D0*TH(1)-W(1))/3.0D0-
+ S2*DCOS(2.0D0*TH(1))+E2*(7.0D0*S2-4.0D0)/24.0D0
C
Y12=9.0D0*E2-34.0D0
C
YF=(2.5D0*S2-2.0D0)*(THF(J)-TH(1))+E2*Y1*DSIN(Y2)*DCOS(Y3)/Y4
C
YS=Y5*DCOS(2.0D0*W(1))/(2.0D0*Y9)+
+ E(1)*S2*(15.0D0*S2-13.0D0)*DCOS(TH(1)+W(1))/2.0D0+
+ E(1)*S2*(15.0D0*S2-13.0D0)*DCOS(3.0D0*TH(1)-W(1))/6.0D0+
+ S2*(15.0D0*S2-13.0D0)*DCOS(2.0D0*TH(1))/2.0D0+
+ (5.0D0*Y6*S4+4.0D0*Y12*S2-56.0D0*E2)/96.0D0
C
Y=THF(J)-W(1)+RJ*YF+RJ*RJ*THF(J)*YS
C
C
C CALCULATE INCLINATION ( SOLUTION )
C
IF(J)=I(1)+SC*RJ*(DCOS(2.0D0*THF(J))/2.0D0+
+ E(1)*DCOS(Y+2.0D0*THF(J))/6.0D0+E(1)*DCOS(Y-2.0D0*THF(J))/2.0D0+
+ E2*(14.0D0-15.0D0*S2)*DSIN(Y2)*DSIN(Y3)/(12.0D0*(5.0D0*S2-4.0D0))-
+ DCOS(2.0D0*TH(1))/2.0D0-E(1)*DCOS(3.0D0*TH(1)-W(1))/6.0D0-
+ E(1)*DCOS(TH(1)+W(1))/2.0D0)
C
C
C CALCULATE LONGITUDE OF THE ASCENDING NODE ( SOLUTION )
C
RJ2=RJ*RJ
C
OMF(J)=OM(1)+C*RJ*(TH(1)-THF(J)+DSIN(2.0D0*THF(J))/2.0D0-
+ E(1)*DSIN(Y)+E(1)*DSIN(Y+2.0D0*THF(J))/6.0D0-
+ E(1)*DSIN(Y-2.0D0*THF(J))/2.0D0-DSIN(2.0D0*TH(1))/2.0D0+
+ E(1)*DSIN(TH(1)-W(1))-E(1)*DSIN(3.0D0*TH(1)-W(1))/6.0D0-
+ E(1)*DSIN(TH(1)+W(1))/2.0D0+E2*Y7*DSIN(Y2)*DCOS(Y3)/Y8)+
+ C*RJ2*THF(J)*(E2*S2*(15.0D0*S2-14.0D0)*DCOS(2.0D0*W(1))/Y9-
+ E(1)*S2*DCOS(TH(1)+W(1))+Y10)
C
ENDIF
C
C
C FORMULA ( SIMPLIFIED SOLUTION )
C
IF(JVER.EQ.2)THEN
C
C
C CALCULATE INCLINATION ( SIMPLIFIED SOLUTION )
C
IF(J)=I(1)+SC*RJ*(DCOS(2.0D0*THF(J))/2.0D0+
+ E(1)*DCOS(3.0D0*THF(J)-W(1))/6.0D0+
+ E(1)*DCOS(THF(J)+W(1))/2.0D0-DCOS(2.0D0*TH(1))/2.0D0-
+ E(1)*DCOS(3.0D0*TH(1)-W(1))/6.0D0-

```

```

      +      E(1)*DCOS(TH(1)+W(1))/2. 0D0)
C
C      CALCULATE LONGITUDE OF THE ASCENDING NODE ( SIMPLIFIED SOLUTION )
C
      OMF(J)=OM(1)+C*PJ*(TH(1)-THF(J)+DSIN(2. 0D0*THF(J))/2. 0D0-
+      E(1)*DSIN(THF(J)-W(1))+E(1)*DSIN(3. 0D0*THF(J)-W(1))/6. 0D0+
+      E(1)*DSIN(THF(J)+W(1))/2. 0D0-DSIN(2. 0D0*TH(1))/2. 0D0+
+      E(1)*DSIN(TH(1)-W(1))-E(1)*DSIN(3. 0D0*TH(1)-W(1))/6. 0D0-
+      E(1)*DSIN(TH(1)+W(1))/2. 0D0)
C
      ENDIF
C
C      FORMULA ( TWO BODY SOLUTION )
C
      IF(JVER. EQ. 3) THEN
C
C      CALCULATE INCLINATION ( TWO BODY SOLUTION )
C
      IF(J)=I(1)
C
C      CALCULATE LONGITUDE OF THE ASCENDING NODE ( TWO BODY SOLUTION )
C
      OMF(J)=OM(1)
C
      ENDIF
C
C      CALCULATE RADIUS ( SOLUTION, SIMPLIFIED, OR TWO BODY )
C
      RF(J)=RADIUS(RJ,A(1),I(1),E(1),W(1),TH(1),THF(J),JVER)
C
C      CONVERT ANGLES TO DEGREES
C
      OMFD(J)=OMF(J)*RTD
      IFD(J)=IF(J)*RTD
      THFD(J)=THF(J)*RTD
      JORBIT(J)=0
10      IF(THFD(J). GT. 360. 0D0) THEN
          THFD(J)=THFD(J)-360. 0D0
          JORBIT(J)=JORBIT(J)+1
          GOTO 10
      END IF
      THJO(J)=JORBIT(J)*2. 0D0*PI+TH(J)-TH(1)
20      IF(OMFD(J). GT. 360. 0D0) THEN
          OMFD(J)=OMFD(J)-360. 0D0
          GOTO 20
      END IF
      THF(J)=THFD(J)/RTD
      OMF(J)=OMFD(J)/RTD
C
C      CALCULATE DELTAS
C
      DR(J)=RF(J)-R(J)
      DID(J)=IFD(J)-ID(J)
      DTHD(J)=THFD(J)-THD(J)
      IF(DABS(DTHD(J)). GE. 180. 0D0) THEN
          IF(DTHD(J). LT. 0. 0D0) THEN

```

```

      DTHD(J)=DTHD(J)+360.0D0
    ELSE
      DTHD(J)=DTHD(J)-360.0D0
    ENDIF
  ENDIF
  DOMD(J)=OMFD(J)-OMD(J)
C
  RETURN
  END
C
C *****
C *
C *      SUBROUTINE INERTIAL      *
C *
C *****
C
  SUBROUTINE INERTIAL
  IMPLICIT DOUBLE PRECISION (A-I,M-Z)
  CHARACTER*20 LINE
  DIMENSION M(100),MD(100),E(100),W(100),WD(100),OM(100),OMD(100)
  DIMENSION I(100),ID(100),F(100),FD(100),EC(100),ECD(100),A(100)
  DIMENSION R(100),H(100),N(100),TH(100),THD(100)
  DIMENSION RF(100),IF(100),IFD(100),OMF(100),OMFD(100),THF(100)
  DIMENSION THFD(100),P(100),JORBIT(100),DR(100),DID(100),DTHD(100)
  DIMENSION DOMD(100),RX(100),RY(100),RZ(100),RFX(100),RFY(100)
  DIMENSION RFZ(100),DRV(100),ARC(100),ARCD(100),DAY(100),HX(100)
  DIMENSION HY(100),HZ(100),VX(100),VY(100),VZ(100),DT(100),NX(100)
  DIMENSION NY(100),NZ(100),RDV(100),EX(100),EY(100),EZ(100)
  DIMENSION NDE(100),EDR(100),V(100),HT(100),RDRF(100),INTA(100)
  DIMENSION EARC(100),EARCD(100),PDR(100)
  DIMENSION ROMA(100),THJO(100),ATE(100),CTE(100)
  COMMON/OBLATE1/DAY,RX,RY,RZ,VX,VY,VZ,DT,HX,HY,HZ,NX,NY,NZ,K,KK
  COMMON/OBLATE2/RDV,R,V,EX,EY,EZ,MU,NDE,EDR,H,N,E,P,I,OM,W,F
  COMMON/OBLATE3/PI,EC,M,A,HT,ER,TH,THD,RTD,MD,WD,OMD,ID,ECD
  COMMON/OBLATE4/FD,LINE,J,THF,THFD,IF,IFD,OMF,OMFD,RF,INT,ROM
  COMMON/OBLATE5/RJ,DR,DID,DTHD,DOMD,ESTERR,ACTERR,TERROR,JVER
  COMMON/OBLATE6/RFX,RFY,RFZ,ARC,ARCD,RDRF,DRV,RJ2,JN,JORBIT
  COMMON/OBLATE7/INTA,ROMA,THJO,ATE,CTE
  COMMON/SPECIAL/EARC,EARCD,PDR,ENG,ENGF
C
  CALCULATE INITIAL ENERGY
C
  ENG=V(1)*V(1)/2.0D0-MU/R(1)
  ENGF=V(1)*V(1)/2.0D0-MU/RF(1)
C
  CALCULATE INERTIAL COORDINATES
C
  RFX(J)=RF(J)*(DCOS(THF(J))*DCOS(OMF(J))-
+      DSIN(THF(J))*DCOS(IF(J))*DSIN(OMF(J)))
  RFY(J)=RF(J)*(DCOS(THF(J))*DSIN(OMF(J))+
+      DSIN(THF(J))*DCOS(IF(J))*DCOS(OMF(J)))
  RFZ(J)=RF(J)*(DSIN(THF(J))*DSIN(IF(J)))
C
  CALCULATE DR VECTOR
C
  DRV(J)=DSQRT((RFX(J)-RX(J))*(RFX(J)-RX(J))+

```

```

+      (RFY(J)-RY(J))*(RFY(J)-RY(J))+
+      (RFZ(J)-RZ(J))*(RFZ(J)-RZ(J))
PDR(J)=DRV(J)/R(J)

C
C
C
CALCULATE ANGLE ERROR

CALL DOT(RX(J),RY(J),RZ(J),RFX(J),RFY(J),RFZ(J),RDRF(J))
ARC(J)=DACOS(RDRF(J)/(R(J)*RF(J)))
CC=RF(J)
CCP=R(J)
BB=ER
AA=DSQRT(BB*BB+CC*CC-2.0D0*BB*CC*DCOS(ARC(J)/2.0D0))
AAP=DSQRT(BB*BB+CCP*CCP-2.0D0*BB*CCP*DCOS(ARC(J)/2.0D0))
CCA=PI-DASIN(CC*DSIN(ARC(J)/2.0D0)/AA)
CCPA=PI-DASIN(CCP*DSIN(ARC(J)/2.0D0)/AAP)
EARC(J)=2.0D0*PI-CCA-CCPA
ARCD(J)=ARC(J)*RTD
EARCD(J)=EARC(J)*RTD

C
C
C
CALCULATE DOWNRANGE AND CROSSRANGE ERRORS

ATE(J)=R(J)*(DTHD(J)/RTD+DCOS(I(J))*DOMD(J)/RTD)
CTE(J)=R(J)*(DSIN(TH(J))*DID(J)/RTD-
+      DCOS(TH(J))*DSIN(I(J))*DOMD(J)/RTD)

C
RETURN
END

C
C
C
*****
*
*      SUBROUTINE RESULTS
*
*****

SUBROUTINE RESULTS
IMPLICIT DOUBLE PRECISION (A-I,M-Z)
CHARACTER*20 LINE
CHARACTER*11 VERSION
DIMENSION M(100),MD(100),E(100),W(100),WD(100),OM(100),OMD(100)
DIMENSION I(100),ID(100),F(100),FD(100),EC(100),ECD(100),A(100)
DIMENSION R(100),H(100),N(100),TH(100),THD(100)
DIMENSION RF(100),IF(100),IFD(100),OMF(100),OMFD(100),THF(100)
DIMENSION THFD(100),P(100),JORBIT(100),DR(100),DID(100),DTHD(100)
DIMENSION DOMD(100),RX(100),RY(100),RZ(100),RFX(100),RFY(100)
DIMENSION RFZ(100),DRV(100),ARC(100),ARCD(100),DAY(100),HX(100)
DIMENSION HY(100),HZ(100),VX(100),VY(100),VZ(100),DT(100),NX(100)
DIMENSION NY(100),NZ(100),RDV(100),EX(100),EY(100),EZ(100)
DIMENSION NDE(100),EDR(100),V(100),HT(100),RDRF(100),INTA(100)
DIMENSION EARC(100),EARCD(100),PDR(100)
DIMENSION ROMA(100),THJO(100),ATE(100),CTE(100)
COMMON/OBLATE1/DAY,RX,RY,RZ,VX,VY,VZ,DT,HX,HY,HZ,NX,NY,NZ,K,KK
COMMON/OBLATE2/RDV,R,V,EX,EY,EZ,MU,NDE,EDR,H,N,E,P,I,OM,W,F
COMMON/OBLATE3/PI,EC,M,A,HT,ER,TH,THD,RTD,MD,WD,OMD,ID,ECD
COMMON/OBLATE4/LINE,J,THF,THFD,IF,IFD,OMF,OMFD,RF,INT,ROM
COMMON/OBLATE5/RJ,DR,DID,DTHD,DOMD,ESTERR,ACTERR,TERROR,JVER

```

```

COMMON/OBLATE6/RFX,RFY,RFZ,ARC,ARCD,RDRF,DRV,RJ2,JN,JORBIT
COMMON/OBLATE7/INTA,ROMA,THJO,ATE,CTE
COMMON/SPECIAL/EARC,EARCD,PDR,ENG,ENGF

```

C

```

DR(1)=0.0D0
DID(1)=0.0D0
DTHD(1)=0.0D0
DOMD(1)=0.0D0
DRV(1)=0.0D0
ARCD(1)=0.0D0
EARCD(1)=0.0D0
PDR(1)=0.0D0
THJO(1)=0.0D0
ATE(1)=0.0D0
CTE(1)=0.0D0

```

C

```

IF(JVER.EQ.1)THEN
  VERSION='SOLUTION'
ELSEIF(JVER.EQ.2)THEN
  VERSION='SIMPLIFIED'
ELSEIF(JVER.EQ.3)THEN
  VERSION='SECULAR'
ENDIF
IF(RJ.EQ.0.0D0)THEN
  VERSION='TWO BODY'
ENDIF

```

C

C

C

```

OUTPUT RESULTS FOR DISSPLA

```

```

IF(JVER.EQ.1)THEN
  WRITE(3,3000) K
  WRITE(3,3100) RJ
ENDIF

```

C

```

DO 10 J = 1, KK
  WRITE(3,3100) DR(J),DID(J),DTHD(J)
  WRITE(3,3100) DOMD(J),DRV(J),EARCD(J)
  WRITE(3,3100) PDR(J),ATE(J),CTE(J)
  WRITE(4,3100) THJO(J)

```

10

C

C

C

```

PRINT RESULTS

```

```

WRITE(6,'( /)')
WRITE(2,'( /)')
WRITE(6,6000) ' RESULTS'
WRITE(2,6000) ' RESULTS'
WRITE(6,6100) LINE
WRITE(2,6100) LINE
WRITE(6,6200) 'J = ',RJ
WRITE(2,6200) 'J = ',RJ
WRITE(6,6300) 'VERSION = ',VERSION
WRITE(2,6300) 'VERSION = ',VERSION
WRITE(6,6100) LINE
WRITE(2,6100) LINE

```

C

```

DO 20 J = K, KK
C
+   WRITE(6,6400) 'POINT = ',J,'ORBIT = ',JORBIT(J),
+   WRITE(2,6400) 'POINT = ',J,'ORBIT = ',JORBIT(J),
+   'ROMBERG ITERATIONS = ',JN
C
+   WRITE(6,6500) 'R = ',R(J),'RF = ',RF(J),'DR = ',DR(J)
+   WRITE(2,6500) 'R = ',R(J),'RF = ',RF(J),'DR = ',DR(J)
C
+   WRITE(6,6500) 'I = ',ID(J),'IF = ',IFD(J),'DI = ',DID(J)
+   WRITE(2,6500) 'I = ',ID(J),'IF = ',IFD(J),'DI = ',DID(J)
C
+   WRITE(6,6500) 'TH = ',THD(J),'THF = ',THFD(J),'DTH = ',DTHD(J)
+   WRITE(2,6500) 'TH = ',THD(J),'THF = ',THFD(J),'DTH = ',DTHD(J)
C
+   WRITE(6,6500) 'OM = ',OMD(J),'OMF = ',OMFD(J),'DOM = ',DOMD(J)
+   WRITE(2,6500) 'OM = ',OMD(J),'OMF = ',OMFD(J),'DOM = ',DOMD(J)
C
+   WRITE(6,6500) 'RX = ',RX(J),'RY = ',RY(J),'RZ = ',RZ(J)
+   WRITE(2,6500) 'RX = ',RX(J),'RY = ',RY(J),'RZ = ',RZ(J)
C
+   WRITE(6,6500) 'RFX = ',RFX(J),'RFY = ',RFY(J),'RFZ = ',RFZ(J)
+   WRITE(2,6500) 'RFX = ',RFX(J),'RFY = ',RFY(J),'RFZ = ',RFZ(J)
C
+   WRITE(6,6500) 'DRV = ',DRV(J),'PDR = ',PDR(J),
+   'EARC= ',EARCD(J)
+   WRITE(2,6500) 'DRV = ',DRV(J),'PDR = ',PDR(J),
+   'EARC= ',EARCD(J)
C
+   WRITE(6,6500) 'RTE = ',DR(J),'ATE = ',ATE(J),
+   'CTE = ',CTE(J)
+   WRITE(2,6500) 'RTE = ',DR(J),'ATE = ',ATE(J),
+   'CTE = ',CTE(J)
C
+   WRITE(6,6600) 'INT = ',INTA(J),'ROM = ',ROMA(J)
+   WRITE(2,6600) 'INT = ',INTA(J),'ROM = ',ROMA(J)
C
20 CONTINUE
C
+   WRITE(6,6500) 'EG = ',ENG,'EGF = ',ENGF
+   WRITE(2,6500) 'EG = ',ENG,'EGF = ',ENGF
C
+   WRITE(6,'( /)')
+   WRITE(2,'( /)')
C
3000 FORMAT(3X,I3)
3100 FORMAT(3(3X,D18.10))
C
6000 FORMAT(3X,A)
6100 FORMAT(3X,A20//)
6200 FORMAT(3X,A,F8.6)
6300 FORMAT(3X,A,A11//)
6400 FORMAT(2(3X,A8,I3/),3X,A21,I3//)
6500 FORMAT(3(3X,A6,F23.15//))

```


6600 FORMAT(3(3X,A6,F23.8/))

C

RETURN

END

C

LIST OF REFERENCES

1. Snider, J. R., *Satellite Motion Around An Oblate Planet: A Perturbation Solution for All Orbital Parameters*, Ph.D. Dissertation, Naval Postgraduate School, Monterey, California, June, 1989.
2. Sagovac, C. P., *A Perturbation Solution of the Main Problem in Artificial Satellite Theory*, Master's Thesis, Naval Postgraduate School, Monterey, California, June, 1990.
3. Struble, R. A., "A Geometrical Derivation of the Satellite Equations," *Journal of Mathematical Analysis and Applications*, Volume 1, 1960, pp. 300-307.
4. Struble, R. A., "The Geometry of the Orbits of Artificial Satellites," *Architectural Rational and Mechanical Analysis*, Volume 7, 1961, pp. 87-104.
5. Struble, R. A., "An Application of the Method of Averaging in the Theory of Satellite Motion," *Journal of Mathematics and Mechanics*, Volume 10, 1961, pp. 691-704.
6. Eckstein, M. C., Shi, Y. Y., and Kevorkian, J., "Satellite Motion for All Inclinations Around an Oblate Planet," *Proceedings of Symposium No. 25, International Astronomical Union*, Academic Press, 1966, pp. 291-322, equations 61.
7. Danielson, D. A. and Snider, J. R., "Satellite Motion Around an Oblate Earth: A Perturbation Solution for All Orbital Parameters: Part I - Equatorial and Polar Orbits," *Proceedings of the AAS/AIAA Astrodynamics Conference*, Stowe, Vermont, August, 1989.
8. Danielson, D. A., Sagovac, C. P., and Snider, J. R., "Satellite Motion Around an Oblate Earth: A Perturbation Solution for All Orbital Parameters: Part II - Orbits for All Inclinations," *Proceedings of the AAS/AIAA Astrodynamics Conference*, Portland, Oregon, August, 1990.
9. Ferziger, J. H., *Numerical Methods for Engineering Application*, John Wiley & Sons, New York, New York, 1981, pp. 32-37.
10. Coffey, S. L. and Alfriend, K. T., "An Analytic Orbit Prediction Program Generator," *Journal of Guidance, Control, and Dynamics*, Volume 7, September-October, 1984, pp. 575-581.
11. Deprit, A., "The Elimination of Parallax in Satellite Theory," *Celestial Mechanics*, Volume 24, June, 1981, pp. 111-153.
12. Coffey, S. L. and Deprit, A., "A Third Order Solution to the Main Problem in Satellite Theory," *Journal of Guidance, Control, and Dynamics*, Volume 5, July-August, 1982, pp. 366-371.
13. Alfriend, K. T. and Coffey, S. L., "Elimination of the Perigee in the Satellite Problem," *Celestial Mechanics*, Volume 32, February, 1984, pp. 163-172.

14. Battin, R. H., *An Introduction to the Mathematics and Methods of Astrodynamics*, American Institute of Aeronautics and Astronautics, New York, New York, 1987, pp. 128-130, pp. 450-470.